MECHANISM UNDERLYING BRADYCARDIA AND LONG QT 2 RELATED ARRHYTHMIAS: INTERPLAY BETWEEN Ca^{2+} OVERLOAD AND ELECTRICAL DYSFUNCTION

by

Jong J. Kim

BS in EE., Yonsei University, Seoul, Korea, 1997

MS in BME, University of Alabam at Birmingham, 2007

Submitted to the Graduate Faculty of

The Swanson School of Engineering in partial fulfillment

of the requirements for the degree of

Doctor of Philosophy

University of Pittsburgh

2011

UNIVERSITY OF PITTSBURGH

SWANSON SCHOOL OF ENGINEERING

This dissertation was presented

by

Jong J. Kim

It was defended on

November 22, 2011

and approved by

Barry London, MD, PhD, Professor, Medicine Department

Partha Roy, PhD, Associate Professor, Bioengineering Department

Sanjeev Shroff, PhD, Professor, Bioengineering Department

Jan Němec, MD, Assistant Professor, Medicine Department

Dissertation Director: Guy Salama, PhD, Professor, Medicine Department

MECHANISM UNDERLYING BRADYCARDIA AND LONG QT 2 RELATED ARRHYTHMIAS: INTERPLAY BETWEEN Ca^{2+} OVERLOAD AND ELECTRICAL DYSFUNCTION

Jong J. Kim, PhD

University of Pittsburgh, 2011

In numerous pathologies, spontaneous Ca^{2+} release (SCR) emanating from the sarcoplasmic reticulum and occurring during the action potential (AP) plateau can drive voltage instability that initiates arrhythmias, but the direct interplay between SCRs and arrhythmogeneis has not been fully understood in bradycardia and in long QT type 2 (LQT2) models.

Simultaneous optical measurement of intracellular Ca^{2+} transient (Ca_iT) and AP were performed in Langendorff-perfused rabbit hearts following AV node ablation. Bradycardia and/or LQT2 was/were induced and the spatial heterogeneity of intracellular Ca^{2+} handling and its link to voltage dispersion were investigated.

Upon switching from 120 to 50 beats/min, AP duration (APD) increased gradually with increasing occurrence of SCRs during the AP plateau ($p<0.01$, $n=7$). SCR was a) regionally heterogeneous, b) spatially correlated with APD prolongation, c) associated with enhanced dispersion of repolarization (DOR), d) reversed by pacing at 120 beats/min and e) suppressed with K201 (1μM) or flecainide (5μM), inhibitors of cardiac ryanodine receptors (RyR2) which reduced APD ($p<0.01$, $n=5$) and DOR ($p<0.02$, $n=5$). Western blots of Ca^{2+} channels/transporters revealed intrinsic spatial distributions of Cav1.2α and NCX (but not RyR2, and SERCA2a) that correlate with the distribution of SCR and underlie the molecular mechanism responsible for SCRs.

In LQT2, lability of Ca_i, voltage, and ECG signals increased during paced rhythm, before the appearance of early afterdepolarizations (EADs). When EADs appeared, Ca_i occasionally rose before voltage upstrokes at the origins of propagating EADs. Localized, areas of SCRs appeared in LQT2 and corresponded to areas of prolonged Ca_iT and APD. Triggered activity appeared after 3-5 min of LQT2 and emanated only at sites with steep membrane potential (V_m) gradients (ΔV_m gradient percentile: 94.9 ± 3.2%, n=6). Pre- or post-treatment with K201 suppressed SCRs and decreased DOR, ΔV_m and ΔCa_i. The reduction of ΔV_m suppressed triggered activity (n=8/9 hearts).

The results show that bradycardia and LQT2 elicit spatially discordant SCR, which is tightly correlated with AP instability. The SCR mediated-enhancement of repolarization gradients and AP prolongation can promote arrhythmogenesis. These findings underscore the importance of a detailed understanding of Ca^{2+}-dependent arrhythmogenic mechanisms for the development of rational treatment strategies.

TABLE OF CONTENTS

LIST OF TABLES

LIST OF FIGURES

ACKNOWLEDGMENTS

I devote all of my honors to my Lord, who I always look to support and guide me in the right direction.

I would like to express deep gratitude to my advisor Dr. Guy Salama. I appreciate you for supporting me and giving me the great opportunity to participate in high level area of cardiac research. It was truly an amazing experience for me to be trained by a highly respected mentor and scientist

I would also like to thank Dr. Jan Němec for his valuable efforts on our projects. His insights were, without a doubt, extremely important to the outcome of our projects. In addition, I would like to thank Dr. Barry London, Dr. Partha Roy, and Dr. Sanjeev Shroff for agreeing to serve on my committee and to offer helpful comments to the projects that have contributed to my dissertation.

I am grateful to my research group, which includes Dr. Rita Papp and Dr. Jonathan Abramson, for their endeavors on our projects. I would like to acknowledge Bethann Gabris who has endlessly assisted me to pursue these projects. I would also like to acknowledge Mr. Divyang Patel for his scientific revision in this dissertation work.

I would like to recognize the financial support of American Heart Association Pre-Doctoral Fellowship, and the Universitiy of Pittsburgh Department of Bioengineering which have assisted me in pursuing my graduate education.

Endless thanks to my family for their love and support. To my mother and dad for their countless prayers, I love you. To my wife, Seejeen, I love you and thank you for your patience and devotion.

1.0 INTRODUCTION

Coordinated propagation of electrical activity throughout the heart ensures synchronized cardiac contraction generating sufficient forces for blood pumping. However, some pathological conditions can transform an electrically stable heart into one that unstable, which leads to the generation of cardiac arrhythmias. In pathological states, interruption in the spatial organization of cardiac wave propagation as a consequence of functional or anatomical conduction barriers can initiate cardiac arrhythmias such as ventricular tachycardia (VT) or ventricular fibrillation (VF).[1, 2] Experimental studies suggest that dispersion of repolarization (**DOR**) or spatial heterogeneity of cardiac activity increases in numerous pathologies of the heart and has been proposed as a fundamental mechanism for the initiation and/or maintenance of arrhythmias when the substrate is challenged with premature depolarization (i.e. premature ectopic beats or triggered activity).[3-6] Intrinsic regional differences in electrophysiological properties and pharmacologic responsiveness of ventricular myocardium have been implicated as a factor of DOR. For example, preferential AP prolongation of M-cells in response to antiarrhythmic class III drugs has been linked to mechanisms fundamental to markedly enhanced transmural DOR under LQT conditions.[7] However, our understanding of the augmentation of DOR throughout a heart under various disease conditions still remains rudimentary.

In addition to DOR, it is well established that triggered activity as a consequence of increases in tissue excitability play an important role in cardiac arrhythmogenesis. Although the

emerging role of altered intracellular Ca^{2+} dynamics in the initiation of arrhythmogenic triggered activity such as early afterdepolarizations (EADs) or delayed afterdepolarizations (DADs) has been extensively reported, the interplay between abnormalities in intracellular Ca^{2+} handling and arrhythmogenesis is not fully appreciated. In normal conditions, cardiac contraction and relaxation are tightly modulated by membrane potential (V_m) and by Ca^{2+} uptake and release which are controlled by proteins on the sarcoplasmic reticulum (SR) membrane ($V_m \rightarrow Ca^{2+}$ coupling). However, in certain diseases an increase in RyR2 open-probability or interruption in Ca^{2+} homeostasis due to an imbalance between Ca^{2+} influx and efflux promotes abnormality in Ca^{2+} handling, such as 'non' voltage gated Ca^{2+} release. The spontaneous Ca^{2+} release from sarcoplasmic reticulum (SR), in turn, elicit V_m instability via Ca^{2+} dependent sarcolemmal transporters ($Ca^{2+} \rightarrow V_m$ coupling).[8-11] Specifically, Ca_i overload in internal Ca^{2+} stores and altered kinetics of Ca_i transients have been documented in ischemia-reperfusion arrhythmias, in congenital and drug-induced forms of LQT that produce a characteric polymorphic ventricular tachycardia, called Torsade de Pointes (TdP), and in heart failure that leads to reentrant arrhythmias.[12-15]

In addition to the impact of spontaneous SR Ca^{2+} release in the initiation of triggered activity, regional variations in intracellular Ca^{2+} [2] handling produce long-short-long-short Ca_i transients that are responsible for spatially discordant V_m instability in heart failure, ischemia, long QT syndrome. Recently, our group reported that spatially inhomogeneous Ca^{2+} oscillations occur before the onset of 'electrical' cardiac arrhythmia during drug-induced LQT2.[16] Such enhanced spatial heterogeneity of Ca_i handling in pathologies can be explained by multiple factors such as intrinsic ion channel/pump distribution, non-uniform ion channel remodeling, local dispersion of sympathetic nerve ganglion, and regional differences of cellular properties.[5,

12, 17, 18] Several experimental studies in animal models have shown that the non uniform distribution of cellular properties produces regional differences of Ca_i handling.[11, 12, 19-21] It is therefore likely that the spatial heterogeneity of Ca_i handling could be linked to local dispersion of action potential (AP) via Ca^{2+} dependent sarcolemmal transporters.[22] The enhanced AP dispersion could serve either as conduction blocks initiating reentrant arrhythmias or as re-excitant activity along the abnormal voltage gradient. However, evidence that high spatiotemporal heterogeneity of Ca_i handling is the underlying mechanism of cardiac arrhythmogenesis is lacking.

It is well established that bradycardia increases the likelihood of triggering TdP associated with delayed repolarization.[23-25] However, the mechanism through which bradycardia facilitates TdP remains unknown. In our previous study, we observed a moderate degree of secondary Ca^{2+} elevation with only bradycardia and the bradycardia dependent abnormality in Ca_i handling was fully reversible by increasing the pacing rate.[16] Despite an extensive body of clinical literature suggesting that tachycardia induced alternations of Ca_i handling is responsible for electrical instability,[26, 27] the interplay between bradycardia-related abnormality in Ca_i handling and electrical instability has not been investigated.

Here, we used simultaneous optical measurement of Ca_i handling and AP dynamics in perfused rabbit hearts, and report for the first time that non-voltage gated secondary Ca^{2+} release (SCR) in drug induced LQT2 or in bradycardia plays a crucial role in the further prolongation of AP. Moreover, the spatial heterogeneity of SCR promotes voltage dispersion across the anterior surface of rabbit hearts. Such Ca^{2+}-dependent augmentation of voltage dispersion promotes lethal cardiac arrhythmias by initiating arrhythmogenic triggered activity along the voltage gradient and/or by providing electrophysiological substrates for reentrant activity.

2.0 SPECIFIC AIMS

The goal of the proposed research is to investigate the interplay between Ca^{2+} overload and electrical dysfunction in bradycardia and in drug-induced long QT type 2. A complete understanding of the mechanism underlying Ca^{2+}-dependent electrical dysfunction and enhancement of spatial organization of tissue excitability may provide more reliable anti-arrhythmic therapies. The specific aims of the proposed research are the following:

Specific Aim #1: To test the hypothesis that bradycardia can promote an imbalance between Ca^{2+} influx and Ca^{2+} efflux, which elicits a secondary Ca^{2+} release (SCR) from internal Ca^{2+} stores. SCR can produce an arrhythmogenic substrate if a) it prolongs APDs through a reverse Ca_i-V_m coupling during AP plateau and b) SCR is spatially heterogeneous resulting in enhanced DOR. This study will provide a mechanistic explanation for bradycardia-dependent arrhythmias, which is an important clinical problem.

Specific Aim #2: To test the hypothesis that secondary Ca^{2+} oscillations (SCa_iO) can promote LQT2 related arrhythmias by initiating triggered activity and by promoting dispersion of repolarization. This includes the impact of SCaO on a) voltage instability, b) the initiation of early afterdepolarizations (EADs) or delayed afterdepolarizations (DADs), and c) enhanced DOR leading to triggered activity along lines of voltage gradients. This study will demonstrate the critical role of spatial heterogeneity of Ca^{2+} abnormalities in the initiation and the maintenance of LQT2-related arrhythmias.

3.0 BACKGROUND

During sinus rhythm, the pacemaker action potential initiates cardiac activation consisting of electrical waves are highly organized from beat-to-beat and control the mechanical contractions associated with each electrical impulse or rhythmic electrical activity. However, during ventricular tachycardia (VT) and ventricular fibrillation (VF), the wave propagation is interrupted by anatomical or functional conduction blocks.[1, 2] The heart loses its rhythmic activity, local muscle contractions become asynchronous with a can-of-worm appearance, and the heart fails to pump blood adequately. The occurrence of arrhythmogenic conduction blocks can be caused by heterogeneities of slowed conduction or of recovery of excitability.[28, 29] More recently, it has been established that disorders in the ion channel kinetics in numerous pathologies produce ionic imbalance between transsarcolemmal membranes. The interruption in ionic homeostasis can also leads to Ca^{2+} overload in internal SR stores, extracellular accumulation of K^+ concentration, and intracellular elevation of Na^+ concentration, which have been implicated as arrhythmogenic risk factors. In this section, the underlying mechanisms for ionic imbalance and the interplay between the ionic imbalance and arrhythmogenesis will be introduced.

3.1 ELECTROPHYSIOLOGY IN MAMMALIAN HEARTS

Rhythmic excitation and contraction (EC) coupling ensures appropriate blood supply throughout the body. During sinus rhythm, the action potential (AP) of a pacemaker initiates a normal regular cardiac activation, electrical waves are organized, and mechanical contractions associated with the electrical activities are rhythmic (see Figure 1). Such electrical activity, called the cardiac AP, is tightly regulated by changes in membrane conductance and ionic movement across the sarcolemmal membrane. The ventricular AP consists of five phases, number 0 – 4 (see Figure 2).[30] Phase 0 represents membrane depolarization as a consequence of rapid activation of voltage gated Na^+ channels (I_{Na}). During phase 1 of AP, partial repolarization occurs immediately after the peak of the AP due to the inactivation of Na^+ channels combined with activation of transient of outward K^+ channels (I_{to}). During phase 2 of the AP, which is the plateau phase that is characteristic of a cardiac AP, Ca^{2+} channels ($I_{Ca,L}$) open and let Ca^{2+} into the cell while delayed rectifier K^+ channels open letting K^+ come out of the cell. The simultaneous activity of two currents acting in opposite directions causes this plateau phase. Phase 3 represents rapid repolarization of AP as a result of activation of outward K^+ currents. Phase 4 is the final phase of AP, and the membrane potential returns to resting potential.

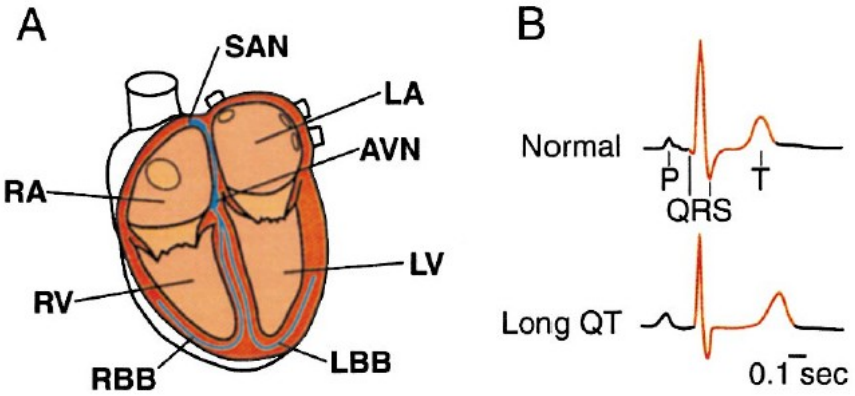

Figure 1. **Heart and conduction system** A) Schematic diagram of heart and conduction system.[30] Cardiac rhythms arising in the SA node (SAN) cause atrial contraction (right atria (RA) and left atria (LA)). In parallel, electrical activity travels to the AV node (AVN) via internodal pathways. After a delay, the sinus rhythm is conducted to the left bundle branch (LBB) and the right bundle branch (RBB) then to the purkinje fibers and the endocardium at the apex of the heart, then finally to the ventricular myocardium (right ventricle (RV) and left ventricle (LV)). B) Examples of normal ECG (top) and long QT ECG (bottom). QT prolongation appears in long QT ECG.

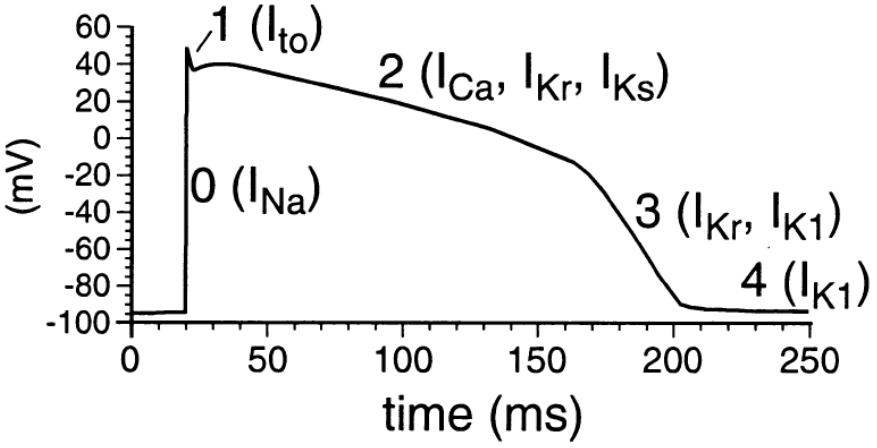

Figure 2. **Cardiac action potential and ion currents** [30] Inward I_{Na} causes a rapid upstroke of cardiac AP (Phase 0). Ito mediates phase 1 notch. ICaLCa,L and delayed rectifying outward K^+ currents (I_{Kr}, and I_{Ks}) sustain AP plateau (Phase 2). Outward I_{Kr} and I_{Ks} mediates rapid AP repolarization (Phase 3) and I_{K1} helps recovery of resting membrane potential (Phase 4).

3.1.1 K^+ dynamics

K^+ channels are ubiquitous membrane proteins that contribute to cardiac electrical activity by regulating membrane resting potential and AP repolarization. The resting membrane potential is determined by the K^+ gradient between the extracellular and cytosolic space. Since activation and the recovery from inactivation of voltage gated I_{Na} and $I_{Ca,L}$ currents are highly dependent on the membrane potential, K^+ dynamics is a dominant factor in regulating tissue excitability.[31] Alternation of extracellular K^+ concentration ($[K^+]_{ex}$) is also recognized as a major factor of automaticity of both pacemaker cells and working myocytes.[32, 33] For instance, a moderate increase in $[K^+]_{ex}$ causes the elevation of resting membrane potential in pacemaker cells.

Furthermore, various K^+ channels contribute to action potential (AP) dynamics. For example, the delayed rectifier current (I_{Kr} and I_{Ks}) elicit AP repolarization. Transient outward current (I_{to}) contributes to the repolarization of phase 1 of AP, and inward rectifier current (I_{K1}) helps recovery to the resting membrane potential by mediating a small hyperpolarizing K^+ current.[30]

3.1.2 Interventions of K^+ dynamics and cardiac arrhythmias

Experimental studies have shown that elevations in $[K^+]_{ex}$, known as hyperkalemia, can be caused by oxygen depletion due to coronary occlusion and are associated with arrhythmogenesis.[34, 35] For example, ischemia-induced hyperkalemia predisposes the heart to the development of lethal reentrant ventricular arrhythmias by causing sustained membrane depolarization that leads to slowing conduction and altered refractoriness.[36] It is also widely

recognized that potassium K^+ deficiency can be associated with a variety of cardiac arrhythmias. For example, it is well known that reduced K^+ concentration in blood serum, known as hypokalemia, decreases the delayed rectifier current (I_{Kr}), and results in cardiac arrhythmias by causing AP prolongation.[37]

In addition, due to the primary roles of K^+ currents in AP repolarization, abnormalities in K^+ currents during APs often induce life-threatening tachyarrhythmias. Typically, inhibition of I_{Kr} is thought to result in arrhythmogenic AP prolongation and promote the occurrence of LQT2-related arrhythmias such as TdP.[38] In addition, abnormal AP shortening reduces refractory periods and provides a favorable substrate for reentrant arrhythmias.[39]

3.1.3 Extracellular K^+ accumulation (EKA) and its role in arrhythmogenesis

Voltage-clamp and K^+ selective electrodes have shown that K^+ accumulation occurs in T-tubules and narrow clefts between cells indicating that K+ concentration ($[K^+]$) in these narrow spaces is not in diffusional equilibrium with the external K^+ concentration (~ 4.7 mM).[40, 41] In normal physiology, K^+ efflux from the cell is pumped back via Na/-K pump - and the local external $[K^+]$ recovers on a beat-to-beat basis.[42] However, at high heart rates or during ischemia, a local EKA rise of 2-5 mM can cause a small but significant depolarization which alters excitability and can change the shape and time course of subsequent APs.[43, 44] Such a spatial and dynamic variation of EKAs can cause variations in tissue excitability, produce local conduction blocks, and has been shown to be sites of premature ectopic beats.[45, 46] High EKAs can occur during stress in physiological conditions such as high heart rates where EKAs may not fully recover from beat to beat resulting in $[K^+]_{ex}$ elevation or from local coronary occlusion and the ensuing ischemia and may worsen during VT and VF. [47, 48] The spatial

variation of EKAs induces inhomogeneous slowing of conduction velocity, which may alternate dynamically to cause blocks of wave propagation that can lead to triggered out-of-phase ectopic beats.[43, 44, 47, 48] The dispersion of EKAs can lead to inhomogeneous tissue excitability, and alternans, and the spatial excitability variation plays an important role in initiating and maintaining cardiac arrhythmias.

3.1.4 Na^+ dynamics

The voltage-gated cardiac Na^+ channel is responsible for the generation of the rapid membrane depolarization during cardiac AP and thereby plays a crucial role in the excitability of cardiomyocytes.[49] In addition, since the AP upstroke velocity also determines impulse conduction velocity in cardiac tissue, this channel also contributes to the conduction of electrical activity through the heart by facilitating intercellular communication via gap junctions.[50] It is also well known that Na^+ dependent transporters such as Na-K pump, Na/Ca exchanger (NCX), and Na/H exchanger (NHE) [51], play a crucial role in regulation of ionic homeostasis.[52]

Due to the crucial role of Na^+ channels in tissue excitability and conductivity, its abnormal activity has been implicated as a major risk factor in various arrhythmogenic models.[53-55] Inherited mutations in SCN5A that encode the α subunits of Na^+ channels result in several different types of arrhythmias. As a consequence, the gain-of-function mutations in the gene increases Na^+ influx during APs, then prolongs cardiac AP, and eventually promotes long-QT type 3 related arrhythmias.[56] Alternatively, deletion or loss-of-function mutations of the gene have been linked to multiple types of arrhythmias including bradycardia, atrioventricular (AV) conduction delay, and Brugada syndrome.[57-60] Also, pharmacological blocks of cardiac Na^+ channels result in slowing conduction and produce marked sudden cardiac death.[61]

In healthy cardiac myocytes, intracellular Na^+ concentration ($[Na^+]_i$) is tightly regulated by Na^+ dependent transporters such as NCX, Na-K ATPase, and NHE. Under some pathological conditions, those regulatory processes can be interrupted and result in $[Na^+]_i$ accumulation.[17, 62] The elevation of $[Na^+]_i$ reverses NCX and promotes sarcoplasmic reticulum (SR) Ca^{2+} overload. Such a cellular Ca^{2+} overload, secondary to Na^+ overload, can increase the propensity of non-voltage gated SR Ca^{2+} release, which is arrhythmogenic.[63]

3.1.5 Ca^{2+} dynamics

Ca^{2+} is primarily responsible for cardiac contraction. Cardiac AP initiated by Na^+ entry across the sarcolemma activates voltage-gated L-type Ca^{2+} channels, and Ca^{2+} entry which triggers SR Ca^{2+} release by a phenomenon known as Ca^{2+} induced Ca^{2+} release (CICR).[64, 65] Transient increases in Ca_i concentration force Ca^{2+} ions to bind to the myofilament protein troponin C and eventually initiate cardiac contraction (see Figure 3). In addition to its role in cardiac contraction, Ca^{2+} regulates ionic influx and efflux via NCX or calcium-gated activated potassium K^+ channels (see Figure 3).[66, 67] In Ca^{2+} mediated signaling pathways, Ca^{2+} regulates many different cellular functions.[68, 69]

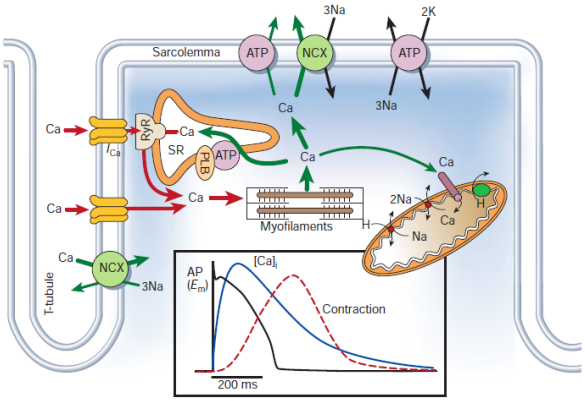

Figure 3. **Schematic diagram of calcium Ca^{2+} induced calcium Ca^{2+} release** [64] Ca^{2+} Influx through voltage gated L- type Ca^{2+} channel induces SR Ca^{2+} release via RyR2. Released Ca^{2+} binds to myofilamenents and initiates cardiac contraction.

3.1.6 Abnormality in Ca_i handling and its role in cardiac arrhythmogenesis

Cardiac contraction is initiated by an increase in intracellular Ca^{2+} concentration ($[Ca^{2+}]_i$) as a result of SR Ca^{2+} release via RyR2 in response to Ca^{2+} entry through the L-type Ca^{2+} channels, known as the phenomenon of CICR.

In general, abnormal Ca_i handling such as SCR has been implicated as a fundamental mechanism that underlies the induction of arrhythmias in numerous cardiac diseases.[11, 16, 70-72] The SCR has been documented in ischemia-reperfusion arrhythmias, congenital and drug-induced forms of long QT that produce polymorphic VT, and in heart failure that leads to reentrant arrhythmias. [8, 14, 70, 73]

In experimental settings, diverse hypotheses for the mechanism underlying SCR have been proposed. For example, in the condition of delayed repolarization or of inhibition of Na-K ATPase by cardiac glycosides, the SR can become overloaded with Ca^{2+}. The SR Ca^{2+} overload makes SR more prone to SCR. Such SCR from the SR propagates as a Ca^{2+} wave by CICR.[63] Some of the Ca^{2+} released during a wave is removed from the cell by the electrogenic NCX

resulting in a net depolarization. This is the cellular mechanism underlying delayed afterdepolarizations (DADs), which often precede certain types of fatal cardiac arrhythmias.[74, 75] More recently it has been proposed that arrhythmogenic SCR can also occur due to the increase in RyR2 open probability as a consequence of increase in CSQ or RyR2 sensitivity to luminal free Ca^{2+} due to CPVT mutations.[76, 77] Redox modification of RyR2 by oxygen free radicals increases RyR2 leakage and facilitates SCR, which triggers ischemia-reperfusion arrhythmias.[71, 78] Protein kinase A (PKA) mediated hyperphosphorylation of RyR2 has been reported in heart failure.[79, 80] If such a SCR occurs before the complete termination of AP repolarization, the SCR elevates cytosolic Ca^{2+} level and results in arrhythmogenic triggered activity such as EADs by promoting Ca^{2+} sensitive inward currents (I_{NCX}).[81, 82]

3.1.7 Regional variation of Ca_i handling and its link to arrhythmogeneis

Some experimental studies in intact rabbit models have reported that gradients of Ca_i transients exist on the basal/apical and endocardial/epicardial axes.[19, 20] For example, the endocardium exhibits a slower uptake of intracellular Ca^{2+} compared with the epicardium, likely as a consequence of the transmural difference of SERCA2a expression. Recently, Sims et al. reported that a higher density of CaV1.2a (L-type Ca^{2+} channel gene) is expressed more at the base than the apex of the LV, and EADs in LQT2 are more pronounced in the base than the apex of the LV of adult female rabbits.[12] Furthermore, a clinical study has shown that the duration of cardiac contraction, which was measured by an ultrasound technique in LQT patients, is transmurally heterogeneous.[83]

3.2 LONG QT TYPE SYNDROME (LQT2))

Long QT syndrome (LQTS) is an abnormal condition in which prolongation of the APD can lead to sudden cardiac death by inducing polymorphic tachyarrhythmias. Among LQTS, LQT2 is the second most common gene location that is affected in long QT syndrome, making up about 25% of all cases. Typically, two different forms of LQT type 2 (LQT2), congenital LQT2 and acquired LQT2, have been characterized.[84-87] First, the congenital form represents a "pure global repolarization disease". The congenital form of LQT2 is caused by mutation of human ether-a-go-go gene (HERG), also known as KCNH2 which encodes the alpha subunit of K^+ channel responsible for I_{Kr}. The loss of function of I_{Kr} delays repolarization of AP and consequently results in APD prolongation. Second, the acquired LQTS is of critical importance because of its prevalence in the clinical setting. The high binding affinity of the HERG channel to a wide range of drugs due to its very susceptible amino acid residues has been a serious public health problem because cardiac and nor-cardiac drugs inadvertently block the I_{Kr} channel from conducting currents, and impairs repolarization of AP.[88] In addition, several factors (e.g., medications, electrolyte abnormalities, and heart failure) delay ventricular repolarization and may lead to lethal arrhythmias.

3.2.1 EADs and DADs in LQT2

Under LQT2 conditions, the EADs are classically attributed to an inward current carried by L-type Ca^{2+} channels.[89] In other words, it has been proposed that under conditions conducive to EADs, the sarcolemma spends a longer period of time in the voltage range where both the activation and inactivation gates of L-type Ca^{2+} channel are partially open. The resulting

enhancement of $I_{Ca,L}$ during phase 3 of ventricular action potential may be sufficient to cause an EAD. Alternatively, secondary Ca^{2+} release from an overloaded SR to the cytoplasm could cause EADs by augmentation of the electrogenic I_{NCX}, a mechanism previously shown to be responsible for the generation of delayed afterdepolarizations (DADs).[11, 14, 81]

3.2.2 Dispersion of repolarization (DOR)

Conventionally, regional differences in outward K^+ currents have been attributed to the DOR.[90-93] In mammalian hearts, K^+ channels are spatially heterogeneous across the wall of the ventricles (epicardium to endocardium) as well along the wall (base to apex). Experimental studies suggest such intrinsic DOR increases in numerous pathologic conditions (bradycardia, LQT, ischemia-reperfusion, and heart failure) and has been proposed as a mechanism fundamental to the initiation and maintenance of arrhythmias.[94-96] Typically, preferential action potential (AP) prolongation of M cells under conditions with reduced I_{Kr} has been proposed as a major underlying mechanism responsible for enhanced transmural DOR in LQT2.[7, 97] Alternatively, functional differences in levels of I_{Kr} along the surface of a heart that can be inhibited by class III anti-arrhythmic agents has been linked to a mechanism underlying epicardial DOR in cryoablated LQT2 models.[11]. In LQT2 models, once triggered activity occurs, enhanced DOR plays a crucial role in maintaining LQT2 related arrhythmias by providing a favorable substrate for unidirectional conduction blocks leading to reentrant arrhythmias.[98]

3.2.3 LQT2 related reentrant arrhythmia

If propagation of cardiac electrical activity is disrupted by anatomical or functional conduction blocks,[1, 2] the heart loses its rhythmic activity, cardiac muscle contraction is locally dissociated, and the heart fails to pump an adequate amount of blood. The arrhythmogenic conduction blocks can be caused by heterogeneous slowing of conduction and/or a spatial dispersion of recovery of excitability.[28, 29] In LQT2 conditions, reentrant activity occurs when the wave propagation of premature ectopic beats is interrupted upon encountering a region of refractory tissue but conducts though excitable areas (unidirectional propagation) leading to functional reentry, which results in LQT2 related polymorphic tachyarrhythmias, known as TdP (see Figure 4).[98, 99] An alternative mechanism has been proposed in optical mapping studies of Langendorff perfused rabbit hearts treated with the I_{Kr} blocker, E4031. In these studies APD prolongation was associated with Ca_i oscillations then became increasingly more severe and elicited EADs where Ca_i preceded the upstroke of EADs. EADs occurred at 2 to 4 sites in the heart and were of sufficient magnitude to propagate and collide with wavefronts emanating from other EADs. TdP was then caused by EADs firing out-of-phase from different sites causing the sinusoidal pattern seen on EKG recordings. Thus, optical images of TdP agreed with the hypothesis of Desertenne that was proposed in 1966.

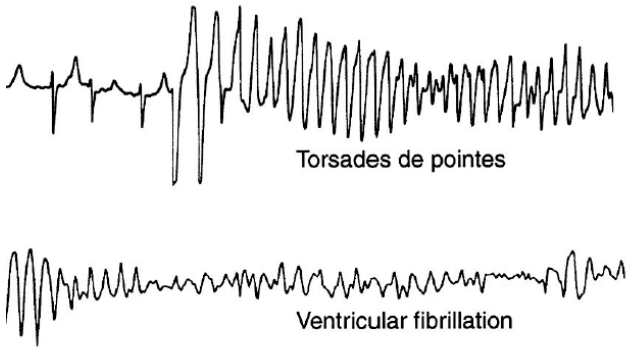

Figure 4. **Typical examples of human ECGs during TdP (top) and ventricular fibrillation (bottom) in LQT conditions** [30] QTc prolongation precedes the occurrence of TdP.

Figure 5. **ECG recording in lead D2 during T-wave alternans in a LQT patient** [100] T-waves alter during 4 consecutive beats (beats I, II, III, IV).

3.2.4 T-wave lability (TWLI)

Electrocardiography (ECG) has been widely used in both clinical and experimental settings for the measurement of electrical activity of a heart. Typically, unusual morphology in ECG represents abnormalities in cardiac rhythms. Abnormal ECG characteristics such as QTc

prolongation and unusual morphology of T wave (alternans and variation) have been reported in LQT patients (see Figure 5).[100-103]Also, in a chronic heart failure model, inter-lead QT dispersion is markedly enhanced and beat to beat variation in repolarization morphology in ECG, known as TWLI, has been thought to be a marker of pro-arrhythmic conditions.[104]

3.2.5 Rate and time dependent APD adaptation and its relevance to LQT2 arrhythmias

APD adaptation, also known as QT accommodation, allows a heart to maintain an acceptable ratio between the period of ventricular filling and ventricular contraction.[105] Most studies attribute APD adaptation to changes in cytosolic Ca^{2+} [2] which in turn alters the kinetics of Ca^{2+}-dependent inactivation of L-type Ca^{2+} channels[64, 65, 106] but others have implicated the rate-dependence of I_{NCX} [107] and of the late Na^{+} current, $I_{Na,L}$.[108] Besides ion channel kinetics, changes in ionic concentrations in the cytoplasm (intracellular Na^{+} and Ca_i) or extracellular K^{+} contribute to APD adaptation.[109, 110] Mathematical simulations of slow heart rate (HR) indicated that the long diastolic intervals result in a complete deactivation of the slow component of the delayed rectifying K^{+} current (I_{Ks}) and complete recovery from inactivation of L-type Ca^{2+}currents ($I_{Ca,L}$) which could theoretically explain APD adaptation in bradycardia.[111-113] Long-term memory, unlike short term memory, is related to pacing induced ion channel remodeling (such as reduction in $I_{Ca,L}$ and I_{to}) taking several days to reach to a new steady-state, and plays an important role in long term APD accommodation. [114]The rate and time dependent APD-accommodation occurring within minutes is thought to be spatially heterogeneous due to the intrinsic heterogeneity of ion channel distribution, specifically I_{Ks} distribution.[113, 115] Such a rate dependent APD prolongation is associated with markedly

enhanced dispersion of APD and explains why LQT2 related arrhythmia is more pronounced during bradycardia.

3.3 STEEP VOLTAGE GRADIENT AND ARRHYTHMOGENESIS

Experimental studies have suggested that steep voltage gradients can be produced by premature stimuli and/or myocardial infarction.[116, 117] Abnormal voltage gradients as a result of heterogeneous ion accumulation and cellular uncoupling across the ischemic border zone can account for the driving force for the diastolic 'injury current' to the normal side of the ischemic border. Such small injury currents can cause a slight depolarization of the normal tissue and may facilitate triggered activity.[116]

3.4 MEASUREMENTS OF CARDIAC AP AND INTRACELLULAR Ca^{2+} DYNAMICS

In the past, although glass pipette microelectrodes have contributed as great deal toward understanding of the ionic basis of the cardiac AP, the application of single cell impalements is not precise for studies requiring simultaneous recording of APs from multiple sites. The spatiotemporal pattern of wave propagation of cardiac electrical activity is an important marker to determine whether cardiac function is rhythmic or arrhythmic. Electrical mapping techniques, by using surface electrodes, have been used to study the spread of cardiac excitation, but the two most basic characteristics, activation and recovery, cannot be identified reliably at the site of recording for conditions other than uniform propagation. In addition, it is not possible to map

while a defibrillating shock is being applied and during slowly changing, low-level depolarization, which is seen in ischemia. Repolarization measured with an electrogram often does not coincide with the actual repolarization at the recording site. Since Salama and Morad for the first time made optical recordings of cardiac AP in 1976, the optical measurements of cardiac APs from the cellular to organ level have made a crucial contribution to cardiac research.[118] The principal theory of optical recordings of cardiac AP is that a membrane binding potentiometric fluorescent dye changes its spectral properties in response to changes in membrane potential. In other words, a membrane binding voltage sensitive dye exhibits wavelength shifts in peak fluorescence and/or absorption due to a change in membrane potential. The major advantages of optical mapping are thought to be 1) the impervious response to electrical defibrillation shock, 2) the fast response to voltage changes, and 3) the high spatiotemporal resolution.[119] In addition to optical recordings of cardiac AP with potentiometric probes, the optical measurements of changes in ion concentration have been widely performed. For example, changes in Ca^{2+} concentration inside cardiomyocytes have been measured with Ca^{2+} sensitive fluorescent probes such as Ca^{2+} indicators Rhod-2 AM and fluo-4.[120, 121]Recently, simultaneous optical measurements of cardiac AP and Ca_i dynamics at high spatial and temporal resolution have been performed and provide a powerful tool to investigate the role of Ca_i anomalies in eliciting cardiac arrhythmias (see Figure 6).

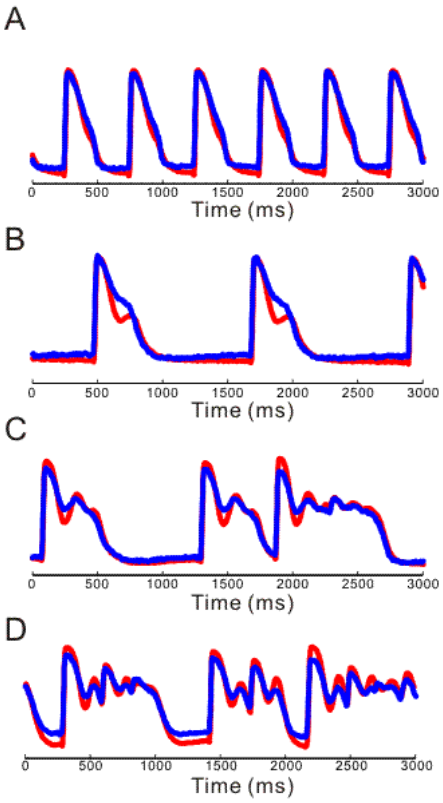

Figure 6. Examples of simultaneous measurement of AP (blue) and Ca_i (red) dynamics in a Langendorff perfused rabbit heart before and after inhibition of I_{Kr} LQT2 was modeled by perfusing with Tyrode's solution containing dofetilide (250 to 500 nM, Pfizer, New York, NY), a selective I_{Kr} blocker and lowering K^+ and Mg^{2+} concentrations by 50 %. A) Baseline recording at 500ms cycle length (CL). B) Baseline recording at 1200ms CL. C) 2 minutes after dofetilide infusion at 1200ms CL. D) 5 minutes after dofetilide infusion at 1200ms CL.

3.5 AGENTS TARGETING ABNORMAL Ca^{2+} HANDLING

Spontaneous SR Ca^{2+} release under diverse pathological conditions has been linked to initiation of cardiac arrhythmias, and suppression of the SCR has been considered as possible anti-arrhythmic therapies.[122, 123] So far, several pharmacological agents have been introduced as SCR suppressors, though their therapeutic strategies may differ.

JTV519, also known as K201 stabilizes RyR2 in the closed state by enhancing the binding affinity of calstabin 2 for RyR2 and preventing the dissociation of calstabin 2 from RyR2.[124] It has been tested in ischemia injury models.[125] Flecainide, which is a well known Na^{+} channel blocker, also suppresses SCR by inhibiting RyR2 channels by open state block, and has been tested in CPVT mutation.[126] Captopril, which was introduced as an angiotensin converting enzyme inhibitor, acts as a reducing agent and thus reduces SCR by protecting against ischemia-induced oxidation.[127]

4.0 BRADYCARDIA INDUCES NON-UNIFORM SECONDARY Ca^{2+} RELEASE THAT ENHANCES ACTION POTENTIAL DURATION, DISPERSION OF REPOLARIZATION AND ARRHYTHMIA RISK

In heart muscle, the influx and efflux of Ca^{2+} across the plasma membrane are precisely balanced during each phasic contraction as is the coordinated Ca^{2+} release and reuptake across the sarcoplasmic reticulum (SR) network. Any deviation or imbalance between influx and efflux can only be small and transient to maintain cytoplasmic Ca^{2+} homeostasis.[128] A fundamental property of mammalian hearts is the force-frequency relationship or 'Staircase Effect' where a change in heart rate causes a transient imbalance between Ca^{2+} influx and efflux until a new steady state is attained where again Ca^{2+} influx equals efflux but at a new state of contractility. The stair case effect is associated with an inverse relationship between action potential (AP) duration (APD) and heart rate (HR) which is critical to achieve a stable state of contractility. The mechanism responsible for APD adaptation as a function of HR remains controversial. Most studies attribute APD adaptation to changes in cytosolic Ca^{2+} [2] which in turn alters the kinetics of Ca^{2+}-dependent inactivation of L-type Ca^{2+} channels[64, 65, 106] but others have implicated the rate-dependence of Na-Ca exchange current, I_{NCX}[107] and of the late Na^+ current, $I_{Na,L}$.[108] Besides ion channel kinetics, changes in ionic concentrations in the cytoplasm (intracellular Na^+ and Ca_i) or extracellular K^+ contribute to APD adaptation.[109, 110] Mathematical simulations of slow HR indicated that the long diastolic intervals result in a complete deactivation of the slow component of the delayed rectifying K^+ current (I_{Ks}) and complete recovery from

inactivation of L-type Ca^{2+}currents ($I_{Ca,L}$) which could theoretically explain APD adaptation in bradycardia.[111-113]

Of all the proposed explanations for APD adaptation, the role of Ca_i cannot be over-emphasized since independent of rate, APD is inversely dependent on external [Ca^{2+}] and Ca_i by one of the mechanisms that mediate $Ca_i \rightarrow V_m$ coupling. During a transition from slow to fast HRs, Ca_i rises due to the greater number of APs per unit time and decreased Ca^{2+} efflux due to shorter diastolic intervals. Higher Ca_i accelerates the Ca^{2+}-dependent inactivation of $I_{Ca,L}$, reduces Ca^{2+} influx per AP which decreases APD; an important negative feedback process that limits total Ca^{2+} influx via $I_{Ca,L}$[129] and enables the system to reach a new steady state. Conversely, a transition from fast to slow HR slows down Ca^{2+} dependent $I_{Ca,L}$ inactivation and the long diastolic intervals allow for the complete recovery of $I_{Ca,L}$ from inactivation which prolong APDs.

HR regulates force generation in a physiological range of HRs but fast or slow HRs create severe Ca^{2+} handling abnormalities that in combination with various pathologies promote arrhythmias.[130] Transitions from slow to fast HR have been extensively studied and shown to create Ca^{2+} alternans that lead to APD and T-wave alternans and arrhythmias. [26] In the setting of ischemia[22, 131] and heart failure[132], arrhythmogenic Ca^{2+} and APD alternans occurred at physiological HR. In contrast, few studies have investigated events associated with bradycardia even though bradycardia is known to be an important co-factor required to trigger Torsade de Pointes in long QT types 2 and 3. In drug-induced long QT type 2 (LQT2), slow HR promotes spontaneous SR Ca^{2+} release that occurs during the AP plateau to produce early afterdepolarizations (EADs) that progress to Torsade de Pointes. [11, 16] At the level of intact hearts, bradycardia prolongs APD but also enhances dispersion of repolarization (DOR),[90,

115] and the enhanced DOR is thought to be a contributing factor to maintain LQT2-related arrhythmias.[133] In ventricular cells, the longer the cycle length the greater the APD prolongation but in intact hearts, the mechanism linking bradycardia to enhanced DOR and arrhythmia vulnerability remains unexplored.

This project investigates APD adaptation during bradycardia in Langendorff perfused rabbit hearts using dual optical mapping of Ca_i and V_m with high resolution CMOS Cameras. The data shows for the first time that bradycardia produces a spatially heterogeneous secondary Ca^{2+} release (SCR) from the SR which modulates APD through $Ca_i \rightarrow V_m$ coupling and correlates with the enhanced dispersion of APD and DOR.

4.1 METHODS

4.1.1 Heart preparations

New Zealand White rabbits (15 female, 60 to 120 days old) were euthanized with pentobarbital (75 mg/kg intravenously) and anticoagulated with heparin (200 U/kg intravenously). The heart was rapidly dissected and perfused with Tyrode's solution containing (in mM): 130 NaCl, 24 $NaHCO_3$, 1.0 $MgCl_2$, 4 KCl, 1.2 NaH_2PO_4, 50 dextrose, 1.25 $CaCl_2$, at pH 7.2-7.4, gassed with 95% O_2 plus 5 % CO_2. Temperature was maintained at 37.0 °C and perfusion pressure was adjusted to ≈70 mmHg with a peristaltic pump. To minimize motion artifact, blebbistatin (Sigma, St Louis, MO 5-10 μM) was added to the perfusate for 5-10 min. The heart was immobilized in a chamber and stained with a voltage-sensitive dye (PGH1: 200 μl of 1 mg/ml dimethyl sulfoxide (DMSO)) and loaded with a Ca^{2+} indicator (Rhod-2 AM, 200 μl

of 1 mg/ml DMSO). Epicardial bipolar pseudo-EKG was continuously monitored. Epicardial pacing with a unipolar electrode on the right ventricle was performed at a baseline cycle length of 0.5 seconds (baseline heart rate (BHR) of 120 beats/minute) or at a slow HR (SHR) with a cycle length of 1.2 seconds (50 beats/minute; profound bradycardia for rabbit hearts). This investigation conformed to the current Guide for Care and Use of Laboratory Animals published by the National Institutes of Health the Institutional Animal Care and Use Committee of the University of Pittsburgh.

4.1.2 Optical apparatus

An optical apparatus consisting of two CMOS Cameras (SciMedia, Ultima One, 100 by 100 pixels, at 250 frames per second) has been used for simultaneous measurement of intracellular Ca^{2+}transients and membrane potential changes, as previously described.[134] The anterior surface of the heart was illuminated with a 520 ± 30 nm excitation beam, and the fluorescence was passed through a dichroic mirror (660 nm) to focus the Rhod-2 and PGH1 fluorescence images on two CMOS Cameras.[134]

4.1.3 Study protocol

The AV node was ablated by cauterization to control heart rate. Hearts were paced at a cycle length of 0.5 s which was taken as a *'baseline heart rate'* (BHR) then the cycle length was lengthened to 1.2 s to impose a bradycardia or a *'slow heart rate'* (SHR). APs and Ca_iT were continuously recorded for 32 s during transitions from fast to slow or slow to fast HRs while measuring changes in AP duration (APD). Changes in HR lead to gradual changes in APD until

a new steady state was attained. The time-course of 'APD adaptation' required continuous recordings of 3-5 minutes to reach a steady state of APDs during transitions from BHR to SHR (bradycardia) and 5-10 minutes in going from SHR to BHR.

Pilot experiments were carried out to select the BHR and the SHR that were used in this study. A slow heart rate of 50 beats/min was chosen because it could be maintained reliably without interruptions by an occasional extra-beat yet was effective to expose spatial heterogeneities of Ca_iT caused by SCR. Similar, but less pronounced effects were observed at 0.9 and 1.0 s cycle lengths. A basic heart rate of 120 beats/min was chosen because a) this HR was well tolerated and did not result in 'run-down' of the preparations, b) capture with pacing electrodes was reliable during uninterrupted recordings and c) spatial heterogeneities of AP and Ca_iT were negligible compared to still faster rates.

4.1.4 Data analysis

T wave (TW) amplitude relative to QRS complex (TW/QRS) in EKG was used to approximate DOR. [135] Activation time at each site was calculated from $(dF/dt)_{max}$ of the local AP or Ca_iT upstroke. APD and Ca_iT duration (Ca_iTD) at each site was calculated from the interval between $(dF/dt)_{max}$ and the recovery of V_m and Ca_iT traces to 20% of baseline (APD_{80} or Ca_iTD_{80}), respectively. Automatic measurement of APD_{80} and Ca_iTD_{80} from all pixels (100 x 100 pixels) was used to calculate mean APD_{80} and Ca_iTD_{80}. The dispersion of APD_{80} and Ca_iTD_{80} was calculated from the SD of APD and Ca_iTD. The time constant (τ) of mean APD (from all 100x100 pixels) adaptation to heart rate changes was calculated by fitting the transitions from BHR to SHR ($\tau_{f\rightarrow s}$) and from SHR to BHR ($\tau_{s\rightarrow f}$) with mono-exponential functions. Briefly, the root mean square of differences between measured and predicted APD

values were used to choose the best curve fit. Rate and time dependent mean APD_{80} and Ca_iTD_{80} and regional variation in 100 x 100 pixels were statistically evaluated. Bradycardia dependent AP/Ca_iT prolongation and dispersions before and after K201 (1 μM) or flecainide (5 μM) perfusion were compared. K201 (3-(4-Benzylcyclohexyl)-1-(7-methoxy-2,3-dihydrobenzo[*f*][1,4]thiazepin-4(5*H*)-yl)propan-1-one) was synthesized according to the procedure reported by Wehrens et al.[136] The area under the curve [137] of Ca_iT at each pixel was normalized by setting the minimum value to zero and the maximum AUC to 1. Maps of AUC were generated at steady state BHR and SHR. AUC was used as a measurement of the relative Ca_i at each site. Scatter plots of AUC versus APD_{80} were used to correlate these two parameters and calculate a correlation coefficient (r) between AUC and APD_{80} at steady state SHR. All 10,000 recordings (100x100 pixels) were used to generate the scatter plots to correlate spatial heterogeneities of SCR to the dispersion of APD_{80}. Regional differences, base of right ventricle (RVB) and apex of left ventricle (LVA) were compared for statistical significance using 2-tailed t-test. Box-whisker diagrams are used to visualize the distribution of the data. The top and bottom whiskers define respectively the maximum and minimum values; the top and bottom of the box define the 75^{th} and 25^{th} percentiles respectively and the line within the box is the median in the data set.

4.1.5 Western blot Analysis

Female New Zealand White rabbits (3 month old) were euthanized, as described above; the hearts were perfused with Tyrode's solution and ventricular tissue samples (~50 mg) were dissected from the anterior RVB and LVA corresponding to "RVB" and "LVA" regions of the optical mapping studies. Proteins were isolated as previously described,[138] were separated by

SDS-PAGE (50 µg/ sample), transferred to PVDF membranes which were probed by standard techniques. After immunolabeling, band intensities were measured with Image J and normalized with respect to β actin. Differences between the RVB and LVA were analyzed with one-tailed t-test and considered significant at $p< 0.05$. Antibodies against Cav1.2α, SERCA2, ERG and β actin were obtained from Santa Cruz Biotech (Cat. #: SC-103588, SC53010, 15968 and 81178, respectively); NCX1, and RyR2 were obtained from Thermo Scientific (Cat. #: MA3-926 and MA3-916, respectively) and Nav1.5 was obtained from Alomone (Cat. #: ASC-005)

4.2 RESULTS

APD_{80} adaptation was reproducible from heart to heart and during repeated cycles (3-4 per heart) of transitions from 120 (BHR) to 50 (SHR) beats/min and back. Figure 7 A illustrates a sequence of two complete cycles of APD adaptation from BHR to SHR. From a steady state heart rate of 120 beats/min (not shown), a transition from BHR to SHR resulted in the expected gradual APD_{80} and QT prolongation which was fully reversed by shifting back to BHR. The mean ΔAPD_{80} in the first episode of 5 minutes of sustained SHR increased by 55.2±10.9% which was similar to % increase in the mean ΔAPD_{80} recorded in second episode of SHR (51.25±8.2%) ($p>0.05$, $n=4$). Panels B and C illustrate optical APs and an EKG recording from bipolar surface electrodes, respectively measured at various time points (labeled: a-e in Figure 7A). An AP recorded at the onset SHR (trace a) is markedly shorter than at steady state SHR (trace b). APs measured at the next set of steady state BHR (traces c and e) are shorter than at steady state SHR (trace d). Similarly, T-wave amplitudes were markedly larger at steady state SHR (arrows on traces b and d) than at BHR (arrows on traces c and e) or the initiation of SHR (arrow on trace a)

(Figure 7C). The increases in T-wave amplitude relative to the QRS amplitude are a measure of enhanced DOR and the ratio of TW/QRS amplitude was statistically greater at steady state SHR than BHR (Figure 7C right panel, $p<0.01$, n=15 trials from 5 hearts).

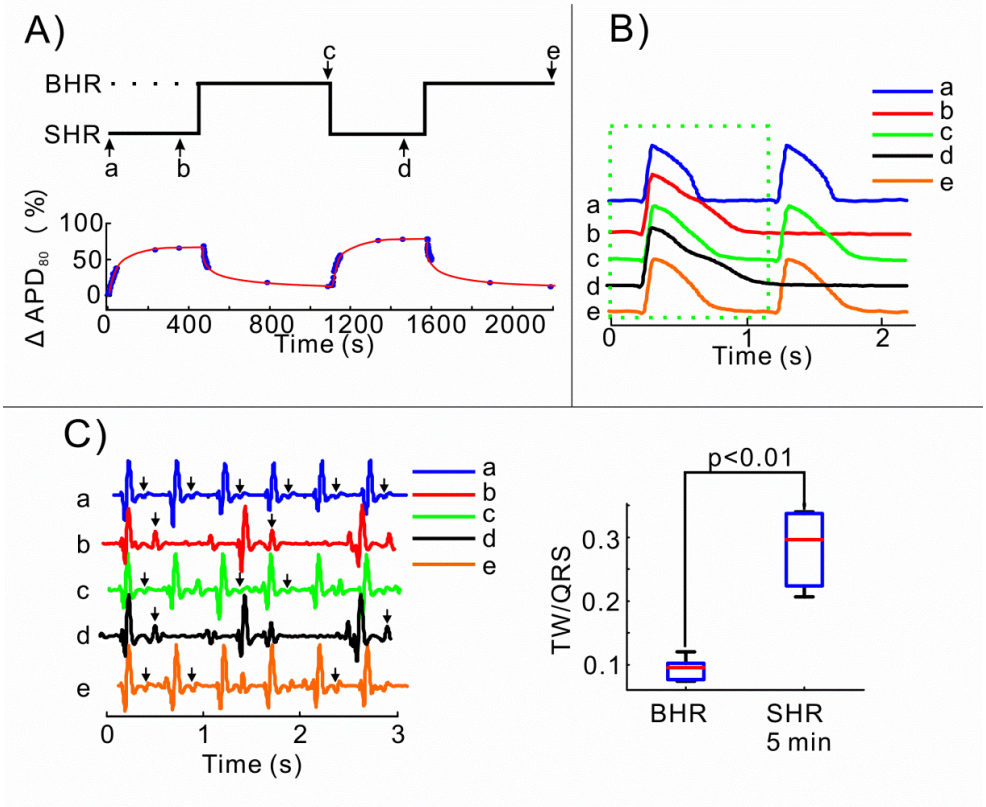

Figure 7. APD_{80} adaptation during transitions from BHR and SHR A) Repeated cycles of pacing from SHR to BHR. Changes in HR (top trace) and the time course of APD_{80} adaptation are shown uninterrupted for 22,000 seconds. B) Optical traces of APs from one of the pixels on the CMOS camera were measured at various time points: a, b, c, d and e, as labeled in panel A (top trace). C) EKG signals were recorded from the epicardium at the same time points: a, b, c, d and e, as depicted in panel A (top trace). The relative amplitude of T-waves measured as the ratio of TW to QRS amplitudes was statistically greater in SHR than BHR which is indicative of an increase in DOR.

APD_{80} adaptation curves showed different time constants in going from BHR to SHR ($\tau_{f\rightarrow s}$ = 48±9.2s) compared to from SHR to BHR ($\tau_{s\rightarrow f}$ =30.4±4.7s; $p<0.05$, n=5 hearts) (Figure 8).

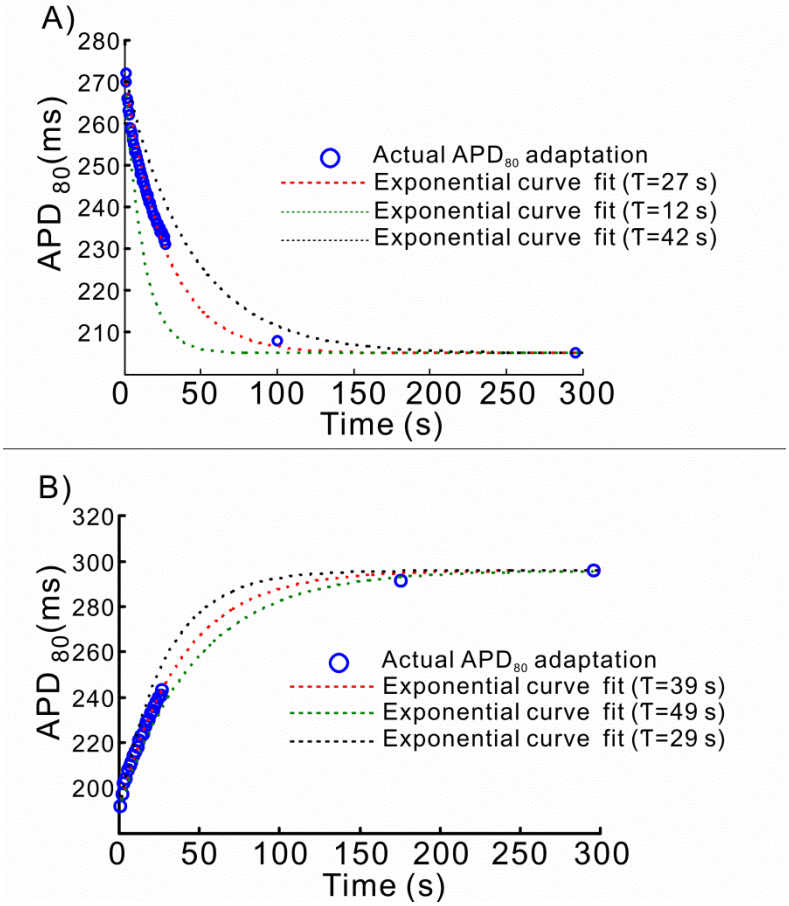

Figure 8. Time constants for APD_{80} adaptation: from BHR to SHR and SHR to BHR A) APD_{80} adaptation during transitions from SHR to BHR. B) APD_{80} adaptation during transition from BHR to SHR. In both cases, the time course of APD80 adaptation to changes of cycle length were fitted to single exponential curves and their time constant ( ) was calculated based on the best-fit of experimentally measured APD_{80} adaptations.

At BHR, AP and Ca_iT signals exhibited the expected rapid rise and monophasic recovery to baseline. During the transition to SHR, diastolic levels of Ca_i decreased gradually and APD_{80} and Ca_iTD_{80} exhibited the expected time-dependent prolongation (Figure 9A). Most interesting was the gradual prolongation of Ca_iTD_{80} which was associated with an increasingly more pronounced "secondary Ca^{2+} rise" (SCR) during the AP plateau and was associated with APD prolongation (Figure 9A, SCR labeled with an arrow, *right traces*). With slow pacing, APDs and Ca_iTDs increased gradually reached a new steady state. The rate dependent, gradual

increase of SCRs (arrow from BHR to SHR) was associated with changes in the shape and time-course of APs, with a linear relationship between Ca_iTD_{80} and APD_{80} (Figure 9A bottom panels). Note the gradual prolongation of Ca_i (*arrow* from short to long durations) and voltage (V_m) traces from BHR, to 16s and 5 min of SHR. Reversal to BHR suppressed SCR gradually, altered the shape of AP repolarization and shortened APD_{80} and Ca_iTD_{80} (*arrow* from long to short duration) (Figure 9B). During APD adaptation, there was a linear relationship between APD_{80} and Ca_iTD_{80} during the transition from BHR to SHR (Figure 9A *bottom traces*) and from SHR to BHR (Figure 9B *bottom traces*).

The distribution of SCR was heterogeneous and was more pronounced at the bast of the right ventricle (RVB) than the apex of the left ventricle (LVA) as was the distribution of APDs. Figure 10A shows an image of a heart and the area viewed by the CMOS Camera, delineated by the black box. Maps of APD_{80} (Figure 10B top panels) and Ca_iTD (Figure 10B bottom panels) are shown for BHR and 32 s and 5 min into SHR. SHR Caused a marked increase in the dispersion of both APD_{80} and Ca_iTD_{80} compared to steady-state BHR ($p < 0.01$, $n = 7$ hearts) (Figure 10B and D). The superposition of Ca_iT measured at BHR, 32 s and 5 min of SHR are shown for three sites (a, b and c) on the anterior surface (Panel A). The traces show that SCR and Ca_iTD_{80} increase during APD adaptation from BHR to SHR in a spatially inhomogeneous, being more pronounced at site *a* on the RVB than sites b and c that are closer to the LVA (Figure 10C). Similarly, the standard deviations [122] of Ca_iTD_{80} and APD_{80} were significantly greater in SHR than BHR ($p<0.01$, $n=7$ hearts, Figure 10D).

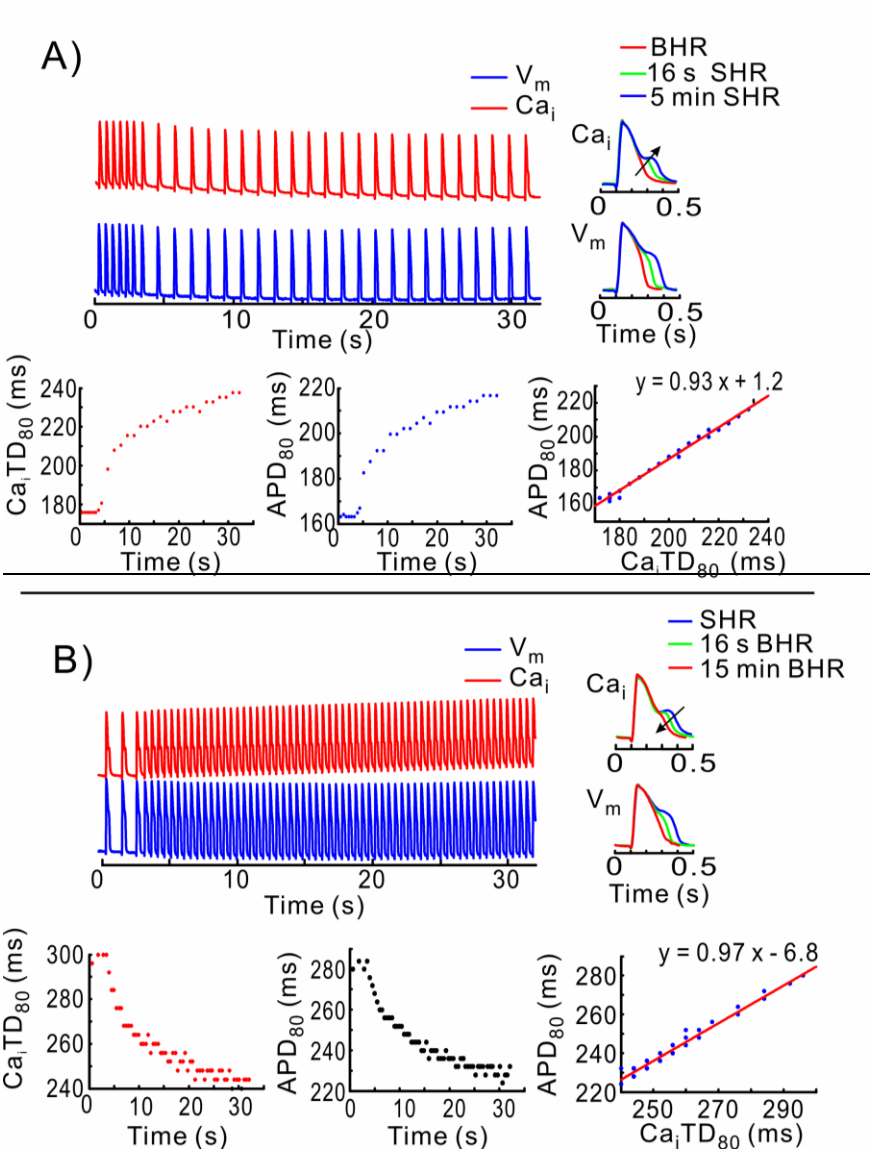

Figure 9. Time-course of APD and Ca_iTD adaptation during first 32 seconds. A) Changes in AP and Ca_i dynamics during a change in heart rate from BHR to SHR (top traces). APD_{80} and Ca_iTD_{80} are plotted as a function of time and APD_{80} vs. Ca_iTD reveals a tight linearly relationship. Inset: superposition of APs and Ca_iTs from the same pixel recorded at different times during adaptation to SHR B) Changes in AP and Ca_i dynamics during the reversal from SHR to BHR. APD_{80} and Ca_iTD_{80} are plotted as a function of time and APD_{80} vs. Ca_iTD are linearly related. Inset: superposition of APs and Ca_iTs from the same pixel recorded at different times during adaptation towards BHR.

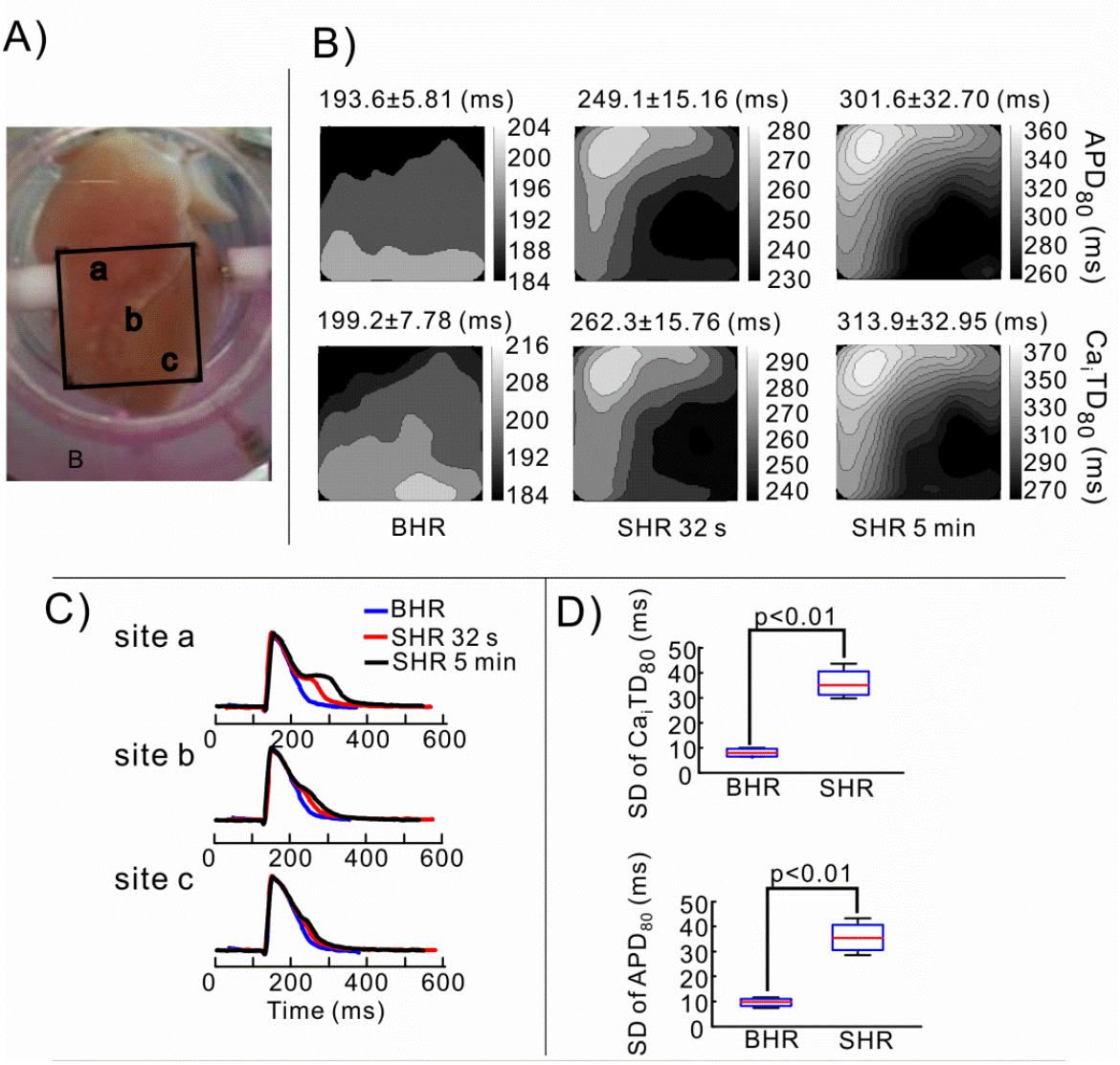

Figure 10. Dispersion of Ca_iTD_{80} and APD_{80} in BHR and SHR A) A picture of the heart with a black box identifying the region of the heart viewed by the CMOS cameras. B) Dispersion of APD_{80} (top panels) and Ca_iTD_{80} (bottom panels) at different time-points from steady state BHR (left panels) to SHR after 32 s (middle panels) and at equilibrium 5 min (right panels). C) Optical traces of Ca_i at site a, b and c, that are identified panel A. D) Standard deviation [122] of Ca_iTD_{80} (top) and APD_{80} (bottom) at steady state BHR and SHR. SDs were calculated from 10,000 recordings (100 x 100 pixels) at 120 beats per minute (bpm) baseline and 5 minute at 50 bpm.

Since the comparison between amplitudes of Ca_iT and APD is widely used to show the impact of Ca^{2+} abnormality on APD prolongation or shortening, correlation of areas under curves (AUCs) of Ca_iT, which approximate amplitudes of SCRs, with APD_{80} was calculated to assess the interplay between Ca_i and V_m. Maps of AUCs and APD_{80} were generated and correlation coefficients were Calculated from scatter plots of AUC vs. $APD_{80.}$ Figure 11A shows the region of a heart viewed by the arrays and Figure 11B and C show the correlation analysis during BHR and SHR, respectively from the same heart. The scatter plot of AUC vs. APD_{80} (Figure 11C, rightmost panel) exposes a particularly poor correlation with r = 0.243 during BHR. In contrast, scatter plots during SHR (Figure 11D, rightmost panel) show a tight correlation with a coefficient r = 0.924. Figure 11D illustrates results from a second heart during SHR where AUCs and APD_{80} were greater in amplitude at the RVB than the LVA and the correlation coefficient of AUCs vs. APD_{80} was 0.987. The hearts in Figure 11A and D were chosen to illustrate the two types of scatter plots that were observed; either a rare bifurcation or non-monotonic AUC vs. APD_{80} relationship (n=1/5) (Figure 11D, rightmost panel) or a monotonic relationship (Figure 11C, n=4/5). Most interesting was the enhanced correlation between AUC and APD_{80} in SHR ($r = 0.93 \pm 0.03$) compared to that in BHR ($r = 0.55 \pm 0.29$) ($p < 0.01$, n = 7 hearts) (Figure 11E). The mean APD_{80} at BHR was not significantly different between RVB and LVA ($p>0.29$, n=7) but became statistically different at SHR ($p<0.05$, n=7) (Figure 11F). In SHR, AUCs were significantly greater at the RVB than the LVA, as shown in AUC maps in Figure 11C and D ($p<0.05$, n=5).

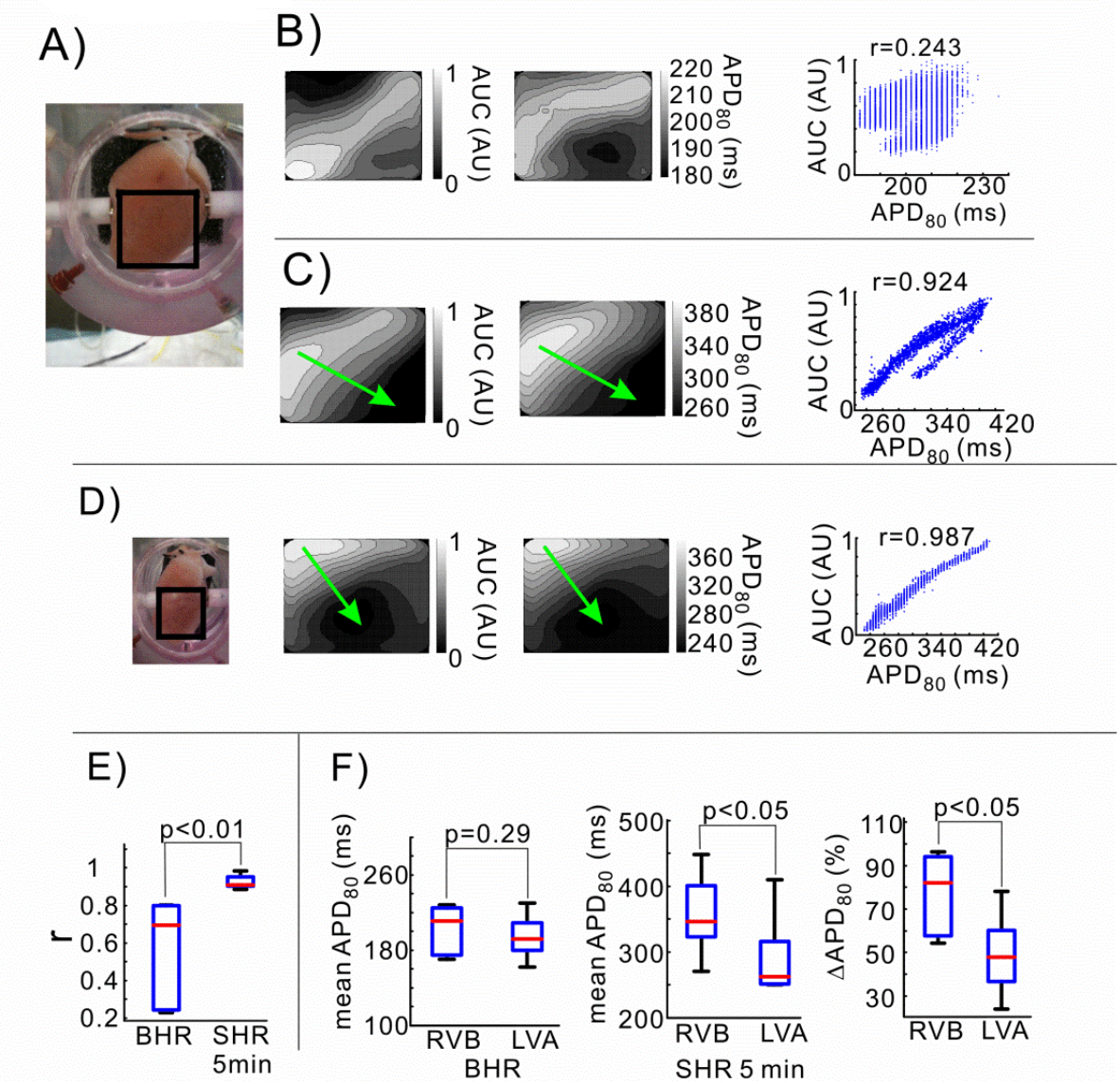

Figure 11. Regional differences of APD_{80} and AUC of Ca_iT in bradycardia A) Image of heart with a box to delineate the field-of-view of the cameras. B) Maps of AUC (of Ca_iT) and of APD_{80} during BHR with scatter plot of AUC vs. APD_{80}, in this case the correlation coefficient, r= 0.243. C) Same heart as in B but during SHR, maps of AUC and APD_{80} exhibit large regional variations from RVB to LVA, arrows depict gradients of large to small AUC and APD_{80}, AUC vs. APD_{80} scatter plot was non-monotonic, with r = 0.924. D) As in C but with a different heart. The field-of-view is delineated by the box and maps of AUC and APD80 exhibit marked regional variations from RVB to LVA, arrows identify direction of long to short Ca_iT and APD_{80}. Scatter plot of AUC vs. APD_{80} was monotonic with r= 0.987. E) Summary analysis of r values showing a higher correlation between AUC and APD_{80} at SHR than BHR, p< 0.01 n=7 hearts. F) Statistical analysis of APD_{80} comparison between RVB and LVA during BHR (p=0.29, NS) after 5 min of SHR (p<0.05 n = 5 hearts); SHR results in statistically significant increase in APD at the base than apex and the percent change in APD, ΔAPD_{80} increased by 80% in RVB compared to 40% in LVA as a result of the bradycardia.

To elucidate the interplay between intracellular Ca^{2+} and voltage, experiments were carried out to assess whether SCR prolonged APDs or prolonged APDs elicited SCRs. In SHR, SCRs are more pronounced and it is reasonable to expect that SCRs might originate from a 'second' release of Ca^{2+} from the SR via cardiac ryanodine receptors (RyR2). Two agents known to stabilize RyR2, K201 (1μM, n=5) and flecainide (5 μM, n=4) were perfused to test their effects on SCR as well as APD and Ca_iTD adaptation. Ca_iTD and APD adaptation was measured during transitions from BHR to SHR before and after perfusion with K201 or flecainide. Plots of the percent change of mean ΔAPD_{80} as a function of time are shown during transitions from BHR to SHR for 24 pixels on the LVA and 24 pixels on the RVB, before and after perfusion with a RyR2 stabilizer. As shown in Figure 12, K201 (panel A) and flecainide (panel B) suppressed SCR and Ca_iTD during SHR (Ca_i traces without or with K201 or with flecainide, respectively in Figure 12A and B) and reduced mean APD_{80} (V_m traces in Figure 12A and B) at pixels on the RVB (K201: $p < 0.01$, n=5; flecainide: $p < 0.01$, n=4) (Figure 12A and B left graphs of ΔAPD80 % vs. time). In contrast to their effect on SCR at the base during SHR, K201 and flecainide did not significantly change AP and Ca_iT at the apex during SHR (Figure 12). It is important to note that K201 and flecainide did not significantly alter the early phase of APD adaptation, meaning the first 10 s of APD prolongation but both suppressed a second phase of APD prolongation from 10-25 s (plots of ΔAPD_{80} % vs. time, Figure 12A and B). As shown in Figure 13, the suppression of SCR by K201 (1 μM) or flecainide (5 μM) markedly reduced the dispersion of APD_{80} at SHR (K201: $p < 0.05$, n=5; flecainide: $p < 0.05$, n=4).

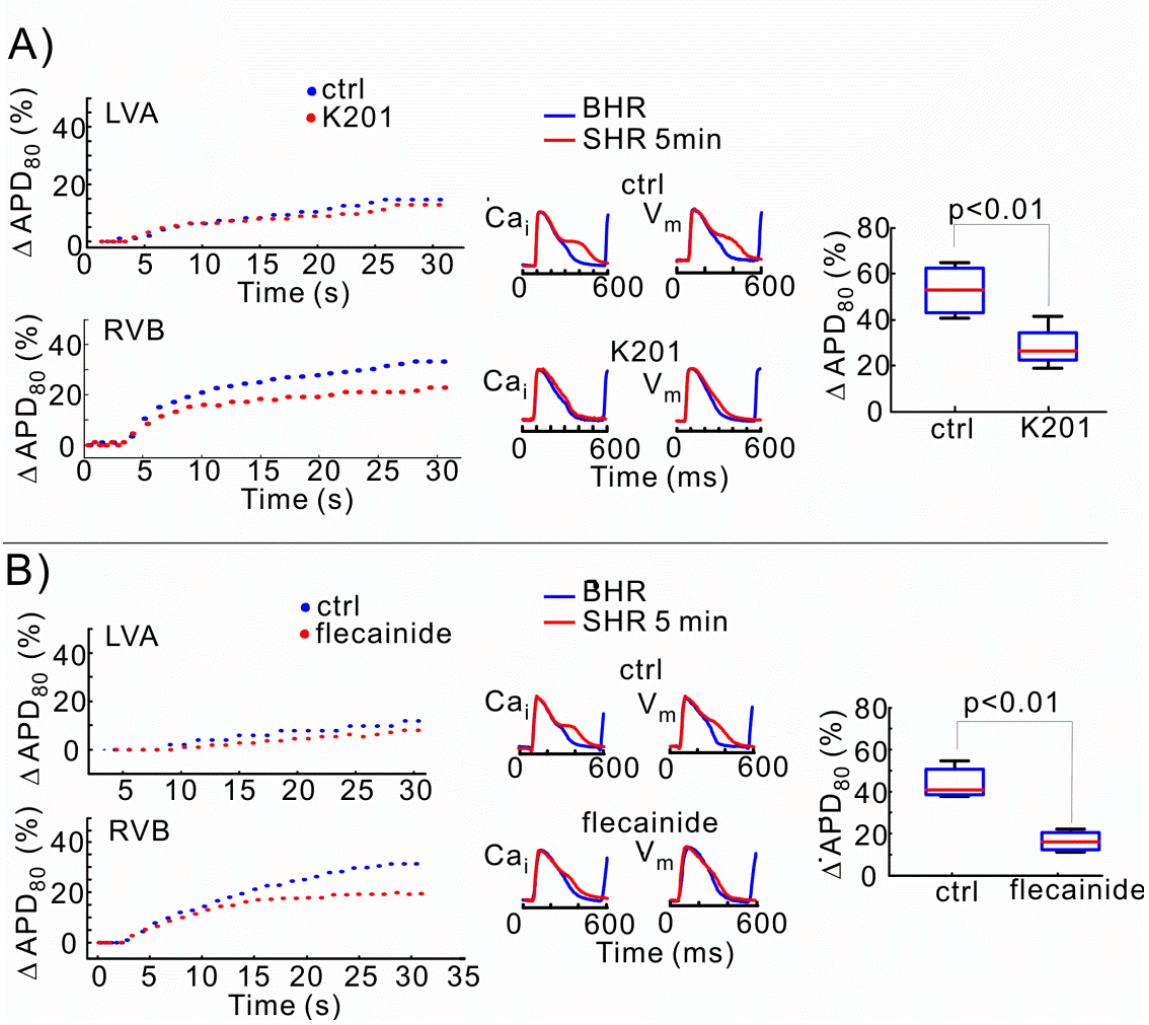

Figure 12. Suppression of SCR by K201 and flecainide A) Percent change of APD_{80} as a function of time during adaptation to SHR for sites on the LVA (top graph) and sites on the RVB (bottom graph) before and after perfusion with 1μM K201; traces of Ca_i and voltage (Vm) are superimposed for BHR and SHR without (top traces) and with K201 (bottom traces). Right graph, plots the summary data (n = 5 hearts) of the % change in ΔAPD_{80} for hearts without (control) and with K210 (1 μM). B) As for panel A but using flecainide (5 μM) instead of K201.

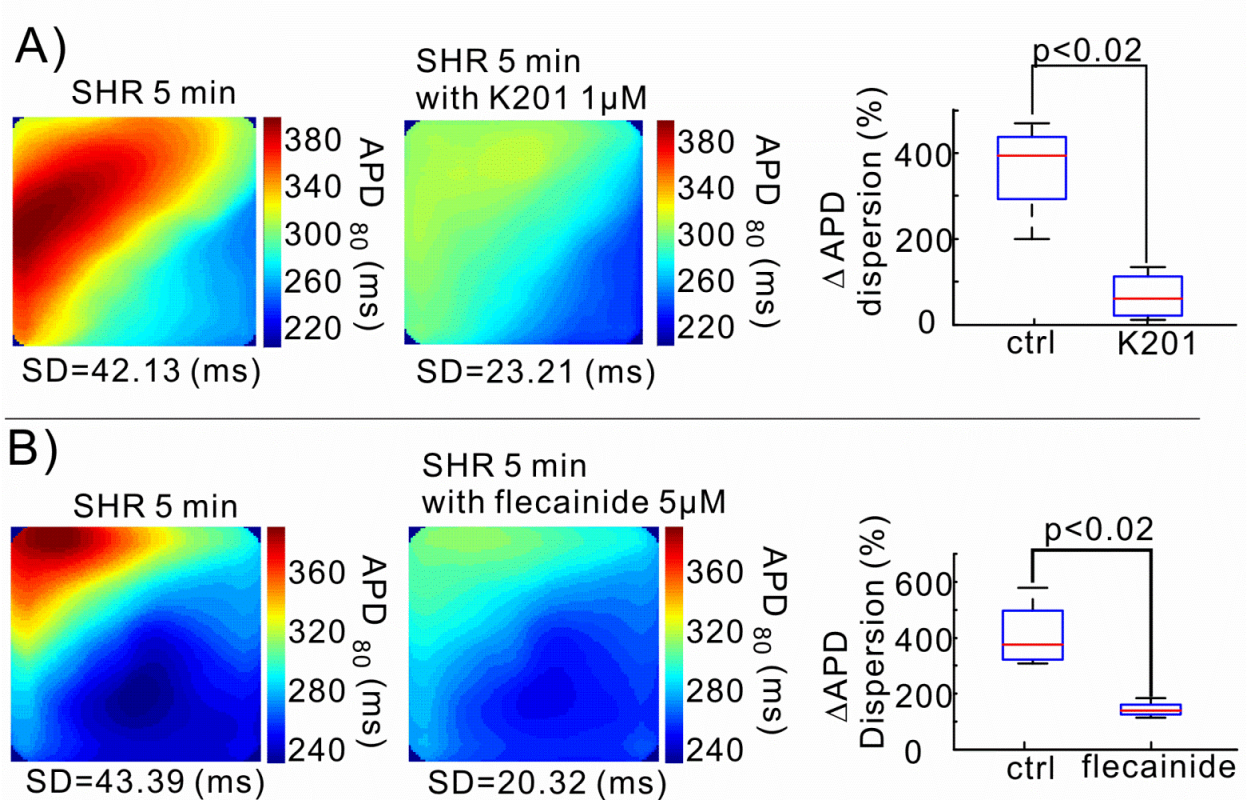

Figure 13. Suppression of SCR reduces DOR A)Maps of APD_{80} (in ms) before (left panel) and after perfusion with K201 (1μM) (middle panel) at SHR, the standard deviation is used to quantitatively measure the dispersion of APD_{80}. Which is significantly greater in controls (ctlr) before K201 than after K201 (right panel) B) Maps of APD_{80} (in ms) before (left panel) and after perfusion with flecainide (5μM) (middle panel) at SHR, the standard deviation is used to quantitatively measure the dispersion of APD_{80}. Which is significantly greater in controls (ctlr) before than after flecainide (right panel)

The higher occurrence of SCR at the RVB compared to LVA was possibly due to intrinsic differences in the expression of ionic channels and/or transporters. As shown in Figure 14, the expressions of L-type Ca^{2+} channel, NCX and voltage-gated Na^{+} channel, Nav1.5 proteins were significantly higher at RBV than LVA ($p<0.05$; n=7). In contrast, the levels of SERCA2A, RyR2 and RERG (Rabbit-ERG) were not significantly different ($p>0.05$; n= 7 hearts). In 5 out of 15 hearts, bradycardia alone was sufficient to produce premature ectopic beats (Figure 15B and D), which were readily eliminated by pacing at BHR (Figure 15C and E). Likewise inhibition of SCR with 1μM of K201 suppressed the onset of ectopic beats at steady state bradycardia (Figure 15F).

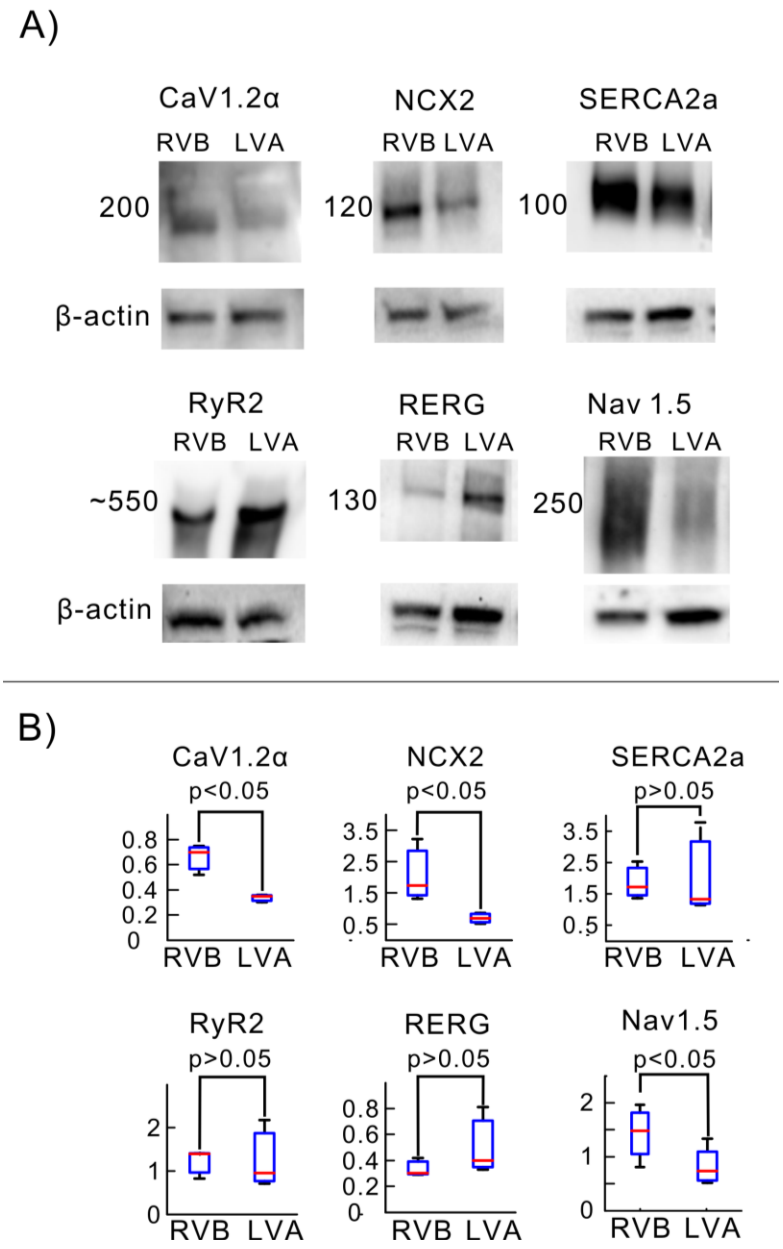

Figure 14. Heterogeneities of Ion Channels and Transporters between RVB and LVA
Ventricular tissues were dissected from the epicardium at the base of the RV (RVB) and the apex of the LV (LVA) and processed for Western blots as described in 'Methods'. Density of peptides was normalized with respect to β-actin to compare levels of channel proteins between RV and LV. A: Illustrates the relative density of RVB versus LVA densities for Cav1.2α, NCX2 (dominant isoform of NCX in heart), SERCA2A, RyR2 and RERG (rabbit ERG). B: Summary of density histograms for each of these channel protein showing a highly significant 2-fold upregulation of Cav1.2α and NCX2 at RVB compared to LVA ($p<0.05$, n=7 hearts). There were no significant differences between RVB and LVA for SERCA2A, RyR2 and RERG ($p>0.05$, n=7 hearts).

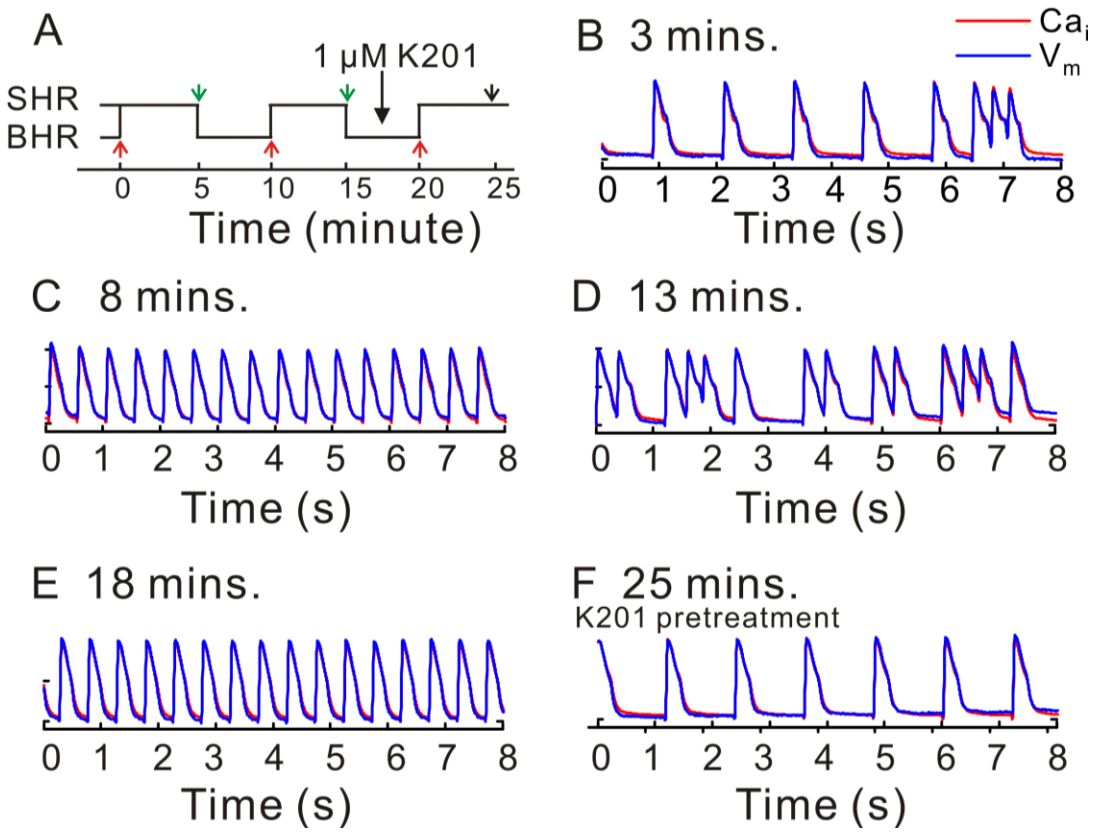

Figure 15. Bradycardia-dependent ectopic beats A) A pacing protocol consisting of 2-cycles of BHR to SHR with 5 min intervals to achieve steady state followed by treatment with K201 and another cycle to examine the effects of RyR2 stabilization. Red arrows indicate the timing of changes in HR from BHR to SHR, and green arrows indicate changes from SHR to BHR. B & D) Premature ectopic beats were reproducible during the two episodes of bradycardia at 3 min and 13 min of the experiment. C & E) The termination of ectopic beats was consistently obtained during the episode of BHR, shown here at 8 and 18 min time points. F) After pretreatment with K201 (1μM), bradycardia-dependent ectopic beats were suppressed.

4.3 DISCUSSION

Change in heart rate is one of the main mechanisms used by mammals to adjust cardiac output to changing demand. The adaptive role of tachycardia in a "fight-or-flight" situation is well accepted as are the beneficial effects of bradycardia during sleep which diminishes energy consumption by the myocardial tissue. Several parameters of cardiac contraction have to adjust to dynamic HR changes. Most prominent is the change in the duration of mechanical (and electrical) systole to maintain an acceptable balance between the time for ventricular ejection and ventricular filling. At the cellular level, this requires shortening of APD and Ca_iT in response to HR increase.

4.3.1 Effects of HR 'in and out' of the physiological range

It is not surprising that unusually rapid or slow heart rates contribute to electrical instability and abnormal Ca^{2+} handling by ventricular myocytes has been implicated as a contributor to this instability. For example, an extensive body of clinical literature suggests that microvolt T-wave alternans (mTWA) is a predictor of ventricular arrhythmias in a wide range of conditions.[139-141] mTWA is known to be a tachycardia-related phenomenon, induced by either exercise or atrial pacing for the purposes of clinical testing.[142] At the cellular level, AP alternans underlies mTWA and is preceded by Ca_iT alternans,[27] which presumably causes AP alternans by changing the NCX current or similar processes that influences $V_m \rightarrow Ca_i$ coupling as well the reverse $Ca_i \rightarrow V_m$ coupling.[143, 144]

Slow ventricular rate is likewise a critical pro-arrhythmic co-factor known to increase propensity to Torsade de Pointes (TdP), a polymorphic ventricular tachycardia associated with

delayed repolarization.[25, 145] In patients with recurrent bouts of TdP, pacing at relatively fast rates is an effective therapeutic maneuver.[146] Abnormal Ca^{2+} handling and spontaneous SR Ca^{2+} release or $I_{Ca,L}$ reactivation are widely accepted as the mechanism of early afterdepolarizations (EADs), the triggered activity which underlies TdP.[14, 81, 147] We have recently reported that in a rabbit model of long QT type-2 related TdP involving bradycardia and I_{Kr} block, oscillations of Ca_iT develop during APD prolongation and precede the appearance of EADs by minutes.[148] The data suggest that the Ca_i oscillations are caused by spontaneous SR Ca^{2+} release that activates a depolarizing NCX current that serves as a trigger to EAD generation. Although I_{Kr} block with dofetilide was required for the appearance of extra Ca_i upstrokes, we observed that bradycardia alone caused a delay or a "plateau" in the normally smooth downslope of Ca_iT. This Ca_iT delay could be eliminated by increasing pacing rate. The experiments reported in this paper were motivated by an effort to elucidate the relationship between bradycardia, Ca^{2+} handling and arrhythmogenesis.

4.3.2 Why is bradycardia arrhythmogenic?

Bradycardia has long been known to prolong APDs and enhance DOR, setting the stage for a more arrhythmogenic substrate with a greater propensity to functional reentry but the mechanisms that enhance DOR are not fully appreciated. Here, we report that bradycardia produces the expected gradual decrease of diastolic Ca_i but also show for the first time that bradycardia promotes *'secondary Ca^{2+} release'* (thus labeled SCR) which is non-uniform on the epicardium and contributes to APD adaptation. SCR differs from spontaneous Ca^{2+} release and Ca^{2+} oscillations because the latter can occur at various times along the AP plateau or even diastole which can lead to the initiation of early and delayed afterdepolarizations, respectively.

Bradycardia-dependent SCR occur as extra Ca^{2+} release 200-300 ms after the AP upstroke, prolong Ca_iTDs, are more pronounced at the RVB and are associated with a delay of ventricular repolarization. The repolarization delay is most likely caused by SCR in response to a change in HR and correlates closely with the spatial and temporal changes in APD.

To address the question whether Ca_iT changes drive AP changes or *vice versa*, we performed experiments with K201 and flecainide, agents known to specifically stabilize RyR2. Both agents eliminated SCR and attenuated AP prolongation and DOR during bradycardia. Both agents have off-target effects which must be carefully considered. K201 (1 μM) inhibited I_{Na}, $I_{Ca,L}$ and I_{Kr} in addition to its effect on RyR2 but these findings in guinea pig myocytes appear to be species dependent.[149, 150] In rabbit myocytes, K201 was fairly specific for RyR2, at 1 μM; it reduced spontaneous SR Ca^{2+} release and Ca^{2+} waves without altering $I_{Ca,L}$ and SR Ca^{2+} content. [151] Flecainide at 5 μM targets voltage-gated Na^+ channels which would reduce intracellular Na^+ and Ca^{2+} load, produce the negative inotropic effect reported for class I anti-arrhythmics[152] which would be expected to prolong not shorten APDs. Flecainide inhibits RyR2 by binding to the open state of the release channel[153] and with respect to APD prolongation; its effect on I_{Na} normally outweighs[154-156] its inhibitory effect on I_{Kr}. [152] Here, both agents reduce bradycardia-induced APD prolongation which argues that both agents primarily suppress SCR originating from the SR Ca^{2+} release by stabilizing RyR2 and not by off-targets effects that would prolong APD. Another compelling argument is that both reduce APD in bradycardia but only at the RVB and have no effect at the LVA or during normal HR. A similar argument suggests a role for SCR in bradycardia-induced DOR and the suppression of DOR by K201 and flecainide. It is likely that the dramatic changes in Ca_iT morphology observed before TdP onset in our LQT2 model represent accentuation of a "normal" Ca_iT response to profound bradycardia.

We have observed that elimination of SCR by K201 blunts a second slow phase of APD prolongation in response to bradycardia. It thus appears that the dynamics of Ca^{2+} handling by ventricular myocytes is another candidate mechanism for AP adaptation to HR change, in addition to the mechanisms mentioned in the introduction. Most likely, the Ca_i handling affects APD by means of $Ca_i \rightarrow V_m$ coupling most likely via NCX. This effect seems to function during bradycardia since the area under the curve of Ca_iT was tightly correlated to APD_{80}, as both varied as a function of time and location until steady state bradycardia was reached (Figure 11). A major difference between Ca_iT measured during baseline and slow HR is the appearance of SCR which implies that SCRs influence APDs. The weak correlation between AUCs and APDs in BHR suggests independence between the two parameters and implies that Ca_i has little effect on the plateau potential and repolarizing K^+ currents. In contrast, SCR in bradycardia augments the forward mode of I_{NCX}, enhances $Ca_i \rightarrow V_m$ coupling and prolongs APDs leading to a high correlation between AUC and APDs. The linear scatter plots suggest that the spatial heterogeneity of AUC is an important determinant of APD_{80} dispersion. QT adaptation time constants measured in human hearts were comparable in magnitude and exhibited a similar trend.[157]

The enhanced correlation of Ca_iT and APD_{80} in bradycardia suggests that SCR raises Ca_i levels during the AP plateau, which stimulates the forward mode of NCX and its depolarizing current, I_{NCX} which raises the plateau potential and prolongs APDs. In the absence of adrenergic activity, SCRs were attributed to the re-activation of RyR2 which would be caused by a higher level of SR Ca^{2+} in a spatially non-uniform manner. The mechanism underlying the regional distribution of SCRs was due to higher levels of expression of Cav1.2α, NCX1 and Nav1.5 (but not RyR2, SERCA2A or RERG) at the RVB than the LVA. In previous reports, we had shown

that in adult female rabbit hearts Cav1.2α and NCX1 were upregulated at the base compared to the apex of left ventricles. The higher levels of mRNA and proteins corresponded to higher levels of their respective current densities $I_{Ca,L}$ and I_{NCX}, measured by patch-clamping myocytes isolated from the base and apex.[138, 158] Higher Nav1.5 at the base could contribute to the higher Ca^{2+} load by increasing intracellular Na^{+} leading to a stimulation of reverse mode and inhibition of the forward mode of I_{NCX}.

The mechanism through which bradycardia promotes SCR is uncertain at this moment. In principle, increased diastolic interval during bradycardia should allow more time for Ca_i removal out of the cell by NCX. However, SR Ca^{2+} pumps can compete effectively with NCX for the removal of Ca_i during bradycardia. The amount of Ca_i transported to the lumen of the SR by SERCA during each cardiac cycle may actually be higher during bradycardia due to: a) longer AP plateau, b) longer duration of Ca^{2+} influx through L-type channels and c) the reduced NCX driving force during more positive plateau potentials. If there is a significant diffusion limitation of Ca^{2+} movement between the uptake and release SR compartments, junctional SR may be replenished after the initial phase of Ca^{2+}-induced Ca^{2+}-release from the non-junctional compartment during each heartbeat to a degree which allows spontaneous Ca^{2+} release through RyR2 in at least some myocytes. This process should be augmented by any intervention which prolongs plateau duration, such as I_{Kr} blockade.

4.4 STUDY LIMITATIONS

The study focused on the epicardium and did not investigate SCR from different regions of the ventricles. Although previous studies demonstrated higher levels of $I_{Ca,L}$ and I_{NCX} occurred at the base of the rabbit epicardium and not the apex or the endocardium,[138, 158] we cannot exclude the possibility of SCR in other regions of the heart. The study provides evidence that bradycardia increases Ca^{2+} in the lumen of the SR in a non-uniform manner resulting in a SCR at the base, and APD prolongation mediated by I_{NCX}. Pilot studies attempted to demonstrate the contribution of NCX to APD prolongation during bradycardia. Unfortunately, the available NCX inhibitors are not sufficiently selective or effective at blocking NCX. Trials with SEA0400 (0.1-2 μM) to block the forward mode of NCX were inconclusive because at these concentrations, inhibition of NCX is partial and at concentrations > 1 μM, $I_{Ca,L}$ is progressively suppressed.[159] An alternative approach of lowering external Na^+ has been successfully used to inhibit I_{NCX} in isolated myocytes but cannot be applied fast enough in perfused hearts. Likewise, caffeine can be effectively use to estimate SR Ca^{2+} load in isolated myocytes but not in perfused hearts. Nevertheless, these limitations do not detract from the validity of the study which exemplifies what can be done at the intact heart level to fully appreciate heterogeneities and complexities that cannot be exposed in studies with isolated myocytes.

4.5 CONCLUSION

In summary, the data presented here describe an acute abnormality of myocardial Ca^{2+} handling caused by bradycardia, which may increase propensity to arrhythmia. A recent elegant study has shown the role of remodeling of Ca^{2+} handling processes for arrhythmia in chronic bradycardia.[160] Additional research in this complex field appears warranted. Clinically, it is possible that RyR2 stabilizers and NCX blockers could have a role in acute treatment of bradycardia-induced TdP, at least until pacing therapy can be instituted. On the cellular level, the mechanisms of SCR clearly merit additional investigation.

5.0 Ca^{2+}OSCILLATIONS AND T-WAVE LABILITY PRECEDE VENTRICULAR ARRHYTHMIAS IN ACQUIRED LONG QT TYPE 2

The prolongation of ventricular action potential duration (APD) and QT interval often leads to life-threatening polymorphic VT that show a characteristic electrocardiographic (ECG) appearance known as TdP. Acquired LQT syndrome (LQTS) is of critical importance because of its prevalence in the clinical setting. Several factors (e.g., medications, electrolyte abnormalities, and heart failure) impair ventricular repolarization and may lead to lethal arrhythmias. LQTS is also of conceptual importance because the congenital form represents a "pure global repolarization disease,"[161] which demonstrates a direct link between repolarization delay and sudden cardiac death.[162] Although the molecular defects leading to prolonged APDs in congenital LQTS have been elucidated in remarkable detail,[163] the mechanism by which impaired repolarization causes VT on the tissue level remains less clear. [14, 164, 165]Two hypotheses that are not mutually exclusive have been proposed. First, prolonged APDs result in triggered activity in the form of early afterdepolarizations (EADs).[162] Second, spatially heterogeneous APD prolongation leads to increased dispersion of refractoriness and may form a substrate for functional reentry. [163, 164]Clinically, prolonged APD is reflected on the surface ECG as QT interval prolongation. Several forms of temporal repolarization instability, such as microvolt T-wave alternans (mTWA)[166, 167] and increased QT interval variability,[168-170] have been linked to sudden cardiac death in clinical and experimental settings. Multiple lines of

evidence suggest that Ca_i alternans leads to APD alternans and mTWA.[27, 61, 144] However, arrhythmias during impaired repolarization are classically associated with bradycardia or pauses, whereas mTWA is usually a tachycardia-induced phenomenon. mTWA is not frequently observed in LQT,[171, 172] and may not be necessary for induction of LQT-related arrhythmias. On the other hand, nonalternans T wave lability (TWL) precedes TdP in LQTS patients[173, 174] as well as in animal models of prolonged repolarization.[162, 175] TWL refers to beat-to-beat changes in T-wave morphology that do not follow an alternans (i.e., ABAB…) pattern. It seems to be a better predictor of arrhythmia than the absolute degree of repolarization delay.

The mechanisms underlying nonalternans repolarization lability are a matter of speculation, and the possible role of abnormal Ca^{2+} handling in this phenomenon remains unexplored. It is possible that TWL is caused by the same process that drives EADs, but generates depolarizations of insufficient amplitude to trigger propagating waves.

EADs have been classically attributed to the spontaneous reactivation of the L-type Ca^{2+} current, $I_{Ca,L}$, during the abnormally long APD and slow AP downstroke.[89, 176] Alternatively, SCR from the SR during phase 2 or phase 3 of the AP can further depolarize the plateau potential through the activation of the electrogenic NCX. A similar mechanism has been documented as the trigger of delayed afterdepolarizations (DADs), but its role for EADs remains controversial. In cryoablated rabbit hearts, simultaneous mapping of transmembrane voltage (V_m) and cytoplasmic free Ca^{2+} in drug-induced LQT2 showed that a rapid increase in Ca_i precedes the rise of V_m at the first sites that fire EADs on the epicardium.[11] The dynamic relationship between Ca_i and V_m during an EAD supports the notion that SR Ca^{2+} overload and spontaneous SR Ca^{2+} release activate an inward NCX current (I_{NCX}), which triggers $I_{Ca,L}$ to produce EADs. However, EADs initiated by oxidative stress (with hydrogen peroxide, H_2O_2 0.2 to 1 mM) were attributed

to Ca^{2+}/calmodulin kinase activation, which increased $I_{Ca,L}$, impaired inactivation of $I_{Ca,L}$ and of voltage-gated Na^{+} current .[177]Still, SR Ca^{2+} release should not be excluded as the trigger of EADs because H_2O_2 acts at numerous targets, including the ryanodine receptor, NCX, and the SR Ca^{2+} pump.

In this report, we investigated the role of Ca_i dynamics on TWL in a noncryoablated rabbit model of LQT2 using simultaneous measurements of Ca_iT, AP, and ECG during paced rhythms and focused on events that precede ventricular ectopy.

5.1 METHODS

5.1.1 Heart preparations

New Zealand White rabbits (female, 60 to 120 days old) were anesthetized with pentobarbital (35 mg/kg intravenously) and anticoagulated with heparin (200 U/kg intravenously). The heart was perfused with Tyrode solution (mM): 130 NaCl, 24 $NaHCO_3$, 1.0 $MgCl_2$, 4 KCl, 1.2 NaH_2PO_4, 50 dextrose, 1.25 $CaCl_2$, gassed with 95% O_2–5 % CO_2. The AV node was destroyed with electrocautery to control heart rate. To minimize motion artifact, blebbistatin (5 to 10 μM for approximately 15 minutes) was added to the perfusate. The heart was immobilized in a chamber and stained with a voltage-sensitive dye (RH 237: 200 μl of 1 mg/ml dimethyl sulfoxide [DMSO]) and loaded with a Ca^{2+} indicator (Rhod-2 AM, 200 μl of 1 mg/ml DMSO). Epicardial bipolar pseudo-ECG was continuously monitored. Epicardial pacing with a unipolar electrode on the right ventricle was performed at cycle length 1.2 seconds (50 beats/minute; bradycardia for rabbit hearts). After baseline recordings, LQT2 was modeled by

perfusing with Tyrode solution containing dofetilide (250 to 500 nM, Pfizer, New York, NY), a selective I_{Kr} blocker and lowering K^+ and Mg^{2+} concentrations by 50 %.[178] This investigation conformed to the current Guide for Care and Use of Laboratory Animals published by the National Institutes of Health.

5.1.2 Optical apparatus

The optical apparatus based on 2 photodiode arrays has been described previously. The anterior surface of the heart was illuminated with a 520 ± 30 nm excitation beam, and the fluorescence was passed through a dichroic mirror (660 nm) to focus the Rhod-2 and RH 237 fluorescence images on two 16 × 16 photodiode arrays (C4675–103, Hamamatsu Corp, Hamamatsu City, Japan). Outputs from the arrays were amplified, digitized at 1 kHz frequency, and stored in computer memory, along with surface ECG.

5.1.3 Data analysis

Automatic measurement of APD and Ca_iTD from all pixels was used to calculate APD and Ca_iTD dispersion, defined as the standard deviation of APD/CTD values. Activation time at each site was calculated from $(dFv/dt)_{max}$ of the local AP upstroke, and APD (Ca_iTD) at each site was the interval from $(dFv/dt)_{max}$ to the recovery of V_m to 10% of baseline (APD_{90} or Ca_iTD_{90}). Isochronal maps of APD and Ca_iTD were generated as previously described. [179]In addition, custom software was created in C^{++} (Microsoft Visual Studio 6.0, Micorsoft Corp., Redmond, WA) for data analysis. Signals were digitally low-pass filtered (3-pole Bessel filter, 20 Hz), and baseline fluctuations were subtracted with a smooth cubic spline. Optical signals were evaluated

from 5 pixels (2-8, 8-2, 8-8, 15-8, 8-15; the numbers stand for the x-y pixel coordinates of the 16 × 16 array). Simultaneous ECG, V_m, and Ca_i signals were displayed, and durations were measured with electronic calipers. During each scan (typically lasting 32 seconds), the interval from pacing stimulus to end of the T-wave (the QT interval equivalent) and the local duration of V_m and Ca_i signals were measured in 2 beats and averaged. The number of Ca_i peaks per AP was determined visually and were averaged over 2 beats from 5 pixels in each of the 32-second scans. Except for the dispersions of APD and Ca_iTD, the average value taken over these 5 pixels was used for subsequent analysis.

The lability of T waves, V_m, and Ca_i signals was calculated as previously reported.[16] Briefly, the ECG , V_m, or Ca_i signals from each beat (unless excluded due to poor signal quality or subsequent PVC) were superimposed using the stimulation artifact, and the root-mean-square of the beat-to-beat differences in signal amplitude measured at corresponding time points of the repolarization segment (150 ms to 900 ms after the stimulus) were calculated. The maximal root-mean-square value (corresponding to the most labile time point) was normalized to the amplitude of the signal-averaged QRS complex (defined as the maximum minus the minimum value, evaluated 10 to 900 ms after stimulation artifact, thus including the QRS complex). The reported T wave, V_m, and Ca_i lability values are taken as a natural logarithm of the normalized root-mean-square values (Table 1).

Table 1. Summary of ECG, V_m, and Ca_i parameters before and after dofetilide. The asterix indicates that Ca_i lability was calculated from 2 beats preceding EAD onset, at the site of EAD origin.

Parameter	Baseline	Dofetilide, before ectopy	*P*
APD (ms)	415 ± 118	678 ± 235	.01
Ca_iTD (ms)	474 ± 144	702 ± 227	.005
QT (ms)	481 ± 105	603 ± 172	.05
No. of Ca_i peaks	1.332 ± 0.387	2.120 ± 0.469	.002
T-wave lability	-4.061 ± 0.944	-2.894 ± 0.950	.002
AP lability	-3.436 ± 0.492	-2.994 ± 0.779	.05
Ca_i lability	-3.338 ± 0.372	-2.970 ± 0.647	.084
Ca_i lability*	-4.049 ± 0.685	-3.356 ± 1.033	.05
V_m x Ca_i correlation	0.9593 ± 0.0231	0.8967 ± 0.0644	.02

The correlation coefficient between V_m and Ca_i signal values during the repolarization segment of the last paced beat not followed by EAD were calculated from 5 pixels as described earlier and averaged. Again, these values were compared to the corresponding values prior to dofetilide perfusion. Unless described otherwise, a 2-tailed paired Student t-test (Excel, Microsoft Corp.) was used to compare signal values obtained from baseline data segments with data segments after dofetilide perfusion, but before the onset of ventricular ectopy. P values of $<.05$ were considered statistically significant.

5.2 RESULTS

TdP was induced by dofetilide perfusion in all hearts (n = 8) in <10 minutes and was preceded by short-coupled premature ventricular beats. Premature ventricular beats on the ECG corresponded to EADs on optical V_m tracings. In all cases, the onset of EADs was preceded by prolongation of APD (415 ± 118 vs. 678 ± 235 ms; $p < .01$) and of Ca_iTD (474 ± 144 vs. 702 ± 227 ms; $p < .005$) as compared with controls. The QT interval determined from epicardial ECG also prolonged markedly (481 ± 105 vs. 603 ± 172 ms; $p < .02$). Occasionally, ectopic ventricular beats with late coupling and V_m tracing suggestive of DADs were observed.

5.2.1 Beat-to-beat lability of repolarization, AP, and CaT

TWL increased in all experiments prior to the onset of arrhythmia (–4.061 ± 0.944 vs. –2.894 ± 0.950; n = 8, $p < .002$). TWL corresponded to discernible changes of T-wave morphology during regular rhythms preceding ventricular arrhythmias (Figure 16). In contrast, macrovolt T-wave alternans was never observed before the onset of ventricular ectopy (n = 8). Similarly, the beat-to-beat lability of optical V_m signals increased prior to VT onset (–3.436 ± 0.492 vs. –2.994 ± 0.779; $p < .05$). There was a trend toward an increase in Ca_iT lability prior to VT onset that did not reach statistical significance (–3.338 ± 0.372 vs. –2.970 ± 0.647; $p = .084$). However, at sites of EAD origin, Ca_iT lability was significantly higher compared with baseline

for the 2 consecutive beats preceding the onset of EADs (–4.049 ± 0.685 vs. –3.356 ± 1.033; $p < .05$). Table 1 summarizes these ECG, V_m, and Ca_i parameters before and after the induction of LQT2 but before the onset of ectopic beats.

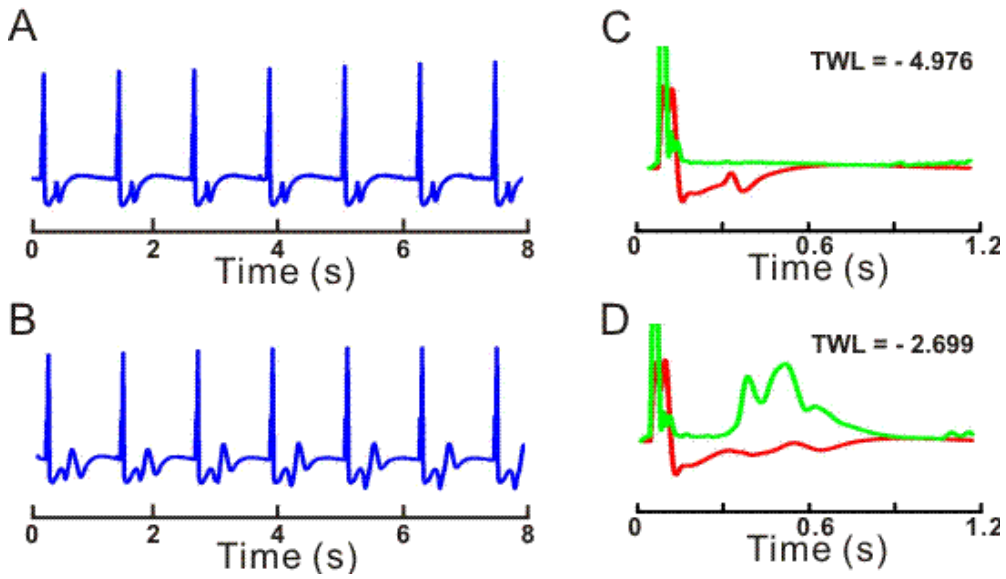

Figure 16. **Prolonged repolarization induces TWL. Examples of ECG recordings during pacing at 50 beats/minute** A) Control. B) LQT2. T-wave morphology is constant in A, but changes on a beat-to-beat basis in B. ECG lability (green traces) is plotted before (C) and during LQT2 (D) and is superimposed on signal-averaged ECG (red traces). The Y-axis for lability is expanded 10-fold with respect to signal-averaged ECG. TWL is calculated as the logarithm of maximum ECG lability measured during the repolarization phase and normalized with respect to the amplitude of signal-averaged QRS. TWL is essentially absent in C and highly pronounced in D. Maximum lability occurs at approximately 470 ms after the pacing stimulus in this case.

One might expect that if Ca_i lability causes V_m lability, then maximum Ca_i lability may occur slightly earlier within a cardiac cycle. However, this did not appear to be the case: the average timing of maximum V_m and Ca_i lability before onset of ectopy was 435 ± 141 and 580 ± 95 ms after pacing spike, respectively ($p=0.044$ by paired t-test). The explanation seems to be that maximum Ca_i lability often occurs towards the end of the AP (late phase 3), when the membrane resistance is lower than during phase 2. Therefore, the effect of Ca_i and I_{NCX} variability on V_m variability may be less than during phase 2. One consistent observation is that

the maximum Ca_i lability occurs later than the second Ca_i peak on signal-averaged Ca_iT (580 ± 95 vs. 430 ± 79 ms, $p < .002$).

5.2.2 Ca_iT oscillations

Aside from beat-to-beat lability, Ca_iT showed other forms of instability. Normal Ca_iTs were monophasic (a single Ca_i peak followed by a recovery to baseline) with Ca_i increasing approximately 10 ms after the rise of V_m. Occasionally, a small secondary rise in Ca_i appeared during phase 3 of the AP at a few sites. Perfusion with dofetilide increased the complexity of Ca_iT kinetics in all hearts, with the appearance of multiple Ca_i peaks (Figures 17 and 18). The average number of Ca_iT peaks occurring during a single AP increased significantly before the onset of EADs (1.332 ± 0.387 vs. 2.120 ± 0.469; $P < .002$). Interestingly, up to 4 distinct Ca_i peaks could be seen in some experiments, whereas the corresponding local AP remained monophasic, with a smooth downstroke during phase 2 and 3 (Figure 19). Ca_i oscillations (Ca_iO) preceded the onset of EADs in all experiments.

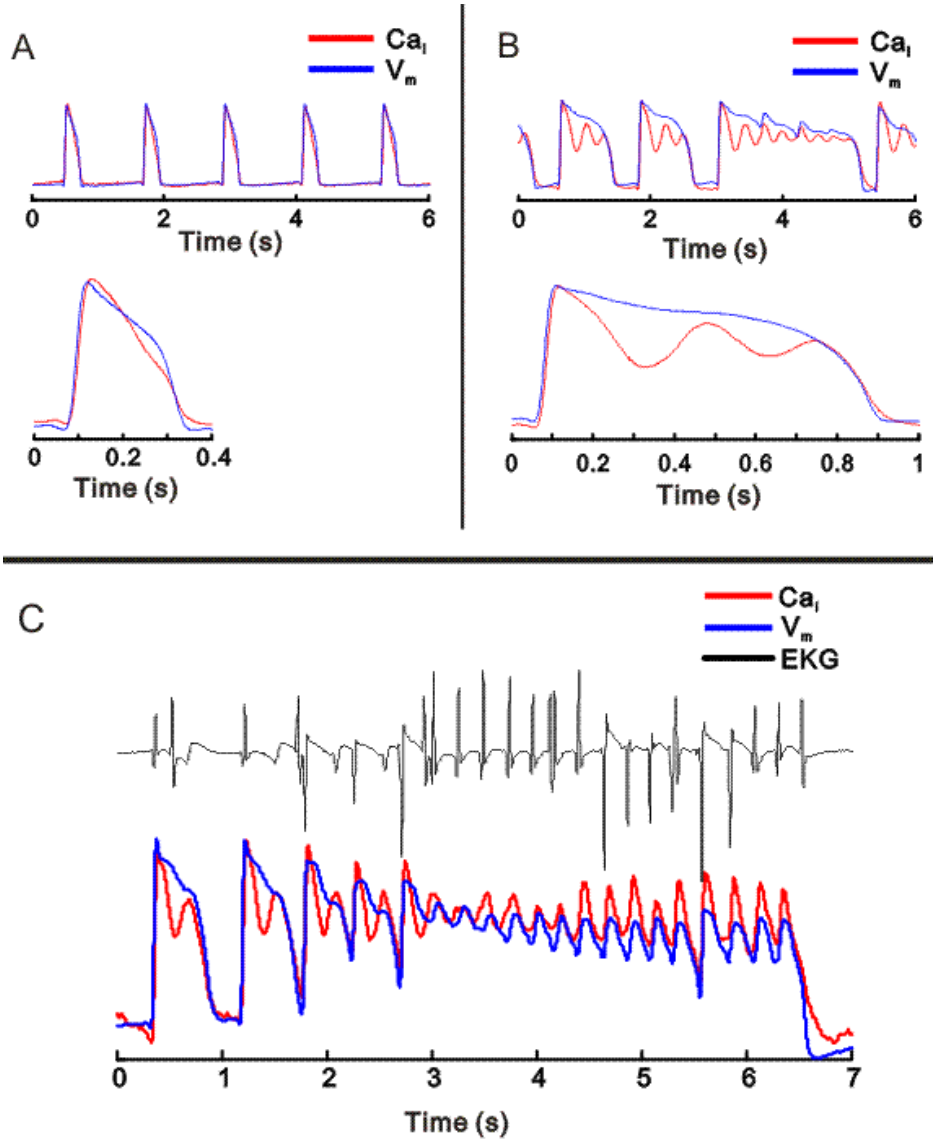

Figure 17. Ca_iO precede EADs. Simultaneous recordings of V_m (blue) and Ca_i (red) before (A) and during LQT2 (B, C) A) V_m and Ca_i are shown at slow (top) and fast (bottom) sweep speeds, and both show monophasic time courses. B) V_m and Ca_i are shown at slow (top) and fast (bottom) sweep speeds. In the first 2 APs, the LQT2 condition prolonged APD and elicited Cai oscillations during the paced beats with no V_m instabilities. The third AP showed multiple Ca_i peaks that were occasionally coincident with EADs. C) An example of TdP onset after the fifth paced beat. The ECG (top trace) and the optical traces of V_m and Ca_i (bottom traces) were recorded simultaneously. The Ca_iO precedes the first EADs at this site.

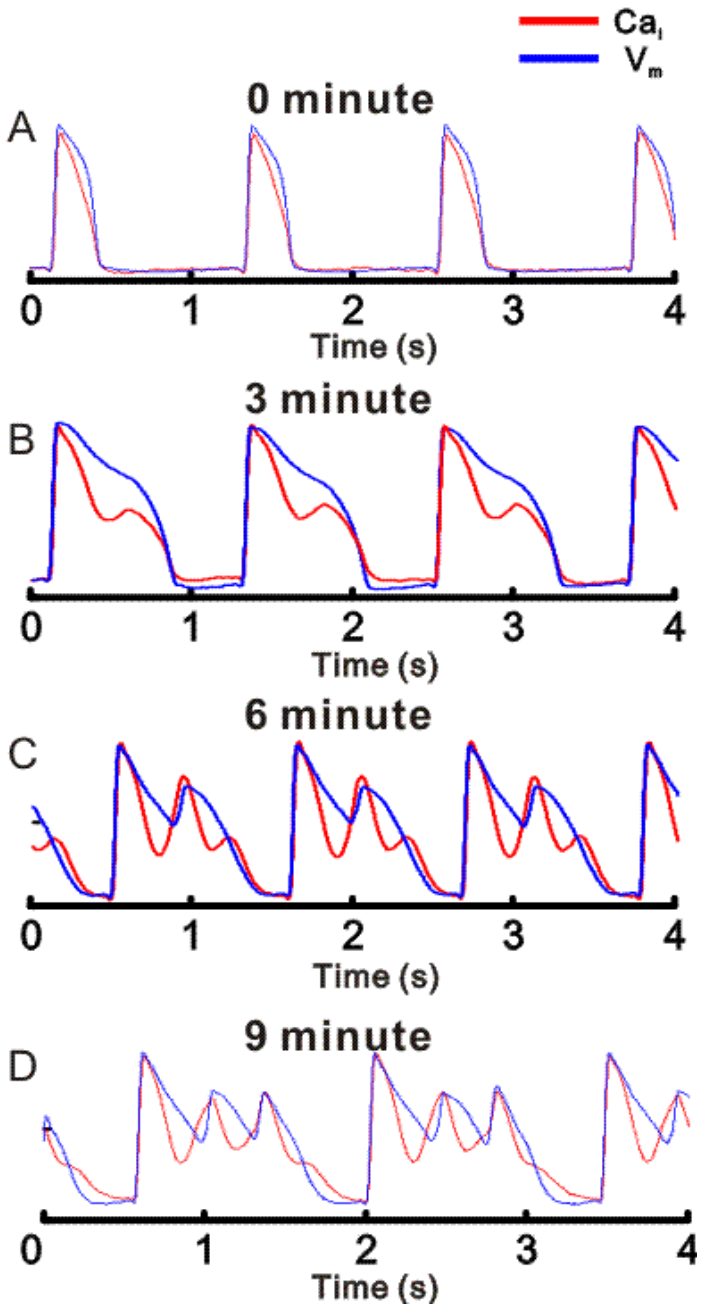

Figure 18. Time-dependent oscillations of Ca_i and the evolution of EADs V_m (blue) and Ca_i (red) measurements (left) during pacing (A, B) and ventricular escape rhythms (C, D). A) In control, V_m and Ca_i are monophasic and similar in shape. B) LQT2 for 3 minutes, a second increase of Ca_i appears during the AP plateau while V_m remains free of EADs. C) LQT2 for 6 minutes promotes more complex Ca_iO that are associated with a single EAD. In this pixel, the Ca_i upstroke precedes the V_m upstroke. D) LQT2 for 9 minutes, 2 consecutive EADs follow each AP upstroke. Prominent Ca_i upstrokes precede EAD upstrokes.

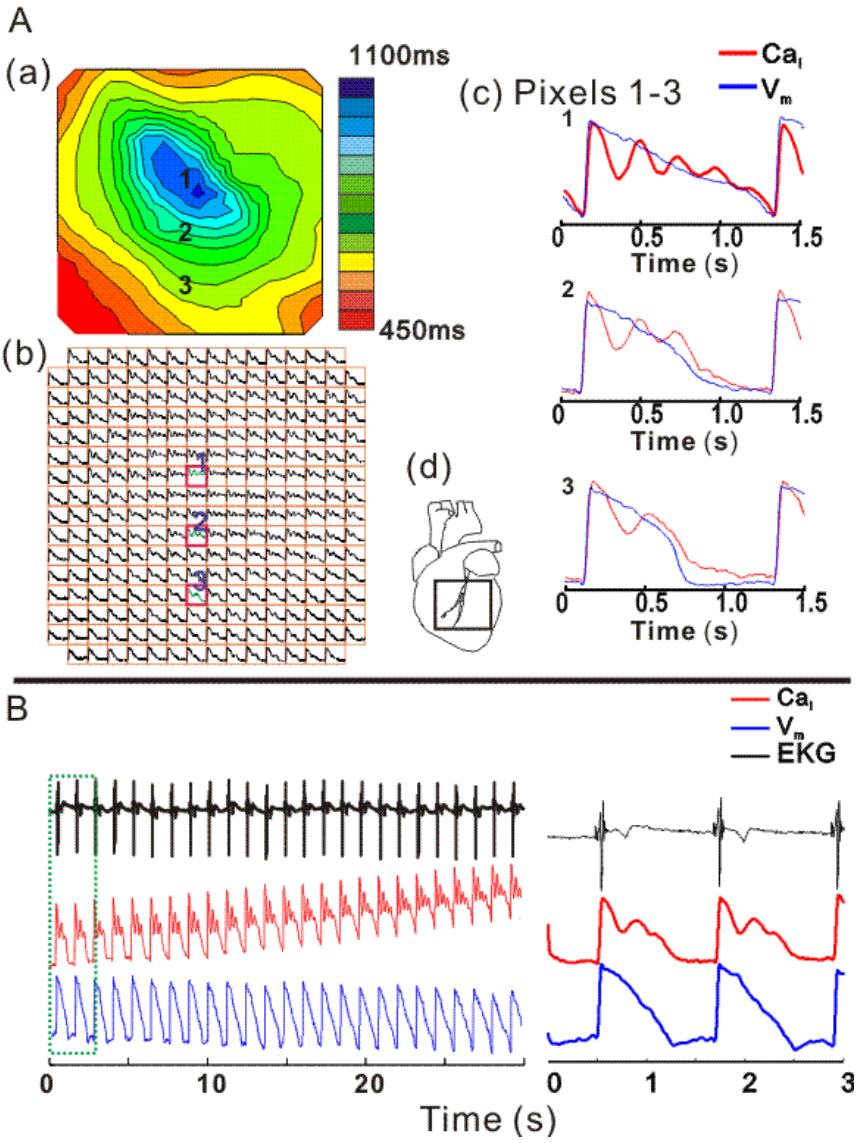

Figure 19. **Spatial and temporal heterogeneity of Ca_iT and APs during LQT2** A) Isochronal map of APD_{90} (A (a), top left) from the anterior surface in LQT2; the field-of-view of the array is shown (inset d), and isochronal lines are 50 ms apart (see color scale). Ca_i signals recorded at each site are depicted in the symbolic map of the photodiode array (b). Simultaneous V_m and Ca_i from a single beat are superimposed for pixels labeled 1, 2, 3 on the maps and are shown at fast sweep speed (c). Marked spatial heterogeneities of Ca_iO appear, with the highest number of Ca_iO found at sites with the longest APDs and decrease to sites with shorter APDs. B) ECG, V_m, and Ca_i recordings from pixel (1) for 30 seconds show a gradual APD prolongation associated with an increasing number of Ca_iO and a rise of diastolic Ca_i. The right panel shows a shorter segment of the signals (green box on left) with better time resolution.

Figure 19A illustrates a marked spatial heterogeneity of V_m and Ca_i signals during dofetilide perfusion, but before the onset of EADs. An isochronal map of APD_{90} shows a marked APD prolongation (pixel 1) that decreased anisotropically. Before the onset of EADs, the correlation between V_m and Ca_i signals during repolarization decreased in all experiments (0.9593 ± 0.0231 vs. 0.8967 ± 0.0644; $p < .02$, 2-tailed sign test), representing an increasing dissociation between the oscillatory Ca_i signal and the monophasic shape and time course of APs. In paced beats immediately preceding the appearance of EADs, the spatial dispersion of Ca_iTD_{90} exceeded the dispersion of APD_{90} (65 ± 29 vs. 52 ± 35 ms; $p < .02$).

During a normal AP, Ca_iTs are tightly controlled by V_m and AP upstrokes preceded the rise of Ca_i with a delay of 10 ± 2 ms. With the appearance of premature ventricular beats, EAD upstrokes often coincided with a secondary Ca_iT peak. In 3 of 8 experiments, the first EAD occurred outside of the field of view of the optical maps. In 2 of 5 experiments where the first EAD fell in the field of view of the array, the second rise of Ca_i preceded the second V_m upstroke by 3 to 5 ms, and this temporal relationship reversed gradually as the EAD propagated away from its origin (Figure 20). In 3 of 8 experiments, EAD upstrokes preceded Ca_i upstrokes but with shorter V_m–Ca_i delays of 5 to 7 ms compared with delays during normal APs. Ca_iO preceding EAD upstrokes (Figures 17B, 18C, and 18D) were routinely observed during complex ectopy, such as bigeminy, trigeminy and VT runs.

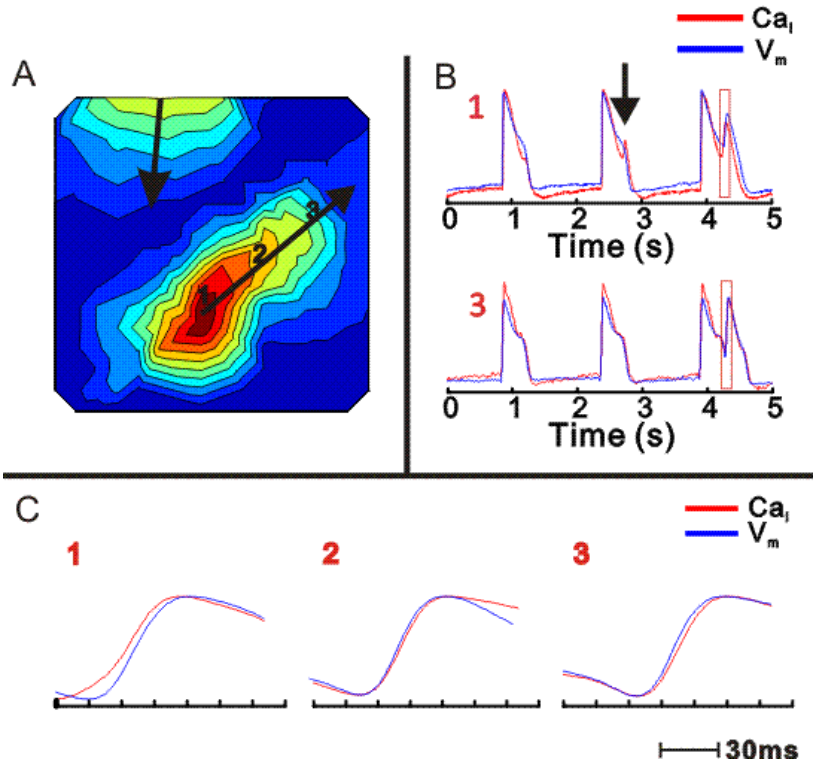

Figure 20. **Propagation of V_m and Ca_i upstrokes during an EAD** A) Isochronal activation map of an ectopic beat (EAD) occurring during an escape rhythm. The origin of the EAD is at site 1. Isochronal lines are 3 ms apart. Note that another independent wavefront emanates from the base of the heart. B) V_m and Ca_i tracings from sites: 1 and 3 in (A). The first AP and Ca_iT are monophasic at site 1; during the second AP, there is a distinct second Ca_i peak without an EAD (arrow). On the third beat, an EAD appears with sufficient magnitude to propagate, as in A. C) The temporal relationship between Ca_i and V_m signals are shown at higher resolution at sites 1 to 3 as labeled in A. At the site of EAD origin (1), Ca_i upstroke precedes V_m upstroke (8 ms); at site 2, V_m is coincident with Ca_i; and at site 3, remote from the EAD origin, V_m precedes Ca_i (3 ms).

As illustrated in Figure 21, a bigeminy pattern on ECG corresponded to a Ca_iO with an EAD during each beat (Figure 21A). Similarly, trigeminy corresponded to beat-to-beat alternations of a large Ca_iO with an EAD followed by a smaller Ca_i oscillation without an EAD on the next beat (Figure 21B). Non sustained runs of polymorphic VT corresponded to long CaT with multiple Ca_iO (Figure 21C).

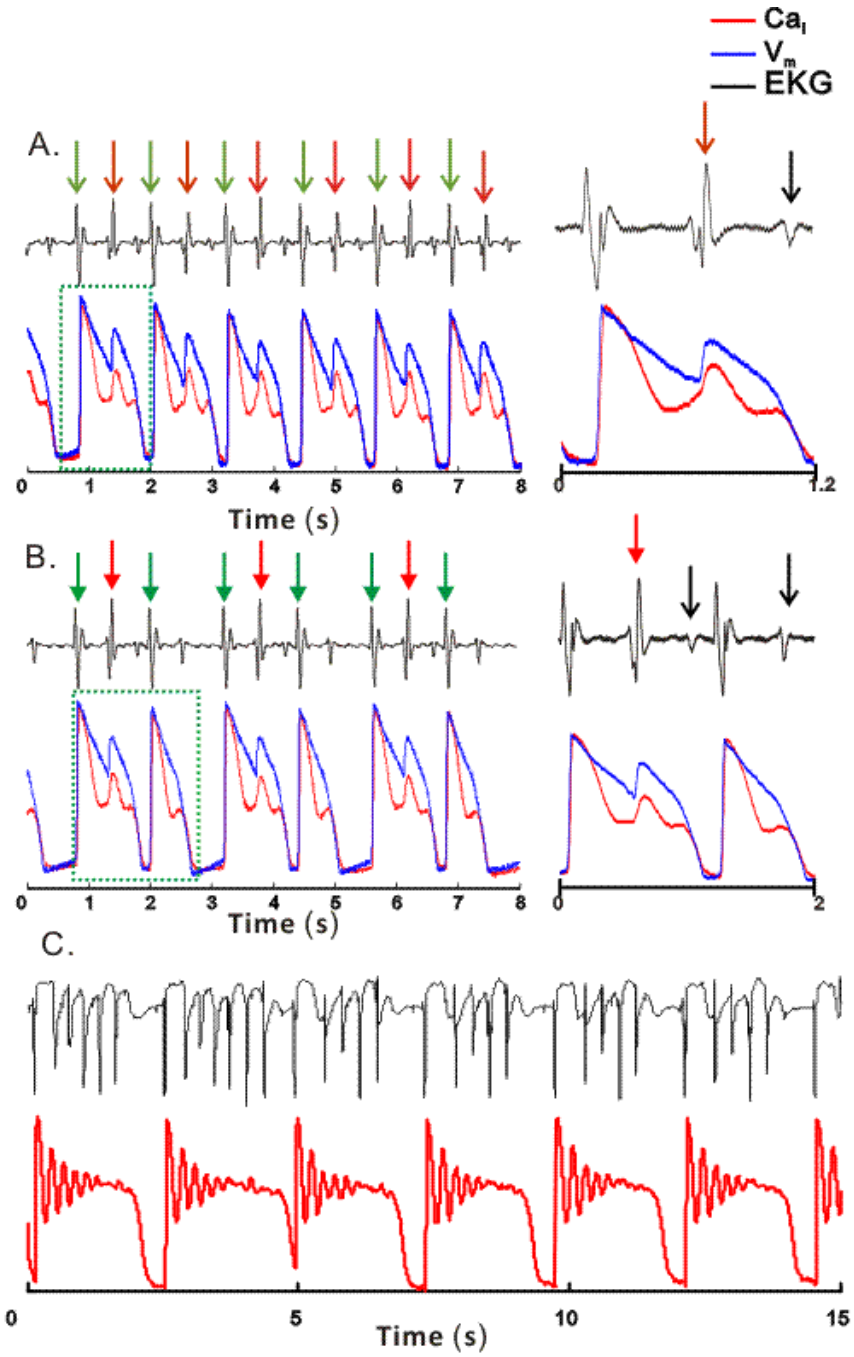

Figure 21. **ECG recordings of complex ectopy: bigeminy and trigeminy correspond to Ca_iO** A) ECG recording of paced rhythm with bigeminy. Each paced beat (green arrows) is followed by a ventricular ectopic beat (red arrow). T-waves on ECG signals are indicated by black arrows. Note that neither V_m nor Ca_i recover to baseline before the ectopic beat; in this sense, the paced/ectopic beat can be understood as a single complex AP. B) An episode of trigeminy from the same experiment. Two paced beats are followed by an ectopic beat. The optical tracings indicate that alternans between a short monophasic paced AP and a bigeminal AP underlies the trigeminal pattern. C) Simultaneous ECG and Ca_i tracing with brief runs of polymorphic VT. Pacing rate was 50 beats/min with 2:1 capture. Each run of polymorphic VT corresponds to a single Ca_iT with multiple secondary Ca_iO.

5.2.3 TdP is suppressed by interventions that abolish Ca_iO

To corroborate the role of spontaneous SR Ca^{2+} release in eliciting EADs and TdP, several interventions were tested to reduce SR Ca^{2+} load in attempts to suppress Ca_iO and the generation of TdP. As shown in Figure 22, nifedipine (5 μM) (Figure 22A) and low external Ca^{2+} (100 μM) (Figure 22B) suppressed Ca_iOs, EADs, and TdP (n = 4 for each intervention), although APD remained prolonged. Restoration of original Ca^{2+} resulted in reappearance of Ca_iO and TdP. In other experiments (n = 3), the hearts were perfused with Tyrode solution containing ryanodine and thapsigargin (10 μM and 200 nM, respectively) to deplete SR before perfusion with dofetilide. In the presence of ryanodine and thapsigargin, dofetilide prolonged APD, but Ca_iO and TdP failed to occur.

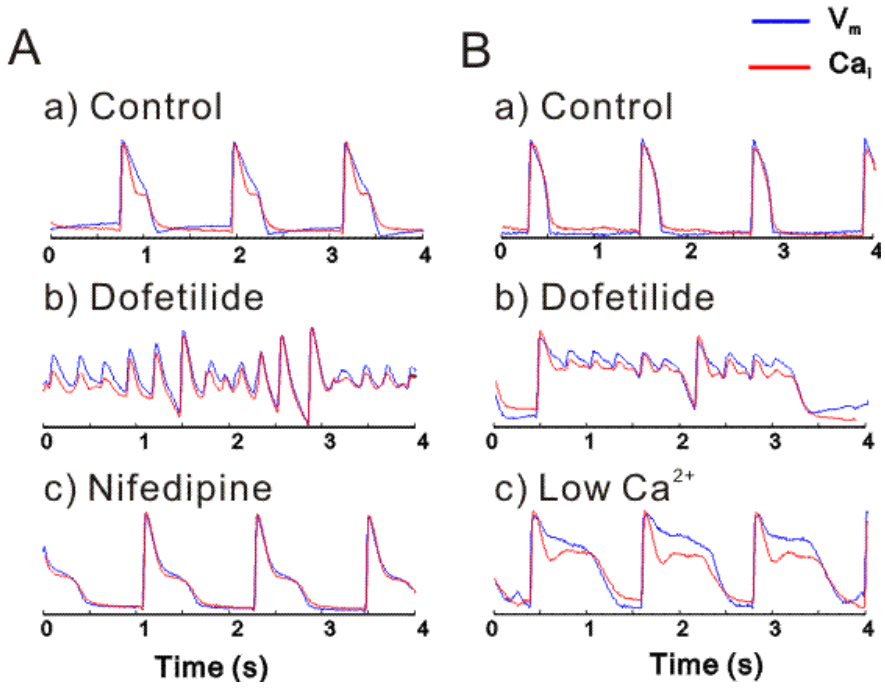

Figure 22. Effect of reduced SR Ca^{2+} load on Ca_iO and TdP TdP was induced with LQT2 solution then nifedipine (5 μM) was added (A) or external Ca^{2+} was lowered (100 μM) (B) in the perfusate. Both interventions attenuated Ca_iO and terminated TdP despite continuous dofetilide perfusion and marked APD prolongation.

5.3 DISCUSSION

The main finding of this report is that under LQT2 conditions, Ca_iT oscillations occur in ventricular myocardium during regular rhythm. They are not caused by oscillations of membrane potential, which they precede by minutes. When EADs do appear, they usually follow Ca_iT upstroke at the site of EAD origin.

Although Ca_i oscillations under LQT conditions have been reported before, they were always described in the presence of EADs and often understood as a consequence of $I_{Ca,L}$ reactivation with consequent calcium-induced Ca^{2+}release. Because the timing of Ca_i and V_m upstrokes is often similar and their relationship may be spatially heterogeneous, this explanation was difficult to disprove. Here, we show that Ca_iT oscillations consistently occur minutes before the appearance of EADs, at the time when AP downstroke remains smooth and monophasic. Interventions that abolish Ca_iT oscillations also abolish TdP. These findings indicate that the secondary Ca_iT peaks are caused by instabilities of intracellular Ca^{2+} handling caused by AP prolongation. These instabilities in turn promote the appearance of EADs, and eventually TdP.

5.3.1 CaT oscillations drive EADs

The driving role of Ca_i oscillations in EAD generation is supported by the analysis of the Ca_iT and AP relationship at the site of EAD focus. At the origins of EADs, the rise of Ca_i preceded the EAD depolarization (n = 2 of 5). At sites remote from EAD foci, V_m preceded Ca_i, which is expected if voltage is responsible for EAD propagation. At sites of earliest EAD upstroke, Ca_i followed the EAD depolarization in 3 of 5 hearts; even then, the short V_m–Ca_i delays (<7 ms) suggested that normal voltage-driven SR Ca^{2+} release did not occur. In such cases,

the EAD most likely emanated from deeper in the myocardial wall and propagated to the epicardial surface. In cryoablated rabbit hearts in which a thin layer of epicardium survives, Ca_i elevation always preceded the EAD depolarization.[11] The cryoablation studies support the interpretation that when EAD depolarizations precede Ca_i elevation, the site of earliest EAD upstrokes correspond to epicardial breakthrough of a transmural depolarization wavefront. The higher spatial dispersion of Ca_iTD compared with APD dispersion just before the onset of EADs also supports the notion that Ca_iTs are not under the control of APs.

5.3.2 Mechanisms linking Ca_iT oscillations to EADs

The most likely mechanism linking secondary Ca_iT upstrokes to membrane depolarization is the NCX current, I_{NCX}, consistent with reports that NCX blockers suppress EADs and TdP.[180] We speculate that Ca_iT oscillations are driven by spontaneous Ca^{2+} release from an overloaded SR. In LQT2, the long AP plateau increases Ca^{2+} influx via $I_{Ca,L}$ because the voltage-dependent component of inactivation is incomplete and long APDs also reduce the driving force for Ca^{2+} efflux via NCX. These changes indirectly increase SR Ca^{2+} uptake due to the increase of sarcolemmal Ca^{2+} entry and the suppression of Ca^{2+} efflux mechanisms. Consistent with this view, nifedipine, low external Ca^{2+}, and ryanodine/thapsigargin eliminated Ca_iT oscillations, EADs, and TdP. Thus, our data indicate that spontaneous Ca^{2+} release from an overloaded SR network is the primary cause of ventricular arrhythmias in LQT2.

In dofetilide-induced LQT2, Ca_iO always appeared before EADs and TdP. Although all Ca_iO are expected to elicit INCX oscillations, not all Ca_iO produced EADs because the ability of I_{NCX} (due to a Ca_iO) to sufficiently depolarize the cell membrane and produce an EAD depends on several factors: (1) the magnitude of the Ca_i elevation, which determines the magnitude of

I_{NCX}; [140] V_m during the plateau phase, a determinant of the magnitude of repolarizing K^+ currents: I_{K1}, residual I_{Kr}, and I_{Ks}; (3) the time point along phase 2 of the AP when I_{NCX} rises, a determinant of the number of L-type Ca^{2+} channels that have recovered from inactivation and can be reactivated; and (4) the activation of the opposing repolarizing K^+ currents (I_{Kr} and I_{Ks}) are also time dependent. The data provide compelling evidence that I_{NCX} is the most reasonable mechanism for the generation of EADs through L-type Ca^{2+} channels reactivation, but it cannot entirely exclude a contribution from spontaneous $I_{Ca,L}$ reactivation.

Nonalternans TWL is caused by the lability of ventricular APs, which is preceded by Ca_iO and Ca_iT lability. Ca_iO are not fully synchronized (Figure 17), and could contribute to AP lability through reverse Ca_i–V_m coupling. In contrast to TWL, alternans of Ca_iT, AP, or TWA was never observed before the onset of ectopy.

5.3.3 Spontaneous SR Ca^{2+} release and arrhythmias

Abnormal Ca^{2+} handling has been implicated in arrhythmogenesis in numerous pathologies,[130] including digoxin toxicity[181] and catecholaminergic polymorphic ventricular tachycardia.[182, 183] VT is triggered by DADs in both of these conditions. DADs are caused by spontaneous SR Ca^{2+} release during diastole and membrane depolarization by INCX.[9] However, the role of spontaneous systolic Ca^{2+} release from SR in the generation of EADs continues to be debated.[184] CaO in the form of sparks and waves have been reported in a wide range of cardiac preparations, ranging from isolated myocytes to intact perfused hearts, and have been implicated as an arrhythmogenic mechanism.[185] In a guinea pig model of ischemia/reperfusion, spontaneous Ca_iO appeared to drive ventricular ectopy.[186] Reperfusion arrhythmias thus represent another clinically relevant situation involving spontaneous Ca^{2+}

release from overloaded SR. The link between delayed repolarization, SR overload, Ca_iT oscillations, and TdP may help the development of diagnostic and treatment strategies in patients with LQTS.

5.4 LIMITATION

Dofetilide was used at a relatively high dose to elicit drug-induced LQT2 because lower doses were less reliable at eliciting TdP. Our LQT2 model shows an extreme degree of impaired repolarization compared to most clinical situations and its clinical relevance must be validated. However, it has the advantage of reproducible TdP induction during an acute study.

5.5 CONCLUSION

In LQT2, APD prolongation promotes Ca_iT oscillations, which precede the appearance of EADs. The data provide a mechanistic explanation for TWL and enhance our understanding of arrhythmogenesis in LQTS. This may lead to improved clinical management of patients with impaired repolarization.

6.0 REGIONAL HETEROGENEITY OF Ca^{2+} KINETICS PROMOTES MEMBRANE POTENTIAL GRADIENTS AND TRIGGERED ACTIVITY IN DRUG-INDUCED LONG QT TYPE 2

Torsade de pointes (TdP) is a lethal polymorphic ventricular tachycardia associated with delayed repolarization as a consequence of congenital or drug-induced/acquired impairment of the rapid rectifying outward potassium current (I_{Kr}), known as long QT type2 (LQT2).[84-87, 187] Enhanced spatial heterogeneity of repolarization (i.e. dispersion of repolarization (DOR)) in LQT2 provides a substrate leading to unidirectional conduction blocks, initiating and sustaining reentrant activity and has long been implicated as a driving force for arrhythmogenesis. [93, 96, 163] The prolongation of M cell action potentials (APs) under conditions with reduced I_{Kr} has been proposed as the underlying mechanism responsible for enhanced transmural DOR in LQT2.[7] Alternatively, it has been reported that functional variations in levels of I_{Kr} that can be inhibited by class III anti-arrhythmic agents play a key role in the genesis of apex/base difference in AP repolarization in cryoablated LQT2 models.[11]

More recently, interruption in Ca^{2+} homeostasis (i.e. imbalance between Ca^{2+} entry and Ca^{2+} efflux) caused by a prolonged AP has been shown to promote Ca^{2+}overload in the sarcoplasmic reticulum (SR). [188-190] The Ca^{2+} overloaded SR, in turn, leads to abnormalities in Ca^{2+} handling such as spontaneous release of Ca^{2+} from the SR. [14, 191, 192] If the spontaneous release of Ca^{2+} from the SR occurs during the plateau phase of an AP, the non

voltage gated elevation in cytosolic free Ca^{2+} levels leads to voltage instability via Ca^{2+} dependent sarcolemmal transporters. [11, 16, 81, 105]

We recently reported that the LQT2-induced abnormality in Ca^{2+} handling was pronounced, spatially inhomogeneous, and tightly correlated with the distribution of AP duration even before the onset of TdP.[16] Although experimental and clinical studies have demonstrated that Ca^{2+} abnormality can be promoted and could be spatially discordant in LQT2 animal models or in LQT2 patients, [12, 83] the direct interplay between spatial heterogeneity of intracellular Ca^{2+} handling and voltage dispersion in LQT2 is not fully appreciated.

We optically measured intracellular Ca^{2+} dynamics and membrane potential (V_m) in a drug-induced LQT2 rabbit model to demonstrate the impact of enhanced spatial heterogeneity of cytosolic Ca^{2+} handling in the augmentation of voltage dispersion, which initiates and sustains LQT2 related arrhythmias.

6.1 METHODS

6.1.1 Heart preparation

Female New Zealand White rabbits (60 to 120 days old) were anesthetized with pentobarbital (35 mg/kg intravenously) and anticoagulated with heparin (200 U/kg intravenously). The heart was excised and perfused on a Langendorff apparatus with Tyrode solution (mM/L): 130 NaCl, 24 $NaHCO_3$, 1.0 $MgCl_2$, 4 KCl, 1.2 NaH_2PO_4, 50 dextrose, 1.25 $CaCl_2$, gassed with 95% O_2–5 % CO_2. The solution temperature was adjusted to 37ºC with a heater. The atrioventricular node was ablated with electrocautery to control heart rate.

Blebbistatin (Sigma-Aldrich, St.Louis, MO; 5 to 10 μM/L for approximately 15 minutes) was added to the perfusate to minimize motion artifact. The heart was immobilized in a chamber and stained with a voltage-sensitive dye (PGH1: 200 μL of 1 mg/mL dimethyl sulfoxide [DMSO] solution) and loaded with a Ca^{2+} indicator (Rhod-2 AM, AnaSpec, Fremont, CA; 200 μL of 1 mg/mL DMSO solution). Epicardial bipolar pseudo-ECG was continuously monitored. Epicardial pacing with a unipolar electrode from the lateral left ventricle was performed at cycle length 1.2 s (50 beats/minute; profound bradycardia for a rabbit heart). After baseline recordings, LQT2 was induced by perfusing the heart with Tyrode's solution containing Dofetilide (500 nM/L, Pfizer, New York, NY) and lowering K^+ and Mg^{2+} concentrations by 50%.[178] This investigation conformed to the current *Guide for Care and Use of Laboratory Animals* published by the National Institutes of Health.

6.1.2 Optical apparatus

The optical apparatus, which is based on two high spatiotemporal resolution CMOS cameras (Ultima Scimedia, Costa Mesa, CA; 100 x 100 pixels, 500-1,000 frames per second), has been used for simultaneous measurement of intracellular Ca^{2+} transients and membrane potential changes. The anterior surface of the heart with a 1.4 cm x 1.4 cm field of view (140 μm x 140 μm pixel resolutions) was illuminated with a 520 ± 30 nm excitation beam generated by a tungsten lamp with an interference filter. The fluorescence beam was divided by a dichroic mirror (660 nm) to focus the Rhod-2 and PGH1 fluorescence signals on two CMOS cameras. The digitized optical signals were saved on computer HD for off-line analysis.

6.1.3 Data analysis

Optical traces of membrane potential (V_m) and intracellular Ca^{2+} transient (Ca_iT) at each pixel were normalized and digitally low-pass filtered (60 Hz cutoff, Butterworth). Activation time at each site was calculated from $(dFv/dt)_{max}$ of the local V_m or Ca_iT upstroke, and action potential (AP) duration (APD) and Ca_iT duration (Ca_iTD) at each pixel was the interval from $(dFv/dt)_{max}$ to the recovery of V_m [2] to 20% of baseline (APD_{80} or $CaiTD_{80}$). APD_{80}/Ca_iTD_{80} and APD/Ca_iTD dispersion was always calculated during paced rhythm, in the absence of triggered activity. Automatic measurement of APD_{80} and $CaTD_{80}$ from all pixels (100 x 100 pixels) was used to calculate APD_{80} and Ca_iTD_{80} dispersion, defined as the standard deviation of APD_{80} (or Ca_iTD_{80}) values. Amplitudes of secondary Ca^{2+} elevation at each pixel were approximated by calculating 'area under curve' [137] of normalized Ca_iT over time-interval from beginning of first secondary Ca^{2+} release (SCR) to end of Ca_iT per AP. A maximal recovery slope (MRS) of normalized Ca_iT at each pixel was calculated from negative maximum value in the first derivative of Ca_iT before the onset of SCRs. A modified phase angle analysis was performed to calculate phase angles of Ca_i and V_m kinetics per AP. Briefly, after local maxima and local minima were defined at a given pixel, individual segments between neighboring local minima and maxima were normalized between 0 to π (rising phase) or $-\pi$ to 0 (falling phase). Earliest rising times of SCRs and V_m re-depolarization at each pixel were calculated from first zero phase angles. Numbers of phase singularities in Ca_iT per AP at each pixel were calculated by counting a total numbers of local maxima and minima per AP. The amplitude of the V_m gradient vector is defined as

$$|\mathrm{grad}(V_m)| = \sqrt{\left(\frac{\partial V_m}{\partial x}\right)^2 + \left(\frac{\partial V_m}{\partial y}\right)^2}$$

The gradients were calculated from discrete data (100x 100 pixels) and we used spatial step of 3 pixel sizes to approximate the partial derivatives in the formula above. Spatial heterogeneity (SH) was calculated as natural logarithm of standard deviation of V_m (or Ca_i) signal amplitude in each 100 x100 pixels, averaged over repolarization time-interval (taken from 100 ms after action potential upstroke to APD_{80}). Data analysis and creation of map images and video clips was performed with software created by the first author in MatLab. Statistical comparison between SH of Ca_i and V_m was performed with paired t-test.

6.2 RESULTS

6.2.1 Increase in spatiotemporal heterogeneity of intracellular Ca^{2+} handling in long QT type 2

At a baseline heart rate of 1.2 s cycle length (CL), moderate bradycardia dependent SCRs, which were fully reversible at 500ms CL, occurred during the plateau phase of the AP. After induction of LQT2 but before the onset of triggered activity, the episodes of SCRs per AP, defined with numbers of local minima and maxima, were more pronounced compared to those at baseline ($p<0.01$, $n=5$) (Figure 23A). Intriguingly, dynamic alternations in the spatial distribution of cytosolic Ca^{2+} levels (or spatial heterogeneity of amplitudes in Ca_iT) were consistently observed in LQT2 as a result of enhanced spatial heterogeneity of Ca_i handling (i.e. kinetics of

Ca^{2+} recovery, onset times of SCRs, and frequencies of SCRs) (Figure 23B&C). Occasionally, sub-millimeter scale spatial heterogeneities of cytosolic Ca^{2+} levels with small 'islands', which were isolated from neighboring pixels, were formed (Figure 24).

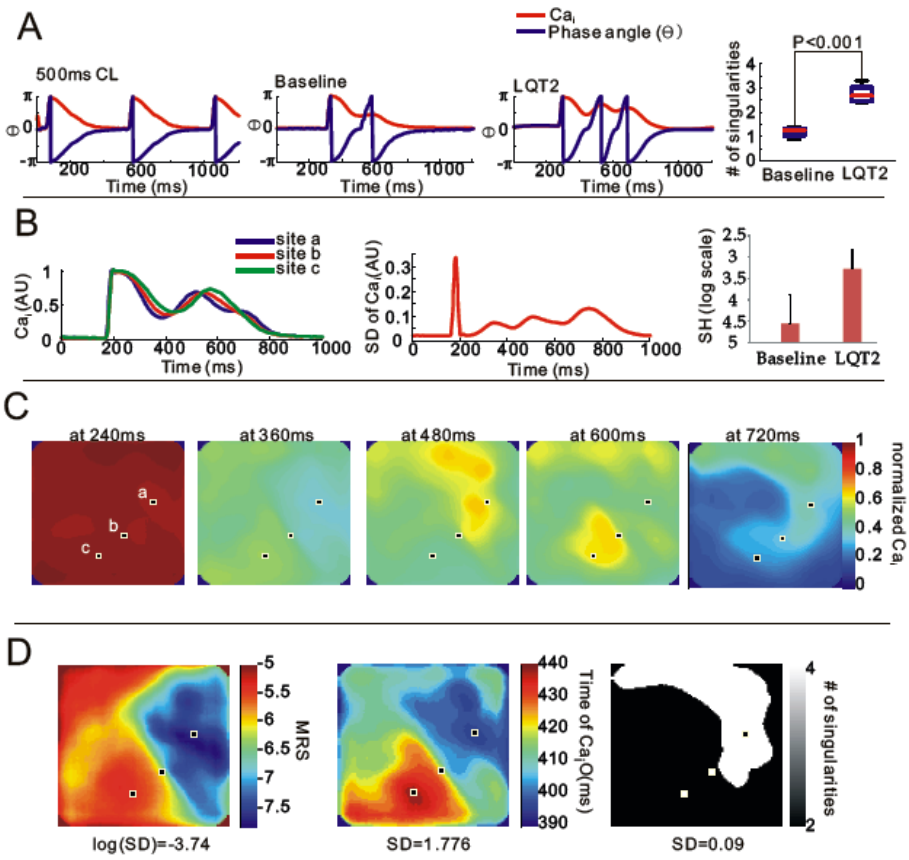

Figure 23. Abnormality in Ca_i handling in LQT2 A) Augmentation of SCRs in LQT2. Left three panels show superimposed traces of Ca_iT and phase angles in different conditions. A heart was paced at 1.2s cycle length before induction of LQT2 (baseline) and during LQT2. A right panel shows statistical comparison of numbers of phase singularities (local maxima and minima) during plateau per AP between baseline and LQT2. B) Dynamics alternation of spatial distribution of Ca_iT amplitude. A left panel shows superimposed traces of Ca_iT in three different sites (a, b, and c in C). A middle panel shows variation of standard deviations of normalized Ca_i amplitude in 100 x 100 pixels with a time dependent manner. A right panel shows the statistical comparison of calculated spatial heterogeneity between baseline and LQT2. C) Snapshots of Ca_i amplitude maps at given times (240ms, 360ms, 480ms, 600ms, and 720ms in B). Square dots indicate site a, b and c in B. D) Spatial heterogeneity of Ca_i handling. A left panel shows a map of maximum recovery slopes (MRSs) of Ca_iTs before the onset of SCRs. A middle panel shows a map of onset times of SCRs. A right panel shows a map of numbers of local maxima and minima during plateau phases of APs. Square dots indicated site a, b, and c.

Regional differences in the delayed recovery of Ca_iT due to the spatial heterogeneity of SCRs eventually led to dispersion of area under curve [137] of Ca_iT per AP and Ca_iTD (Figure 25A). Spatial distribution of calculated AUC was correlated with the dispersion of Ca_iTD_{80} in LQT2 ($r=0.932\pm0.065$, $n=5$). The AUC distribution in LQT2 reflected one of baseline ($r=0.88\pm0.054$, $n=5$), but was more pronounced than in baseline ($p<0.02$, $n=5$) (Figure 25B).

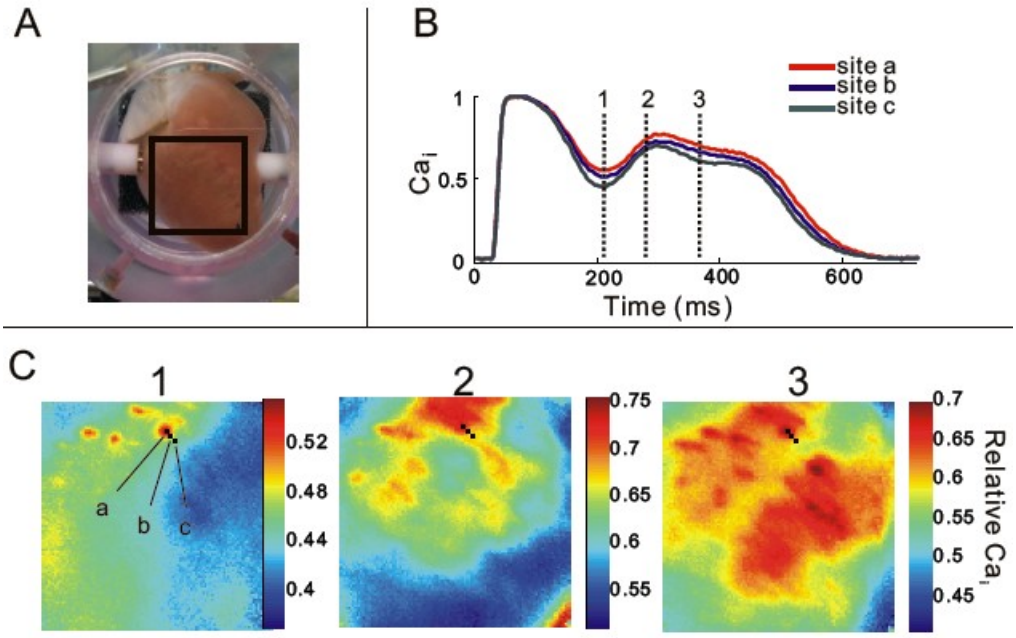

Figure 24. Sub-millimeter scale heterogeneity of Ca_i handling A) A picture of a Langendorff perfused heart. A black square (1.4 cm x 1.4 cm) indicates a field of view of optical mapping. B) Superimposed optical traces of normalized Ca_i in site a, b and c in C. Vertical dot lines labeled with 1, 2 and 3 indicate time lines of Ca_i mapping in C. C) Maps of normalized Ca_i amplitudes at a given time. 1, 2, and 3 indicate the corresponding time lines in B. square dots indicate site a, b, and c with 400 μm distances.

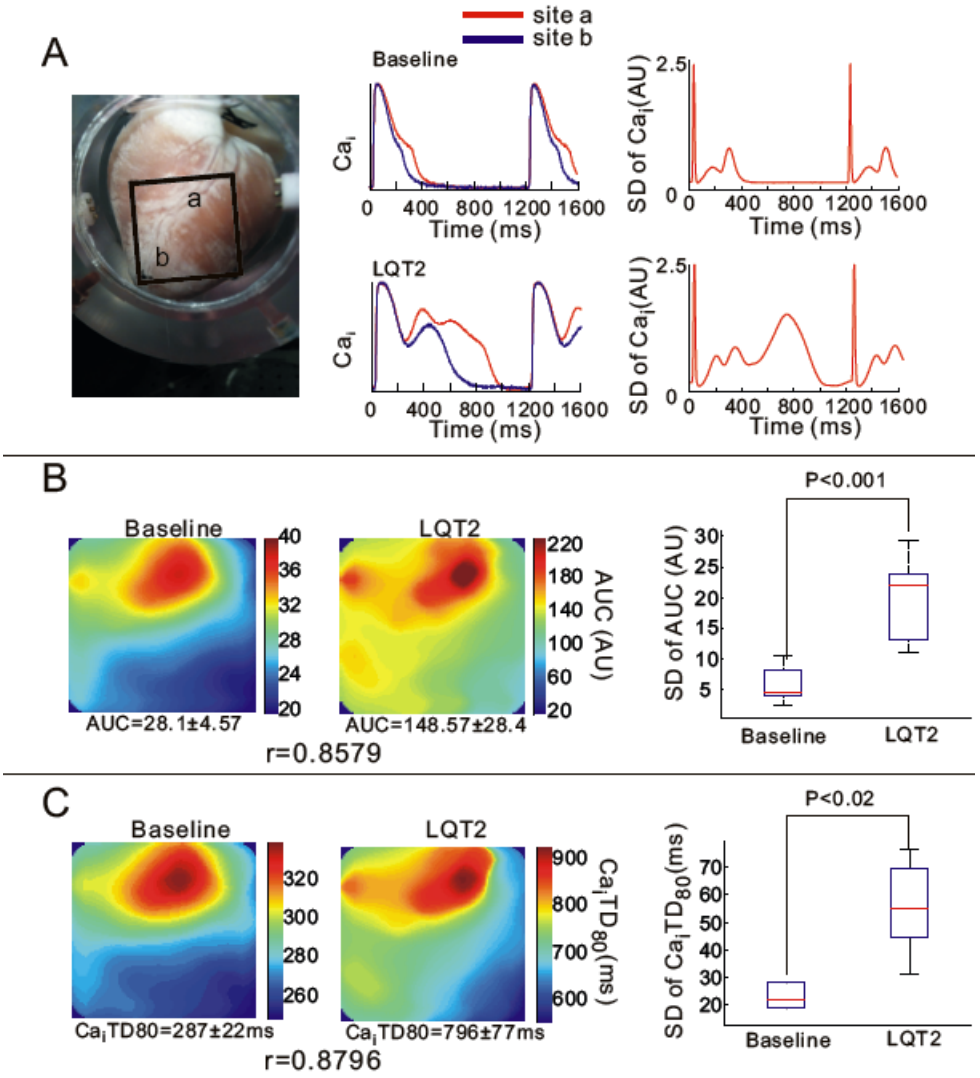

Figure 25. Spatial heterogeneity of AUC and dispersion of Ca_iTD_{80} A) A picture of a Langendorff perfused heart. A black square indicates a field of view of optical mapping. a, and b in the square indicate site a and b in the middle panel. A middle panel shows superimposed optical traces of normalized Ca_i in site a and b in A during baseline (top) and LQT2 (bottom). A right panel shows a time course of variation of SD of normalized Ca_i amplitudes in 100x100 pixels during baseline (top) and LQT2 (bottom). B) Spatial heterogeneity of AUC (of Ca_iT). Left two panels show spatial distribution of AUC during baseline (left) and LQT2 (right). A right panel shows statistical comparison of SD in AUC between baseline and LQT2. C) Spatial heterogeneity of Ca_iTD_{80}. Left two panels show spatial distribution of Ca_iTD_{80} during baseline (left) and LQT2 (right). A right panel shows statistical comparison of SD in Ca_iTD_{80} between baseline and LQT2.

6.2.2 Spatiotemporal interplay between SCRs and V_m re-depolarization in LQT2

In LQT2, the calculated spatial heterogeneity of Ca_iT amplitudes was more striking than calculated regional differences in V_m ($p<0.01$, n=6) (Figure 26A). The spatial organization of cytosolic Ca^{2+} levels was closely correlated to dispersion of V_m during the plateau phase of APs at a given time (Figure 26B&C). To investigate whether spatial organization of SCRs promotes V_m dispersion or regional differences in V_m instability elicits spatial heterogeneity of SCRs, we compared the rise times of SCRs with those of phase 2 EADs. Highly selective suppression of SCRs with RyR2 stabilizer, 1μM of K201, was also performed to further elucidate the interplay between SCR and Vm. SCRs during the plateau phase of APs in LQT2 always preceded phase 2 EADs (time delay= 9.2±5.2ms, n=50,000) (Figure 26D). This time delay between SCRs and phase 2 EADs caused a loss in the spatial correlation between Ca_i and V_m because the spatial heterogeneity of Ca_i occurred before V_m dispersion (Figure 26E). Suppression of SCRs eliminated phase 2 EADs (Figure 26E). Furthermore, more oscillatory events were observed at regions with longer APD_{80}/Ca_iTD_{80} (Figure 27 B). The delayed recovery of APs due to phase 2 EADs corresponding to SCRs in LQT2 (r=0.9546±0.0319, n=5) promoted further prolongation of AP duration, and regional differences in the delayed recovery of APs resulted in augmented dispersion of repolarization (Figure 27B). Suppression of SCRs with K201 significantly reduced dispersion of repolarization in LQT2 ($p<0.01$. n=5). These findings suggest that the spatial heterogeneity of SCRs in LQT2 is a driving force of voltage dispersion and/or DOR.

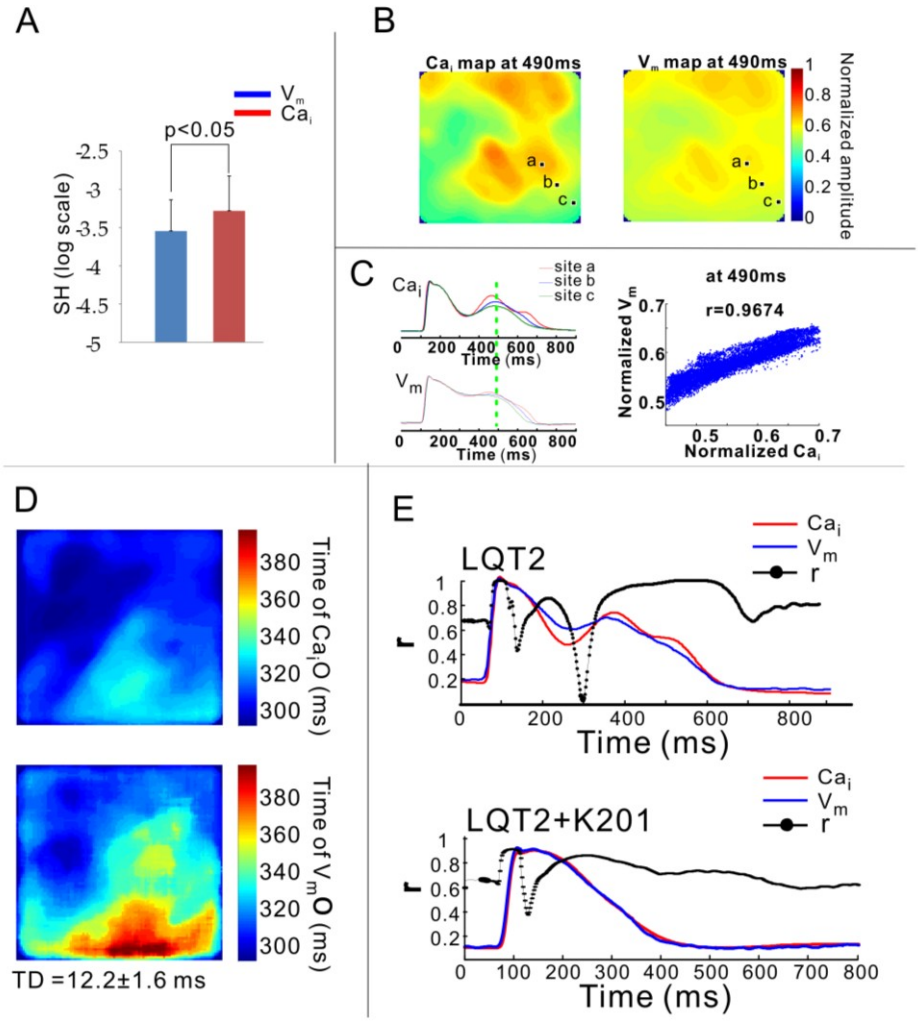

Figure 26. Spatiotemporal coupling between Ca_i and V_m A) statistical comparison between calculated spatial heterogeneity (SH) of Ca_i and V_m. B) Maps of normalized Ca_i and V_m amplitudes at a given time. Square dots indicate site a, b, and c for C. C) Spatial correlation between Ca_i and V_m amplitudes. A left panel shows superimposed optical traces of normalized Ca_i (top) and V_m (bottom). A vertical dot line indicates a timeline of Ca_i and V_m mapping in B. A right panel shows a scatter plot of Ca_i vs. V_m. r represents correlation coefficient between Ca_i and V_m amplitudes. D) Maps of times of SCRs/Ca_i oscillations (top) and EADs/V_m oscillations (bottom). The rise of SCR precedes the rise of EADs in all 100 x 100 pixels. E) Continuous spatial correlation during a single AP in LQT2 (top) and in LQT2 with 1μM of K201 perfusion (bottom) at the same pixel. **r** represents a spatial correlation coefficient between Ca_i and V_m. Higher r values show that either Ca_i or V_m causes the other.

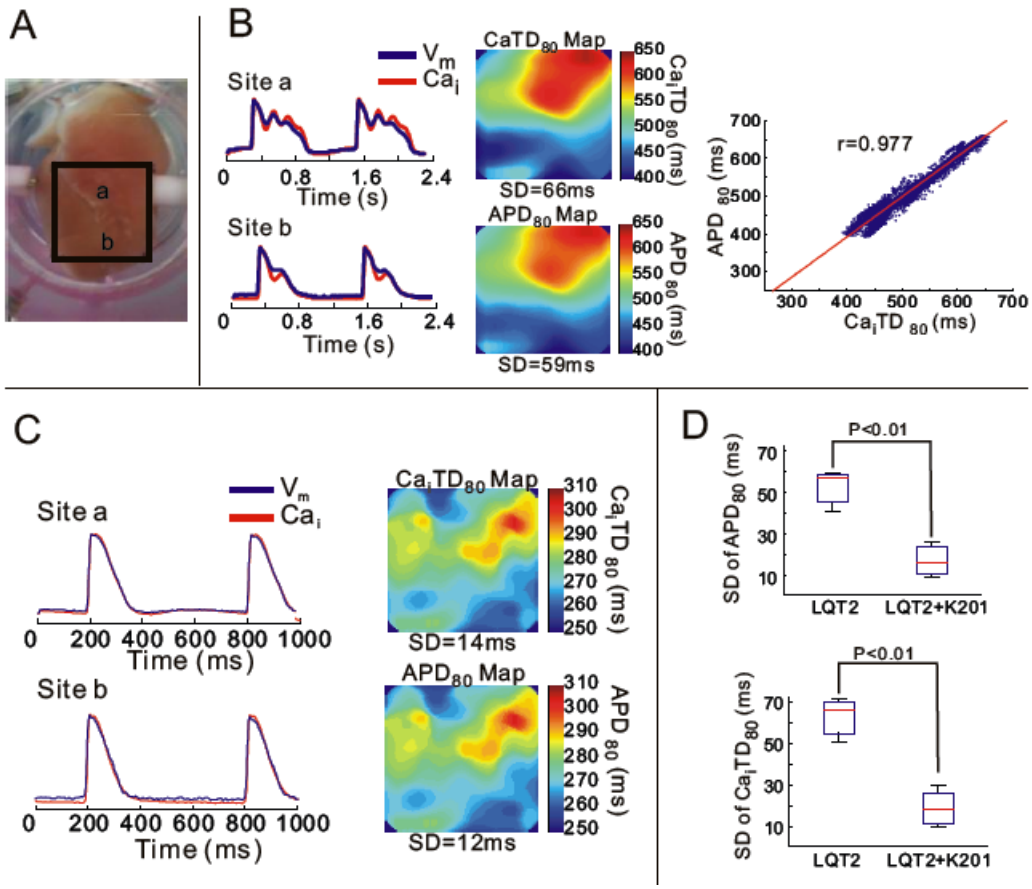

Figure 27. Correlation between spatial heterogeneity of Ca_iTD_{80} and dispersion of APD_{80} A) A picture of a Langendorff perfused heart. A black square indicates a field of view of optical mapping. a, and b in the square indicate site a and b in B. B) Tight linear relationship between dispersion of Ca_iTD_{80} and APD_{80}. A left panel shows superimposed optical traces of normalized Cai and Vm in site a (top) and b (bottom) in A. A middle panel shows maps of Ca_iTD_{80} and APD_{80}. A right panel shows a scatter plot of Ca_iTD_{80} vs. APD_{80}. C) Decreases in dispersion of Ca_iTD_{80} and APD_{80} after suppression of SCRs with 1μM of K201. A left panel shows superimposed optical traces of normalized Ca_i and V_m in site a (top) and b (bottom) in A. A right panel shows maps of Ca_iTD_{80} and APD_{80}. D) Statistical comparison of dispersion of APD_{80} (top) and Ca_iTD_{80} (bottom) in LQT2 before and after K201 infusion.

6.2.3 The impact of enhanced V_m dispersion during phase 3 of APs in the initiation of arrhythmogenic triggered activity

Abnormally high V_m dispersion, which was correlated with the spatial heterogeneity of cytosolic Ca^{2+} levels, was observed during phase 3 of APs before the onset of triggered activity in LQT2 (Figure 28A). To test the role of enhanced voltage dispersion during phase 3 of APs in the initiation of triggered activity, V_m gradients immediately before the onset of triggered activity was calculated. Intriguingly, such V_m gradients preceding the onset of triggered activity were spatially lined up with the origins of triggered activity (Figure 28B&C). The triggered activity was more pronounced at regions with higher V_m gradients (>94 percentile) (Figure 28D). The triggered activity was completely suppressed by reducing V_m gradients as a result of suppression/prevention of SCRs with K201 in 8 out of 9 hearts (pre-perfusion of 1μM of K201 in 4 hearts and post-perfusion of 1μM of K201 in 5 hearts) (Figure 28E). These findings suggest that abnormally enhanced V_m gradients during phase 3 of APs in LQT2 are Ca^{2+} dependent and can play a crucial role in the initiation of triggered activity.

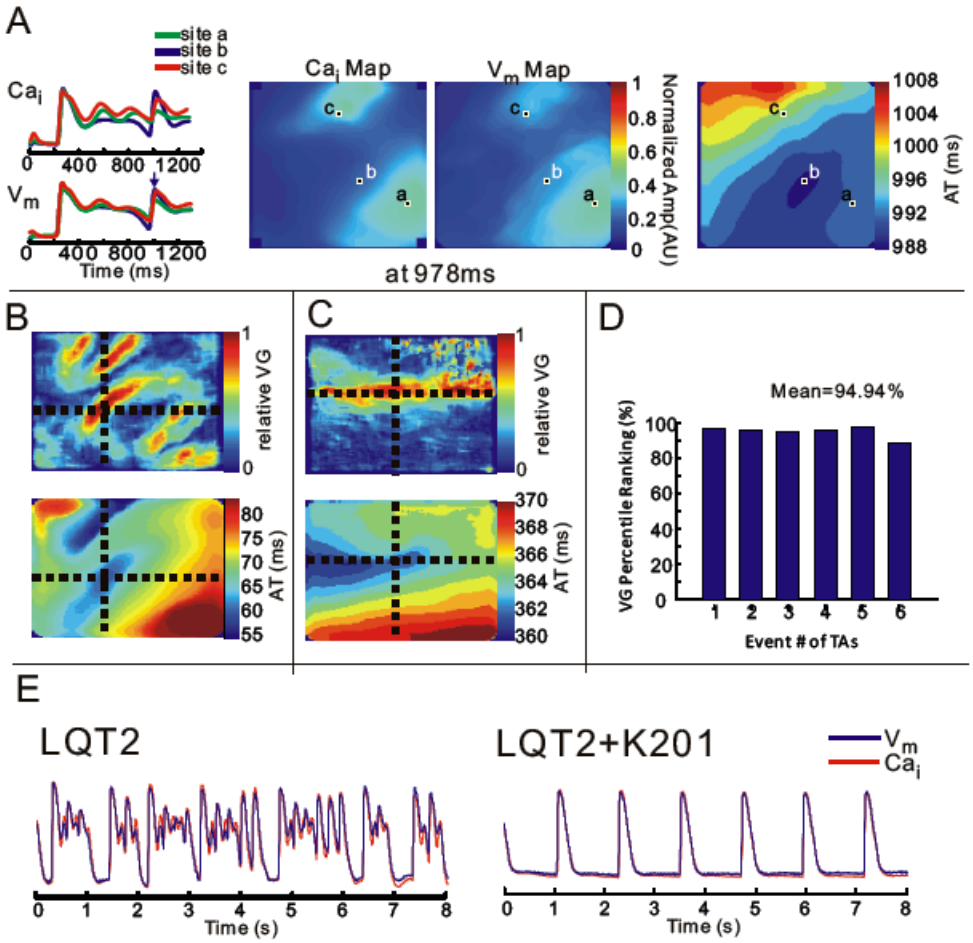

Figure 28. V_m gradients and triggered activity A) An example of V_m gradients and triggered activity in LQT2. A left panel shows superimposed optical traces of normalized Ca_i (top) and V_m (bottom) in site a, b and c. A middle panel shows maps of normalized Ca_i and V_m amplitude 10ms before the onset of triggered activity. A right panel shows a map of activation of triggered activity. B & C) Spatial correlations between V_m gradients and the origins of triggered activity in two different hearts. D) Percentile ranks of V_m gradients at the origins of triggered activities in six different hearts. E) Elimination of triggered activity after reduction of V_m gradients with K201 perfusion. A left panel shows superimposed optical traces of normalized Ca_i and V_m during LQT2 arrhythmia. A right panel shows superimposed optical traces of normalized Ca_i and V_m after suppression of LQT2 arrhythmia with K201 perfusion in the same heart. VG: V_m gradient, and AT: activation time.

6.2.4 The role of SCEs in the initiation of local early afterdepolarizations (EADs) and propagating delayed afterdepolarizations (DADs)

Previously, we reported that secondary Ca^{2+} oscillations, which precede V_m instability, are capable of eliciting reactivation of the L-type calcium channel via Na-Ca exchangers leading to triggered activity such as EADs and DADs.[16] We further investigated the direct interplay between SCRs and triggered activity without mediation of V_m gradients. In addition to triggered activity along the V_m gradients, numerous EADs and DADs were observed in this LQT2 models (Figure 29A). At the origination points of EADs and DADs (or the earliest sites of occurrence), a rise of Ca_i always preceded the rise of V_m re-depolarizations. The majority of early phase EADs were localized without propagation and were spatially discordant. Occasionally, local propagation of EADs occurred and was driven by voltage (Figure 29B). On the other hand, once DADs were initiated with consistently preceding SCRs to V_m re-depolarization during phase 4 of APs, global propagation of DADs was persistent and driven by voltage (Ca_iTs follow APs) (Figure 29C). These observations are consistent with our previous studies.

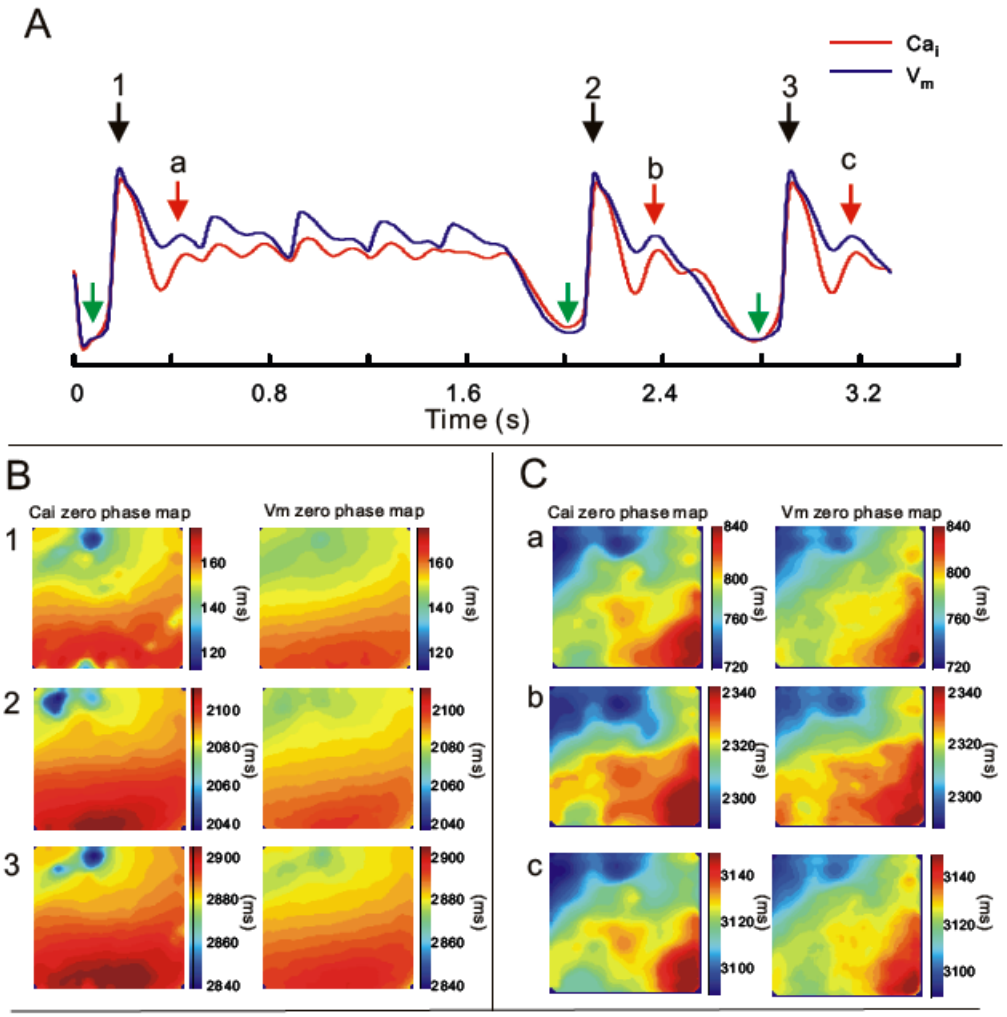

Figure 29. EADs and DADs in LQT2 A) Superimposed optical traces of normalized Ca_i and V_m during LQT2 arrhythmia. Green arrows indicate a diastolic elevation of Ca_i and V_m. Black arrows labeled with 1, 2, and 3 indicate DADs. Red arrows labeled with a, b, and c indicate EADs occurring immediate after DADs. B) Zero phase maps of Ca_i (left) and V_m (right) during DADs indicated in A. At the origins of DADs, rising of Ca_iT precedes rising of V_m. In the regions of DAD propagation, rising of V_m precedes to rising of Ca_i. C) Zero phase maps of Ca_i and V_m during EADs indicated in A. Most of early phase EADs were localized without propagation, but once propagation of EADs occurred, rising of V_m precedes rising of Ca_i.

6.3 DISCUSSION

LQT2 is known to increase the spatial heterogeneity of AP repolarization (i.e. dispersion of repolarization (DOR)) and has been widely implicated as an arrhythmogenic factor. However, mechanisms fundamental to LQT2 related augmentation of DOR and its impact of arrhythmogenesis remain unclear. Here, we report for the first time that spatially discordant abnormality in Ca_i handling promotes V_m gradients, which is responsible for triggered activity in LQT2. This Ca^{2+} dependent dispersion of repolarization offers an alternative to the M-cell hypothesis to explain increase in repolarization gradient in LQT2. Consideration of the mechanisms of these interesting findings requires further discussion.

6.3.1 Transmural DOR vs. epicardial DOR

Because I_{Ks} current density in midmyocardial cells (M cells) is relatively weak, M cells are more sensitive to many APD-prolonging conditions than epicardial and endocardial cells.[193] The preferential AP prolongation of M-cells has been linked to underlying mechanisms of markedly enhanced 'transmural' DOR in LQT2.[7, 97] Conversely, experimental studies have shown that heterogeneous AP prolongation occurs along the surface of a heart in various species in LQT2.[11, 93, 96, 194] It is controversial whether or not electrotonic influence of subepicardial M-cells contributes to the large epicardial dispersion of repolarization (Base → Apex). However, it is unlikely that M-cells promote epicardial DOR since 1) M cells reside throughout the deep subepicardial layers without any base-apex preference[98, 195] and 2) cryoablation of septum and conduction system except for a 1 mm thick layer of epicardium shows marked base to apex gradients of repolarization in LQT2. Thus, other factors rather than

M-cells may account for epicardial repolarization gradients.[11, 196] Alternatively, it has been proposed that there is a functional difference in the level of I_{Kr} along the epicardium that can be blocked by class III antiarrhythmic drugs.[11] However, experimental evidence supporting this hypothesis is lacking.

6.3.2 Possible effects of Ca^{2+} abnormality on AP prolongation

Intriguingly, AP prolongation in LQT2 is often associated with oscillatory events and modulated with agents which increase $I_{Ca,L}$.[7] The role of Ca_i handling in further AP prolongation in LQT2 is not fully demonstrated, but it is possible that cytosolic Ca^{2+} elevation during AP plateau due to spontaneous SR Ca^{2+} release could produce membrane potential instability (i.e. EADs) and eventually result in further repolarization delay in LQT2. Previously, we reported that oscillations in Ca_iT occurred on the surface of the heart in a rabbit LQT2 model before the onset of TdP and were correlated with further AP prolongation.[16, 197] It is not surprising that spontaneous elevation (oscillation) in Ca_i level, which is not voltage gated, delays AP repolarization as a consequence of positive Ca_i-V_m coupling via Ca^{2+} dependent sarcolemmal transporters namely as NCX, but the interplay between Ca_i handling and AP prolongation in LQT2 has not been fully understood.

6.3.3 Markedly enhanced Ca^{2+} heterogeneity in LQT2

Ca^{2+} homeostasis (i.e. balance between transmembrane Ca^{2+} influx and Ca^{2+} efflux) in cardiac myocytes is tightly modulated by membrane potential and by the Ca^{2+} uptake and release controlled by proteins on the SR. Experimental studies have shown that these processes are

altered in numerous pathologies and result in changes in systolic and diastolic Ca^{2+}.[70, 71, 78, 80, 198] Specifically, conditions with delayed repolarization alter the amount of Ca_i uptake in the lumen of the SR by SERCA during each cardiac cycle due to the delayed voltage dependent inactivation of L-type Ca^{2+} channels (increase in Ca^{2+} influx) and the reduced NCX driving force (decrease in Ca^{2+} efflux). Thus, beat to beat basis imbalance between Ca^{2+} entry and Ca^{2+} efflux results in gradual SR Ca^{2+} overload leading to spontaneous SR Ca^{2+} release. The next question is whether or not this phenomenon can be spatially heterogeneous. Experimental results have suggested that intercellular Ca^{2+} diffusion through gap junctions may facilitate synchronous spontaneous Ca^{2+} releases in neighboring cells.[197, 199] On the other hand, it was reported that spontaneous SR Ca^{2+} release can be persistent and even more pronounced when gap junctions are inhibited.[143] This observation suggests that intracellular oscillatory events in a single cell can result from its own intrinsic properties rather than intercellular synchronization.

Here, after induction of LQT2, the spatial and temporal complexity of cytosolic Ca^{2+} levels was significantly enhanced as a consequence of spatiotemporal changes in Ca_i kinetics. This is consistent with clinical observations showing that the relaxation of cardiac contraction in LQT2 patients was spatially inhomogeneous.[83] The underlying mechanisms of mechanical dispersion in LQT2 and its influence to voltage dispersion remain elusive. It is possible that this spatial heterogeneity of Ca_i handling in LQT2 reflect repolarization gradients. However, since Ca^{2+} uptake in SR by SERCA and spontaneous Ca^{2+} release are not fully voltage dependent, regional variations in intrinsic properties of Ca_i dynamics are likely to cause the Ca^{2+} heterogeneity. Experimental studies have shown that in mammalian hearts, Ca_i handling molecules such as Cav1.2α, NCX1, and SERCA2a are differentially expressed across the ventricular wall as well as along the epicardial surface and this regional difference is pronounced

more in female than in male.[12, 20, 21, 200] As a result, intrinsic inhomogeneous distribution of Ca^{2+} handling molecules could explain markedly enhanced Ca^{2+} heterogeneity in LQT2.

6.3.4 Spatial similarity of Ca^{2+} abnormality between bradycardia and LQT2

In a previous chapter, it was shown that bradycardia alone elicits spontaneous Ca^{2+} releases, which are spatially inhomogeneous and tightly correlated with the regional expression of Ca^{2+} handling molecules. The similarity in spatial distribution of Ca_i handling between bradycardia baseline and bradycardia-LQT2 (Figure 25B) illustrates that complex spatial patterns of Ca_i handling in LQT2 may reflect intrinsic heterogeneity of Ca_i handling, which was already accentuated in bradycardia alone. Even if this conjecture is accepted, it is unclear why the submillimeter-scale spatial heterogeneity of Ca_i should only appear after LQT2 induction. In addition to complex heterogeneity in Ca_i dynamics, Ca_i signaling mechanisms are likely to be activated and to complicate the system through positive and negative feedback processes. Additional experiments are required to fully elucidate the answer to this problem.

6.3.5 Correlation of Ca^{2+} and V_m gradients

In numerous pathologies, spatially discordant alternations in cytosolic Ca^{2+} handling are responsible for the dispersion of V_m instability/alternans, presumably due to positive Ca_i-V_m coupling via electrogenic Ca^{2+} dependent Na-Ca exchangers.[10, 26, 102] The most striking observation in this report is that spatiotemporal alternations in Ca_i handling in LQT2 were tightly correlated with dynamic changes in V_m dispersion. The notions 1) that SCRs, whose regional variation is responsible for the spatial heterogeneity of Ca_i, always precede early phase

membrane re-depolarization, 2) that spatial heterogeneity of Ca_i and Ca_iTD are consistently bigger than spatial heterogeneity of V_m and APD respectively, and 3) that perfusion with 1μM K201, which acts exclusively on ryanodine receptors and specifically affects Ca_i handling,[151] abolished the spatial heterogeneity shows that the regional variation of Ca_i handling can promote voltage dispersion.

6.3.6 V_m gradients initiate triggered activity

Repolarization gradients in LQT2 have been shown to initiate unidirectional conduction blocks and have been separated from that of spontaneous SR Ca^{2+} release which initiates triggered activity such as early afterdepolarizations (EADs) and delayed afterdepolarizations (DADs). In this model, triggered activity was initiated in the steepest region of voltage gradients (3.12±0.64 mV/mm^2, n=6). A voltage gradient along the direction of propagation of electrical activity is normal and facilitates synchronized contraction throughout the heart. However, in experimental studies, steep voltage gradients in pathologies can generate arrhythmogenic triggered activity.[116, 201] For example, in myocardial infarct models, a voltage gradient across the ischemic border zone can lead to a diastolic injury current at the normal side of the ischemic border. Such small injury currents can slightly depolarize the normal tissue and facilitate the occurrence of triggered activity. [116] Although it is well established that gradients of diastolic Ca^{2+} levels promote repolarization gradients in numerous pathologies,[20, 22, 26, 102] the direct interplay between Ca^{2+} dependent voltage gradients and triggered activity has not been established.

Here, we observed that LQT2 mediated triggered activity is also initiated by V_m gradients during phase 3 of APs. Despite high spatial correlation between origins of triggered activity and

voltage gradients in this study, further investigation of clear mechanistic explanation on the impact of Ca^{2+} mediated voltage gradients in the initiation of triggered activity is required. Theoretically, regional differences in cytosolic Ca^{2+} levels can generate voltage dispersion via electrogenic NCX during the plateau phases of APs. If electrotonic currents from 'donor' cells are sufficient to partially depolarize 'recipient' cells, triggered reactivation of L-type channels can initiate triggered activity.

In cryoablated rabbit LQT2 models, Maruyama et al. recently reported similar observations. According to the report, enhanced voltage gradients during phase 3 of APs can promote phase 3 EADs that lead to triggered activity. Intriguingly, they argued that the late phase voltage dispersion in acquired LQT syndrome was independent of regional variations in Ca^{2+} handling because the phase 3 EADs were not suppressed with BAPTA infusion.[196] However, the efficacy of BAPTA in chelating Ca^{2+} in intact animal models is controversial.[10] In contrast, we observed here that highly specific inhibition of secondary Ca^{2+} release with 1μM of K201, a dose at which it selectively decreases the RyR2 open probability, consistently eliminated triggered activity. Previous interventions into cytosolic Ca^{2+} handling with partial inhibition of L-type Ca^{2+} channels with nifedipine or by reducing $[Ca^{2+}]_o$ suppressed triggered activity.[16] Such experimental evidence supports that triggered activity is Ca^{2} -dependent.

Since we tested the role of voltage gradients in the initiation of triggered activity on the surface of hearts, further investigation is required to elucidate whether a steep voltage gradient on the surface of hearts account for the triggered activity or the triggered activity is initiated in deeper regions and propagates to the surface along the voltage gradient. However, experimental evidence has shown that triggered activity was observed in cryoablated rabbit hearts under similar LQT2 conditions,[11, 196] which suggests that TA may not originate intramurally. In the

canine wedge model of LQT2, breakthrough sites of triggered activity occurred consistently along the epicardial voltage gradient and not deep inside the ventricular walls.[202] If the triggered activity originates intramurally independent of voltage gradient, the breakthrough pattern of TA could not follow epicardial voltage gradient but rather propagates to earlier recovery areas.

6.3.7 Non voltage-gradient mediated triggered activity such as EADs and DADs in LQT2

In a way, the observed requirement for steep V_m gradient in triggering propagated EADs is not surprising: secondary Ca_i oscillations occurring during the AP plateau in the absence of local V_m gradient would be expected to cause a "local" EAD, but no propagation because the EADs may not be sufficient to initiate propagating triggered activity – this is a phenomenon we have repeatedly observed (Figure 7). On the other hand, Ca_i oscillations that occur even in the absence of a local V_m gradient in excitable tissue can certainly cause propagating ectopic beats, also known as DADs, which has been consistently observed by our group and others (Figure 29).[11, 16, 196, 203]

6.4 LIMITATIONS

Optical recordings of membrane potential and Ca^{2+} dynamics on the anterior surface of rabbit hearts revealed a complex spatial heterogeneity of Ca_i handling which was responsible for voltage dispersion leading to triggered activity in LQT2. The 2D nature of optical mapping does not provide LQT2 related enhancement of transmural differences in Ca_i handling and its link to triggered activity which originates from deeper layers of the ventricles. In addition, positive coupling of Ca_i-V_m via I_{NCX} most likely accounted for Ca_i dependent V_m dispersion in LQT2, but due to the lack of a reliable NCX inhibitor, further assessment of the NCX mediated interplay between Ca_i heterogeneity and V_m dispersion was not fully investigated.

6.5 CONCLUSION

In summary, we report that a marked increase of Ca_iT heterogeneity develops under LQT2 conditions, with the formation of unexpectedly small, irregularly shaped regions of elevated Ca_i. We propose that the increase in Ca_iT heterogeneity contributes to augmentation of V_m gradients and DOR and is highly arrhythmogenic by generating triggered activity or by initiating reentrant circuits. The suppression of TdP by a RyR2 selective K201 concentration underscores the importance of a detailed understanding of arrhythmogenic mechanisms for the development of rational treatment strategies.

APPENDIX A

INTRACELLULAR Ca^{2+} OSCILLATIONS AND T-WAVE LABILITY (TWL) PRECEDE TORSADE DE POINTES (TDP) IN A RABBIT MODEL OF LONG QT TYPE 2 (LQT2)

Authors: *Jan Nemec, Jong Kim, Bethanny Gabris, Guy Salama, University of Pittsburgh, Pittsburgh, PA* ; *J. Am. Coll.Cardiol.*2010;55;A2.E16 doi:10.1016/S0735-1097(10)60017-4

Background: Action potential (AP) prolongation results in TdP in clinical and experimental LQT2, but the exact mechanism remains uncertain. T-Wave alternans has been proposed as a marker of arrhythmic risk and is elicited by APD and Ca^{2+} alternans. However, non-alternans TWL hasbeen associated with TdP in LQT syndrome. We hypothesized that TWL at constant heart rate precedes TdP in a LQT2 model and that it is caused by abnormal Cai dynamics.

Methods: Female rabbit hearts were perfused, AV node was ablated and ventricles paced at 50 beats per minute. Epicardial ECG was recorded during optical mapping (RH 237 and Rhod-2 AM) of AP and Cai. LQT2 was mimicked by Dofetilide (D; 500 nM/L) and decrease in $[K^+]_o$ and $[Mg^{2+}]_o$. TWL was calculated as logarithm of root-mean-square of differences between T wave amplitude from subsequent beats.

Results: D prolonged AP durations and induced TdP (n=8/8). Baseline Ca transient (CaT) was usually monophasic. Occasionally, a small secondary peak was observed. The number of CaT peaks per AP during paced rhythm increased upon D addition and prior to VT onset compared to

baseline in all cases (Number of CaT per AP: 1.33±0.39 vs 2.32±0.47, $p<0.002$). This was accompanied by increased TWL (-4.06±0.94 vs -2.89±0.95, $p<0.002$).

Conclusions: TWL precedes TdP in rabbit LQT2 model. Complex Ca dynamics (>1 CaT peak per AP) occurs during prolonged AP, promoting TWL and TdP. Possible mechanisms include secondary Ca2+ release from an overloaded sarcoplasmic reticulum and enhanced Na/Ca exchange current.

APPENDIX B

ACQUIRED LQT2 LEADS TO MARKED SPATIAL HETEROGENEITY (SH) OF Ca^{2+} TRANSIENT

Authors: *Jong J. Kim, Jan Nemec, Guy Salama, University of Pittsburgh, Pittsburgh, PA*; J. Am. Coll. Cardiol. doi:10.1016/S0735-1097(11)60003-X 2011;57;E3.

Background: Enhanced dispersion of repolarization (DOR) in LQT2 and abnormalities of intracellular Ca2+ [2] have been proposed as arrhythmogenic mechanism of Torsade de Pointes (TdP). However, the interplay and relative roles of DOR and SH of Cai is not understood.

Methods: Simultaneous optical maps of membrane voltage (Vm) and Cai were recorded from the anterior surface of Langendorff rabbit hearts (n=7) paced at 50 bpm after AV node ablation. After perfusion with normal Tyrode (baseline; B), LQT2 was induced by adding dofetilide (0.5 μM) and reducing K+ (2 mM). Standard deviation of Vm and Cai signal amplitude was calculated in each 100x100 pixel frame and averaged over repolarization time-interval (from 100 ms after action potential upstroke to APD80). SH was calculated from paced beats as natural logarithm of this average at B and during LQT2.

Results: Irregular regions of elevated Cai (~2x3 mm) appeared during phase 2 and 3 of action potential. During LQT2, SH of Cai exceeded SH of Vm in all hearts (-3.28±0.45 vs -3.55±0.41; $p<0.01$), although high Cai correlated with high Vm. At B, SH of Vm and Cai were similar and

significantly lower than during LQT2.

Conclusions: SH of Cai transient during LQT2 exceeds SH of Vm. Regions of elevated Cai exhibit complex oscillations on a mm scale. SH of Cai may reflect intrinsic regional differences of Cai handling mechanisms accentuated by repolarizationdelay of LQT2 rather than follow SH of Vm. Instead, SH of Cai appears to enhance SH of Vm, elevate DOR and facilitate TdP.

APPENDIX C

BRADYCARDIA ELICITS A SECONDARY Ca_i ELEVATION DURING THE ACTION POTENTIAL (AP) PLATEAU WHICH IS SPATIALLY HETEROGENEOUS, PROLONGS AP DURATIONS (APD) FURTHER, ENHANCES DISPERSION OF REPOLARIZATION (DOR) AND MAY EXPLAIN THE ARRHYTHMOGENIC PROPERTIES OF BRADYCARDIA

Authors: *Jong J. Kim, Jan Nemec, Rita Papp, and Guy Salama, University of Pittsburgh, Pittsburgh, PA*; AHA 2011 Scientific Session APS.403.03a

Introduction: Bradycardia is known to prolong APD and DOR and is a factor that promotes arrhythmia in long QT type 2. In numerous conditions, spontaneous Ca^{2+} release from sarcoplasmic reticulum has been shown to trigger early afterdepolarizations, ectopic activity that initiate arrhythmias, but the interplay between secondary Ca^{2+} elevation (SCE) and membrane excitability has not been demonstrated in bradycardia.

Objectives: To correlate voltage-depolarization during the AP plateau to SCE during bradycardia.

Methods: Dual optical mapping of intracellular calcium transient (CaT) and AP was performed in Langendorff perfused rabbit hearts. After AV node ablation, CaT and AP dynamics were investigated at physiological (120 beats per minute (bpm)) and slow heart rate (50 bpm).

Results: Upon changing HR from 120 to 50 bpm, APD gradually increased with a time-constant of 53.8±8.9 s, consistent with clinical QT measurements. The shift from 120 to 50 bpm elicited SCE during the AP plateau that was a) regionally heterogeneous, b) associated with enhanced depolarization of the AP plateau and was reversed by pacing at 120 bpm. Regional differences of SCE at 50 bpm were significantly increased ($P<0.01$, n=7) and were correlated with dispersion of APD ($r=0.9277\pm0.03$, n=7). SCE and APD prolongation were more pronounced at the base of right ventricles than the apex of left ventricles ($P<0.01$, n=7). Suppression of SCE with K201 (1 μM/L) (to stabilize RyR2) reduced APD ($P<0.01$, n=5) and DOR ($P<0.02$, n=5). The molecular basis of the spatial distribution of SCE is currently being correlated to the intrinsic distributions of Ca^{2+} handling channels and transporters (Cav1.2α, RyR2, NCX and SERCA2a).

Conclusion: These data show for the first time that bradycardia elicits SCE which contributes to AP prolongation and its spatial heterogeneity increases DOR. These changes explain why bradycardia is a critical factor to trigger Torsade de Pointes in LQT2.

APPENDIX D

THE ROLE OF SPATIAL HETEROGENEITIES OF INTRACELLULAR Ca^{2+} OSCILLATIONS (Ca_iO) IN LONG QT TYPE 2 (LQT2)-RELATED ARRHYTHMIAS

Authors: *Jong J. Kim, Jan Nemec, and Guy Salama, University of Pittsburgh, Pittsburgh, PA*;

Heart Rhythm, Vol 8, No. 5, PO6-113, May Supplement 2011

Introduction: Spontaneous Ca^{2+} release from internal stores, Ca_iO and dispersion of refractoriness (DOR) have been implicated as underlying mechanisms of Torsade de Pointes (TdP) in LQT2. DOR remains a fundamental arrhythmogenic mechanism because it generates conduction blocks and the steep voltage (V_m) gradients that sustain reentry. Enhanced DOR is partly due to intrinsic heterogeneities of ionic currents but may also depend on spatial and dynamic heterogeneities of Ca_iO.

Methods: Simultaneous optical maps of membrane voltage (Vm) and Cai were recorded from the anterior surface of Langendorff rabbit hearts (n=7) paced at 50 bpm after AV node ablation. After perfusion with normal Tyrode's, LQT2 was induced with dofetilide (0.5 μM) and low K^+ (2 mM) and Mg^{2+} (0.5mM). Time delays between Ca_iO and Vm was quantitatively analyzed using phase maps. Spatial correlation between Ca_iO amplitudes and DOR/Vm dispersion in LQT2 but before the onset of triggered activity (TA) was investigated. Cai and Vm heterogeneities were mapped and correlated to the origins of TA.

Results: Spontaneous Ca_iO preceded phase 2 and 3 depolarization by 9.1503±5.1874ms. Local CTD_{80} was dependent on the amplitude of Ca_iO and was spatially correlated to APD_{80} (COE = 0.9546±0.0319, n=5). The spatial heterogeneity of preceding Ca_iO was correlated to Vm dispersion (COE=0.8172±0.093, n=5). TA occurred primarily at the boundaries of high and low Vm.

Conclusions: Spatial heterogeneities of Ca_iO can alter local V_m dynamics resulting in enhanced DOR or large Vm gradient that can initiate TA and provide the substrate of local conduction blocks needed to sustain TdP.

BIBLIOGRAPHY

1. Rogers, J.M., et al., *Incidence, evolution, and spatial distribution of functional reentry during ventricular fibrillation in pigs.* Circ Res, 1999. **84**(8): p. 945-54.

2. Pogwizd, S.M., J.P. McKenzie, and M.E. Cain, *Mechanisms underlying spontaneous and induced ventricular arrhythmias in patients with idiopathic dilated cardiomyopathy.* Circulation, 1998. **98**(22): p. 2404-14.

3. Wang, Z., et al., *Differential distribution of inward rectifier potassium channel transcripts in human atrium versus ventricle.* Circulation, 1998. **98**(22): p. 2422-8.

4. Schram, G., et al., *Differential distribution of cardiac ion channel expression as a basis for regional specialization in electrical function.* Circ Res, 2002. **90**(9): p. 939-50.

5. Mantravadi, R., et al., *Autonomic nerve stimulation reverses ventricular repolarization sequence in rabbit hearts.* Circ Res, 2007. **100**(7): p. e72-80.

6. Nattel, S., et al., *Arrhythmogenic ion-channel remodeling in the heart: heart failure, myocardial infarction, and atrial fibrillation.* Physiol Rev, 2007. **87**(2): p. 425-56.

7. Antzelevitch, C., et al., *The M cell: its contribution to the ECG and to normal and abnormal electrical function of the heart.* J Cardiovasc Electrophysiol, 1999. **10**(8): p. 1124-52.

8. Hoeker, G.S., et al., *Spontaneous calcium release in tissue from the failing canine heart.* Am J Physiol Heart Circ Physiol, 2009. **297**(4): p. H1235-42.

9. Fujiwara, K., et al., *Burst emergence of intracellular Ca2+ waves evokes arrhythmogenic oscillatory depolarization via the Na+-Ca2+ exchanger: simultaneous confocal recording of membrane potential and intracellular Ca2+ in the heart.* Circ Res, 2008. **103**(5): p. 509-18.

10. Ogawa, M., et al., *Calcium dynamics and ventricular fibrillation.* Circ Res, 2008. **102**(5): p. e52.

11. Choi, B.R., F. Burton, and G. Salama, *Cytosolic Ca2+ triggers early afterdepolarizations and Torsade de Pointes in rabbit hearts with type 2 long QT syndrome.* J Physiol, 2002. **543**(Pt 2): p. 615-31.

12. Sims, C., et al., *Sex, age, and regional differences in L-type calcium current are important determinants of arrhythmia phenotype in rabbit hearts with drug-induced long QT type 2.* Circ Res, 2008. **102**(9): p. e86-100.

13. Prunier, F., et al., *Prevention of ventricular arrhythmias with sarcoplasmic reticulum Ca2+ ATPase pump overexpression in a porcine model of ischemia reperfusion.* Circulation, 2008. **118**(6): p. 614-24.

14. Volders, P.G., et al., *Progress in the understanding of cardiac early afterdepolarizations and torsades de pointes: time to revise current concepts.* Cardiovasc Res, 2000. **46**(3): p. 376-92.

15. Weiss, J.N., et al., *Early afterdepolarizations and cardiac arrhythmias.* Heart Rhythm.
16. Nemec, J., et al., *Calcium oscillations and T-wave lability precede ventricular arrhythmias in acquired long QT type 2.* Heart Rhythm. **7**(11): p. 1686-94.

17. Garciarena, C.D., et al., *Chronic NHE-1 blockade induces an antiapoptotic effect in the hypertrophied heart.* J Appl Physiol, 2009. **106**(4): p. 1325-31.

18. Chen, J.B., et al., *Multiple Ca2+ signaling pathways regulate intracellular Ca2+ activity in human cardiac fibroblasts.* J Cell Physiol. **223**(1): p. 68-75.

19. Katra, R.P. and K.R. Laurita, *Cellular mechanism of calcium-mediated triggered activity in the heart.* Circ Res, 2005. **96**(5): p. 535-42.

20. Laurita, K.R., et al., *Transmural heterogeneity of calcium handling in canine.* Circ Res, 2003. **92**(6): p. 668-75.

21. Chen, G., et al., *Regional genomic regulation of cardiac sodium-calcium exchanger by oestrogen.* J Physiol. **589**(Pt 5): p. 1061-80.

22. Qian, Y.W., et al., *Spatial heterogeneity of calcium transient alternans during the early phase of myocardial ischemia in the blood-perfused rabbit heart.* Circulation, 2001. **104**(17): p. 2082-7.

23. Oka, Y., et al., *Atrioventricular block-induced Torsades de Pointes with clinical and molecular backgrounds similar to congenital long QT syndrome.* Circ J. **74**(12): p. 2562-71.

24. Steinbrecher, U.P. and D.H. Fitchett, *Torsade de pointes. A cause of syncope with atrioventricular block.* Arch Intern Med, 1980. **140**(9): p. 1223-6.

25. Subbiah, R.N., et al., *Torsades de pointes during complete atrioventricular block: Genetic factors and electrocardiogram correlates.* Can J Cardiol. **26**(4): p. 208-12.

26. Pruvot, E.J., et al., *Role of calcium cycling versus restitution in the mechanism of repolarization alternans.* Circ Res, 2004. **94**(8): p. 1083-90.

27. Chudin, E., et al., *Intracellular Ca(2+) dynamics and the stability of ventricular tachycardia.* Biophys J, 1999. **77**(6): p. 2930-41.

28. Quan, W. and Y. Rudy, *Unidirectional block and reentry of cardiac excitation: a model study.* Circ Res, 1990. **66**(2): p. 367-82.

29. Rohr, S., J.P. Kucera, and A.G. Kleber, *Slow conduction in cardiac tissue, I: effects of a reduction of excitability versus a reduction of electrical coupling on microconduction.* Circ Res, 1998. **83**(8): p. 781-94.

30. Keating, M.T. and M.C. Sanguinetti, *Molecular and cellular mechanisms of cardiac arrhythmias.* Cell, 2001. **104**(4): p. 569-80.

31. Dominguez, G. and H.A. Fozzard, *Influence of extracellular K+ concentration on cable properties and excitability of sheep cardiac Purkinje fibers.* Circ Res, 1970. **26**(5): p. 565-74.

32. Katzung, B.G. and J.A. Morgenstern, *Effects of extracellular potassium on ventricular automaticity and evidence for a pacemaker current in mammalian ventricular myocardium.* Circ Res, 1977. **40**(1): p. 105-11.

33. Lu, H.H., *Shifts in pacemaker dominance within the sinoatrial region of cat and rabbit hearts resulting from increase of extracellular potassium.* Circ Res, 1970. **26**(3): p. 339-46.

34. Eisner, D.A. and W.J. Lederer, *The relationship between sodium pump activity and twitch tension in cardiac Purkinje fibres.* J Physiol, 1980. **303**: p. 475-94.

35. Kline, R.P. and M. Morad, *Potassium efflux in heart muscle during activity: extracellular accumulation and its implications.* J Physiol, 1978. **280**: p. 537-58.

36. Terkildsen, J.R., E.J. Crampin, and N.P. Smith, *The balance between inactivation and activation of the Na+-K+ pump underlies the triphasic accumulation of extracellular K+ during myocardial ischemia.* Am J Physiol Heart Circ Physiol, 2007. **293**(5): p. H3036-45.

37. El-Sherif, N. and G. Turitto, *Electrolyte disorders and arrhythmogenesis.* Cardiol J. **18**(3): p. 233-45.

38. Lankipalli, R.S., et al., *Mechanisms underlying arrhythmogenesis in long QT syndrome.* J Electrocardiol, 2005. **38**(4 Suppl): p. 69-73.

39. Bosch, R.F., et al., *Ionic mechanisms of electrical remodeling in human atrial fibrillation.* Cardiovasc Res, 1999. **44**(1): p. 121-31.

40. Clark, R.B., et al., *T-tubule localization of the inward-rectifier K(+) channel in mouse ventricular myocytes: a role in K(+) accumulation.* J Physiol, 2001. **537**(Pt 3): p. 979-92.

41. Swift, F., et al., *Slow diffusion of K+ in the T tubules of rat cardiomyocytes.* J Appl Physiol, 2006. **101**(4): p. 1170-6.

42. Nakao, M. and D.C. Gadsby, *[Na] and [K] dependence of the Na/K pump current-voltage relationship in guinea pig ventricular myocytes.* J Gen Physiol, 1989. **94**(3): p. 539-65.

43. Kagiyama, Y., J.L. Hill, and L.S. Gettes, *Interaction of acidosis and increased extracellular potassium on action potential characteristics and conduction in guinea pig ventricular muscle.* Circ Res, 1982. **51**(5): p. 614-23.

44. Kleber, A.G., C.B. Riegger, and M.J. Janse, *Extracellular K+ and H+ shifts in early ischemia: mechanisms and relation to changes in impulse propagation.* J Mol Cell Cardiol, 1987. **19 Suppl 5**: p. 35-44.

45. Coronel, R., et al., *Distribution of extracellular potassium and its relation to electrophysiologic changes during acute myocardial ischemia in the isolated perfused porcine heart.* Circulation, 1988. **77**(5): p. 1125-38.

46. Buchanan, J.W., Jr., T. Saito, and L.S. Gettes, *The effects of antiarrhythmic drugs, stimulation frequency, and potassium-induced resting membrane potential changes on conduction velocity and dV/dtmax in guinea pig myocardium.* Circ Res, 1985. **56**(5): p. 696-703.

47. Harris, A.S., et al., *Excitatory factors in ventricular tachycardia resulting from myocardial ischemia; potassium a major excitant.* Science, 1954. **119**(3085): p. 200-3.

48. Hill, J.L. and L.S. Gettes, *Effect of acute coronary artery occlusion on local myocardial extracellular K+ activity in swine.* Circulation, 1980. **61**(4): p. 768-78.

49. Weidmann, S., *The effect of the cardiac membrane potential on the rapid availability of the sodium-carrying system.* J Physiol, 1955. **127**(1): p. 213-24.

50. Shaw, R.M. and Y. Rudy, *Ionic mechanisms of propagation in cardiac tissue. Roles of the sodium and L-type calcium currents during reduced excitability and decreased gap junction coupling.* Circ Res, 1997. **81**(5): p. 727-41.

51. Tracy, C.M., et al., *Evidence that cocaine slows cardiac conduction by an action on both AV nodal and His-Purkinje tissue in the dog.* J Electrocardiol, 1991. **24**(3): p. 257-62.

52. Bers, D.M., W.H. Barry, and S. Despa, *Intracellular Na+ regulation in cardiac myocytes.* Cardiovasc Res, 2003. **57**(4): p. 897-912.

53. Splawski, I., et al., *Variant of SCN5A sodium channel implicated in risk of cardiac arrhythmia.* Science, 2002. **297**(5585): p. 1333-6.

54. Bezzina, C.R., M.B. Rook, and A.A. Wilde, *Cardiac sodium channel and inherited arrhythmia syndromes.* Cardiovasc Res, 2001. **49**(2): p. 257-71.

55. Morita, H., et al., *Ventricular arrhythmia induced by sodium channel blocker in patients with Brugada syndrome.* J Am Coll Cardiol, 2003. **42**(9): p. 1624-31.

56. Rivolta, I., et al., *A novel SCN5A mutation associated with long QT-3: altered inactivation kinetics and channel dysfunction.* Physiol Genomics, 2002. **10**(3): p. 191-7.

57. Kyndt, F., et al., *Novel SCN5A mutation leading either to isolated cardiac conduction defect or Brugada syndrome in a large French family.* Circulation, 2001. **104**(25): p. 3081-6.

58. Herfst, L.J., et al., *Na+ channel mutation leading to loss of function and non-progressive cardiac conduction defects.* J Mol Cell Cardiol, 2003. **35**(5): p. 549-57.

59. Benson, D.W., et al., *Congenital sick sinus syndrome caused by recessive mutations in the cardiac sodium channel gene (SCN5A).* J Clin Invest, 2003. **112**(7): p. 1019-28.

60. Akai, J., et al., *A novel SCN5A mutation associated with idiopathic ventricular fibrillation without typical ECG findings of Brugada syndrome.* FEBS Lett, 2000. **479**(1-2): p. 29-34.

61. Lopez-Barbeito, B., et al., *Diphenhydramine overdose and Brugada sign.* Pacing Clin Electrophysiol, 2005. **28**(7): p. 730-2.

62. Eisner, D.A., W.J. Lederer, and R.D. Vaughan-Jones, *The dependence of sodium pumping and tension on intracellular sodium activity in voltage-clamped sheep Purkinje fibres.* J Physiol, 1981. **317**: p. 163-87.

63. Venetucci, L.A., et al., *The sarcoplasmic reticulum and arrhythmogenic calcium release.* Cardiovasc Res, 2008. **77**(2): p. 285-92.

64. Bers, D.M., *Cardiac excitation-contraction coupling.* Nature, 2002. **415**(6868): p. 198-205.

65. Altamirano, J. and D.M. Bers, *Voltage dependence of cardiac excitation-contraction coupling: unitary Ca2+ current amplitude and open channel probability.* Circ Res, 2007. **101**(6): p. 590-7.

66. Blaustein, M.P. and W.J. Lederer, *Sodium/calcium exchange: its physiological implications.* Physiol Rev, 1999. **79**(3): p. 763-854.

67. Magleby, K.L. and B.S. Pallotta, *Calcium dependence of open and shut interval distributions from calcium-activated potassium channels in cultured rat muscle.* J Physiol, 1983. **344**: p. 585-604.

68. Viatchenko-Karpinski, S., et al., *Abnormal calcium signaling and sudden cardiac death associated with mutation of calsequestrin.* Circ Res, 2004. **94**(4): p. 471-7.

69. Berridge, M.J., M.D. Bootman, and H.L. Roderick, *Calcium signalling: dynamics, homeostasis and remodelling.* Nat Rev Mol Cell Biol, 2003. **4**(7): p. 517-29.

70. Jiang, D., et al., *RyR2 mutations linked to ventricular tachycardia and sudden death reduce the threshold for store-overload-induced Ca2+ release (SOICR).* Proc Natl Acad Sci U S A, 2004. **101**(35): p. 13062-7.

71. Terentyev, D., et al., *Redox modification of ryanodine receptors contributes to sarcoplasmic reticulum Ca2+ leak in chronic heart failure.* Circ Res, 2008. **103**(12): p. 1466-72.

72. Wehrens, X.H., et al., *FKBP12.6 deficiency and defective calcium release channel (ryanodine receptor) function linked to exercise-induced sudden cardiac death.* Cell, 2003. **113**(7): p. 829-40.

73. Hearse, D.J. and R. Bolli, *Reperfusion induced injury: manifestations, mechanisms, and clinical relevance.* Cardiovasc Res, 1992. **26**(2): p. 101-8.

74. Burashnikov, A. and C. Antzelevitch, *Block of I(Ks) does not induce early afterdepolarization activity but promotes beta-adrenergic agonist-induced delayed afterdepolarization activity.* J Cardiovasc Electrophysiol, 2000. **11**(4): p. 458-65.

75. Baartscheer, A., et al., *SR calcium handling and calcium after-transients in a rabbit model of heart failure.* Cardiovasc Res, 2003. **58**(1): p. 99-108.

76. Meli, A.C., et al., *A Novel Ryanodine Receptor Mutation Linked to Sudden Death Increases Sensitivity to Cytosolic Calcium.* Circ Res.

77. Sy, R.W., et al., *Arrhythmia characterization and long-term outcomes in catecholaminergic polymorphic ventricular tachycardia.* Heart Rhythm. **8**(6): p. 864-71.

78. Belevych, A.E., et al., *Redox modification of ryanodine receptors underlies calcium alternans in a canine model of sudden cardiac death.* Cardiovasc Res, 2009. **84**(3): p. 387-95.

79. Shan, J., et al., *Role of chronic ryanodine receptor phosphorylation in heart failure and beta-adrenergic receptor blockade in mice.* J Clin Invest. **120**(12): p. 4375-87.

80. Chen, K.Y. and T.G. Huang, *[Hyperphosphorylation of type 2 ryanodine receptor in chronic heart failure]*. Zhonghua Xin Xue Guan Bing Za Zhi, 2007. **35**(7): p. 675-7.

81. Szabo, B., et al., *Role of Na+:Ca2+ exchange current in Cs(+)-induced early afterdepolarizations in Purkinje fibers.* J Cardiovasc Electrophysiol, 1994. **5**(11): p. 933-44.

82. Huffaker, R.B., J.N. Weiss, and B. Kogan, *Effects of early afterdepolarizations on reentry in cardiac tissue: a simulation study.* Am J Physiol Heart Circ Physiol, 2007. **292**(6): p. H3089-102.

83. Haugaa, K.H., et al., *Transmural differences in myocardial contraction in long-QT syndrome: mechanical consequences of ion channel dysfunction.* Circulation. **122**(14): p. 1355-63.

84. Moric Janiszewska, E., et al., *Expression of genes KCNQ1 and HERG encoding potassium ion channels Ik(r), Ik(s) in long QT syndrome.* Kardiol Pol. **69**(5): p. 423-9.

85. Sanguinetti, M.C. and M. Tristani-Firouzi, *hERG potassium channels and cardiac arrhythmia.* Nature, 2006. **440**(7083): p. 463-9.

86. Curran, M.E., et al., *A molecular basis for cardiac arrhythmia: HERG mutations cause long QT syndrome.* Cell, 1995. **80**(5): p. 795-803.

87. Abbott, G.W., et al., *MiRP1 forms IKr potassium channels with HERG and is associated with cardiac arrhythmia.* Cell, 1999. **97**(2): p. 175-87.

88. Perry, M., et al., *Structural determinants of HERG channel block by clofilium and ibutilide.* Mol Pharmacol, 2004. **66**(2): p. 240-9.

89. January, C.T. and J.M. Riddle, *Early afterdepolarizations: mechanism of induction and block. A role for L-type Ca2+ current.* Circ Res, 1989. **64**(5): p. 977-90.

90. Bryant, S.M., et al., *Regional differences in the delayed rectifier current (IKr and IKs) contribute to the differences in action potential duration in basal left ventricular myocytes in guinea-pig.* Cardiovasc Res, 1998. **40**(2): p. 322-31.

91. Litovsky, S.H. and C. Antzelevitch, *Transient outward current prominent in canine ventricular epicardium but not endocardium.* Circ Res, 1988. **62**(1): p. 116-26.

92. Clark, R.B., et al., *Heterogeneity of action potential waveforms and potassium currents in rat ventricle.* Cardiovasc Res, 1993. **27**(10): p. 1795-9.

93. London, B., et al., *Dispersion of repolarization and refractoriness are determinants of arrhythmia phenotype in transgenic mice with long QT.* J Physiol, 2007. **578**(Pt 1): p. 115-29.

94. Misier, A.R., et al., *Increased dispersion of "refractoriness" in patients with idiopathic paroxysmal atrial fibrillation.* J Am Coll Cardiol, 1992. **19**(7): p. 1531-5.

95. Wu, J., J. Wu, and D.P. Zipes, *Early afterdepolarizations, U waves, and torsades de pointes.* Circulation, 2002. **105**(6): p. 675-6.

96. Baker, L.C., et al., *Enhanced dispersion of repolarization and refractoriness in transgenic mouse hearts promotes reentrant ventricular tachycardia.* Circ Res, 2000. **86**(4): p. 396-407.

97. Antzelevitch, C., et al., *Heterogeneity within the ventricular wall. Electrophysiology and pharmacology of epicardial, endocardial, and M cells.* Circ Res, 1991. **69**(6): p. 1427-49.

98. Akar, F.G., et al., *Unique topographical distribution of M cells underlies reentrant mechanism of torsade de pointes in the long-QT syndrome.* Circulation, 2002. **105**(10): p. 1247-53.

99. Woosley, R.L., et al., *Mechanism of the cardiotoxic actions of terfenadine.* Jama, 1993. **269**(12): p. 1532-6.

100. Priori, S.G., et al., *Evaluation of the spatial aspects of T-wave complexity in the long-QT syndrome.* Circulation, 1997. **96**(9): p. 3006-12.

101. Sung, R.K., et al., *QTc Prolongation and Family History of Sudden Death in a Patient with Desmin Cardiomyopathy.* Pacing Clin Electrophysiol.

102. Shimizu, W. and C. Antzelevitch, *Cellular and ionic basis for T-wave alternans under long-QT conditions.* Circulation, 1999. **99**(11): p. 1499-507.

103. Pastore, J.M., et al., *Mechanism linking T-wave alternans to the genesis of cardiac fibrillation.* Circulation, 1999. **99**(10): p. 1385-94.

104. Barr, C.S., et al., *QT dispersion and sudden unexpected death in chronic heart failure.* Lancet, 1994. **343**(8893): p. 327-9.

105. Seethala, S., et al., *Effect of beta-adrenergic stimulation on QT interval accommodation.* Heart Rhythm. **8**(2): p. 263-70.

106. Papp, Z., et al., *Calcium-dependent modulation of the plateau phase of action potential in isolated ventricular cells of rabbit heart.* Acta Physiol Scand, 1999. **167**(2): p. 119-29.

107. Eisner, D.A., K.M. Dibb, and A.W. Trafford, *The mechanism and significance of the slow changes of ventricular action potential duration following a change of heart rate.* Exp Physiol, 2009. **94**(5): p. 520-8.

108. Guo, D., et al., *Contribution of late sodium current (I(Na-L)) to rate adaptation of ventricular repolarization and reverse use-dependence of QT-prolonging agents.* Heart Rhythm. **8**(5): p. 762-9.

109. Faber, G.M. and Y. Rudy, *Action potential and contractility changes in [Na(+)](i) overloaded cardiac myocytes: a simulation study.* Biophys J, 2000. **78**(5): p. 2392-404.

110. Boyett, M.R. and B.R. Jewell, *A study of the factors responsible for rate-dependent shortening of the action potential in mammalian ventricular muscle.* The Journal of physiology, 1978. **285**: p. 359-80.

111. Arnold, L., et al., *The dependence on heart rate of the human ventricular action potential duration.* Cardiovasc Res, 1982. **16**(10): p. 547-51.

112. Hund, T.J. and Y. Rudy, *Rate dependence and regulation of action potential and calcium transient in a canine cardiac ventricular cell model.* Circulation, 2004. **110**(20): p. 3168-74.

113. Viswanathan, P.C., R.M. Shaw, and Y. Rudy, *Effects of IKr and IKs heterogeneity on action potential duration and its rate dependence: a simulation study.* Circulation, 1999. **99**(18): p. 2466-74.

114. Shvilkin, A., et al., *Evolution and resolution of long-term cardiac memory.* Circulation, 1998. **97**(18): p. 1810-7.

115. Verduyn, S.C., et al., *Role of interventricular dispersion of repolarization in acquired torsade-de-pointes arrhythmias: reversal by magnesium.* Cardiovasc Res, 1997. **34**(3): p. 453-63.

116. Coronel, R., et al., *Injury current and gradients of diastolic stimulation threshold, TQ potential, and extracellular potassium concentration during acute regional ischemia in the isolated perfused pig heart.* Circ Res, 1991. **68**(5): p. 1241-9.

117. Pollard, A.E., et al., *Modulation of triggered activity by uncoupling in the ischemic border. A model study with phase 1b-like conditions.* Cardiovasc Res, 2002. **56**(3): p. 381-92.

118. Salama, G. and M. Morad, *Merocyanine 540 as an optical probe of transmembrane electrical activity in the heart.* Science, 1976. **191**(4226): p. 485-7.

119. Efimov, I.R., V.P. Nikolski, and G. Salama, *Optical imaging of the heart.* Circ Res, 2004. **95**(1): p. 21-33.

120. Del Nido, P.J., et al., *Fluorescence measurement of calcium transients in perfused rabbit heart using rhod 2.* Am J Physiol, 1998. **274**(2 Pt 2): p. H728-41.

121. Fast, V.G., *Simultaneous optical imaging of membrane potential and intracellular calcium.* J Electrocardiol, 2005. **38**(4 Suppl): p. 107-12.

122. Hwang, H.S., et al., *Inhibition of cardiac Ca2+ release channels (RyR2) determines efficacy of class I antiarrhythmic drugs in catecholaminergic polymorphic ventricular tachycardia.* Circ Arrhythm Electrophysiol. **4**(2): p. 128-35.

123. Hunt, D.J., et al., *K201 (JTV519) suppresses spontaneous Ca2+ release and [3H]ryanodine binding to RyR2 irrespective of FKBP12.6 association.* Biochem J, 2007. **404**(3): p. 431-8.

124. Wehrens, X.H., et al., *Enhancing calstabin binding to ryanodine receptors improves cardiac and skeletal muscle function in heart failure.* Proc Natl Acad Sci U S A, 2005. **102**(27): p. 9607-12.

125. Kawabata, H., K. Nakagawa, and K. Ishikawa, *A novel cardioprotective agent, JTV-519, is abolished by nitric oxide synthase inhibitor on myocardial metabolism in ischemia-reperfused rabbit hearts.* Hypertens Res, 2002. **25**(2): p. 303-9.

126. van der Werf, C., et al., *Flecainide therapy reduces exercise-induced ventricular arrhythmias in patients with catecholaminergic polymorphic ventricular tachycardia.* J Am Coll Cardiol. **57**(22): p. 2244-54.

127. Menshikova, E.V. and G. Salama, *Cardiac ischemia oxidizes regulatory thiols on ryanodine receptors: captopril acts as a reducing agent to improve Ca2+ uptake by ischemic sarcoplasmic reticulum.* J Cardiovasc Pharmacol, 2000. **36**(5): p. 656-68.

128. Barry, W.H. and J.H. Bridge, *Intracellular calcium homeostasis in cardiac myocytes.* Circulation, 1993. **87**(6): p. 1806-15.

129. Altamirano, J. and D.M. Bers, *Effect of intracellular Ca2+ and action potential duration on L-type Ca2+ channel inactivation and recovery from inactivation in rabbit cardiac myocytes.* American journal of physiology. Heart and circulatory physiology, 2007. **293**(1): p. H563-73.

130. Salama, G., *Arrhythmia genesis: aberrations of voltage or Ca2+ cycling?* Heart Rhythm, 2006. **3**(1): p. 67-70.

131. Qian, Y.W., et al., *Spatial heterogeneity of action potential alternans during global ischemia in the rabbit heart.* Am J Physiol Heart Circ Physiol, 2003. **285**(6): p. H2722-33.

132. Wilson, L.D., et al., *Heart failure enhances susceptibility to arrhythmogenic cardiac alternans.* Heart Rhythm, 2009. **6**(2): p. 251-9.

133. el-Sherif, N., et al., *QTU prolongation and polymorphic ventricular tachyarrhythmias due to bradycardia-dependent early afterdepolarizations. Afterdepolarizations and ventricular arrhythmias.* Circ Res, 1988. **63**(2): p. 286-305.

134. Salama, G. and S.M. Hwang, *Simultaneous optical mapping of intracellular free calcium and action potentials from Langendorff perfused hearts.* Curr Protoc Cytom, 2009. **Chapter 12**: p. Unit 12 17.

135. Yan, G.X. and C. Antzelevitch, *Cellular basis for the normal T wave and the electrocardiographic manifestations of the long-QT syndrome.* Circulation, 1998. **98**(18): p. 1928-36.

136. Wehrens, X.H., et al., *Protection from cardiac arrhythmia through ryanodine receptor-stabilizing protein calstabin2.* Science, 2004. **304**(5668): p. 292-6.

137. Zhou, S., et al., *Nonreentrant focal activations in pulmonary veins in canine model of sustained atrial fibrillation.* Am J Physiol Heart Circ Physiol, 2002. **283**(3): p. H1244-52.

138. Chen, G., et al., *Regional genomic regulation of cardiac sodium-calcium exchanger by oestrogen.* The Journal of physiology, 2011. **589**(Pt 5): p. 1061-80.

139. Bloomfield, D.M., et al., *Microvolt T-wave alternans and the risk of death or sustained ventricular arrhythmias in patients with left ventricular dysfunction.* J Am Coll Cardiol, 2006. **47**(2): p. 456-63.

140. Costantini, O., et al., *The ABCD (Alternans Before Cardioverter Defibrillator) Trial: strategies using T-wave alternans to improve efficiency of sudden cardiac death prevention.* J Am Coll Cardiol, 2009. **53**(6): p. 471-9.

141. Rosenbaum, D.S., et al., *Electrical alternans and vulnerability to ventricular arrhythmias.* N Engl J Med, 1994. **330**(4): p. 235-41.

142. Verrier, R.L., et al., *Microvolt T-wave alternans physiological basis, methods of measurement, and clinical utility-consensus guideline by international society for holter and noninvasive electrocardiology.* J Am Coll Cardiol, 2011. **58**(13): p. 1309-24.

143. Plummer, B.N., et al., *Spontaneous calcium oscillations during diastole in the whole heart: the influence of ryanodine reception function and gap junction coupling.* Am J Physiol Heart Circ Physiol. **300**(5): p. H1822-8.

144. Walker, M.L., et al., *Hysteresis effect implicates calcium cycling as a mechanism of repolarization alternans.* Circulation, 2003. **108**(21): p. 2704-9.

145. Oka, Y., et al., *Atrioventricular block-induced Torsades de Pointes with clinical and molecular backgrounds similar to congenital long QT syndrome.* Circ J, 2010. **74**(12): p. 2562-71.

146. Kay, G.N., et al., *Torsade de pointes: the long-short initiating sequence and other clinical features: observations in 32 patients.* J Am Coll Cardiol, 1983. **2**(5): p. 806-17.

147. Choi, B.R., F. Burton, and G. Salama, *Cytosolic Ca2+ triggers early afterdepolarizations and Torsade de Pointes in rabbit hearts with type 2 long QT syndrome.* The Journal of physiology, 2002. **543**(Pt 2): p. 615-31.

148. Nemec, J., et al., *Calcium oscillations and T-wave lability precede ventricular arrhythmias in acquired long QT type 2.* Heart rhythm : the official journal of the Heart Rhythm Society, 2010. **7**(11): p. 1686-94.

149. Kimura, J., et al., *Effects of a novel cardioprotective drug, JTV-519, on membrane currents of guinea pig ventricular myocytes.* Japanese journal of pharmacology, 1999. **79**(3): p. 275-81.

150. Kiriyama, K., et al., *Effects of JTV-519, a novel anti-ischaemic drug, on the delayed rectifier K+ current in guinea-pig ventricular myocytes.* Naunyn-Schmiedeberg's archives of pharmacology, 2000. **361**(6): p. 646-53.

151. Loughrey, C.M., et al., *K201 modulates excitation-contraction coupling and spontaneous Ca2+ release in normal adult rabbit ventricular cardiomyocytes.* Cardiovasc Res, 2007. **76**(2): p. 236-46.

152. Wang, D.W., et al., *Comparison of the effects of class I anti-arrhythmic drugs, cibenzoline, mexiletine and flecainide, on the delayed rectifier K+ current of guinea-pig ventricular myocytes.* J Mol Cell Cardiol, 1996. **28**(5): p. 893-903.

153. Hilliard, F.A., et al., *Flecainide inhibits arrhythmogenic Ca2+ waves by open state block of ryanodine receptor Ca2+ release channels and reduction of Ca2+ spark mass.* Journal of molecular and cellular cardiology, 2010. **48**(2): p. 293-301.

154. Ikeda, N., et al., *Effects of flecainide on the electrophysiologic properties of isolated canine and rabbit myocardial fibers.* J Am Coll Cardiol, 1985. **5**(2 Pt 1): p. 303-10.

155. Malfatto, G., A. Zaza, and M. Facchini, *Different effects of antiarrhythmic drugs on the rate-dependency of QT interval: a study with amiodarone and flecainide.* J Cardiovasc Pharmacol, 2007. **50**(5): p. 535-40.

156. Sarubbi, B., et al., *Compared effects of sotalol, flecainide and propafenone on ventricular repolarization in patients free of underlying structural heart disease.* Int J Cardiol, 1998. **66**(2): p. 157-64.

157. Seethala, S., et al., *Effect of beta-adrenergic stimulation on QT interval accommodation.* Heart rhythm : the official journal of the Heart Rhythm Society, 2011. **8**(2): p. 263-70.

158. Sims, C., et al., *Sex, age, and regional differences in L-type calcium current are important determinants of arrhythmia phenotype in rabbit hearts with drug-induced long QT type 2.* Circulation research, 2008. **102**(9): p. e86-100.

159. Birinyi, P., et al., *Effects of SEA0400 and KB-R7943 on Na+/Ca2+ exchange current and L-type Ca2+ current in canine ventricular cardiomyocytes.* Naunyn-Schmiedeberg's archives of pharmacology, 2005. **372**(1): p. 63-70.

160. Tsuji, Y., et al., *Ca(2+)-related signaling and protein phosphorylation abnormalities play central roles in a new experimental model of electrical storm.* Circulation, 2011. **123**(20): p. 2192-203.

161. Burashnikov, A. and C. Antzelevitch, *Reinduction of atrial fibrillation immediately after termination of the arrhythmia is mediated by late phase 3 early afterdepolarization-induced triggered activity.* Circulation, 2003. **107**(18): p. 2355-60.

162. Hinterseer, M., et al., *Relation of increased short-term variability of QT interval to congenital long-QT syndrome.* Am J Cardiol, 2009. **103**(9): p. 1244-8.

163. Morita, H., J. Wu, and D.P. Zipes, *The QT syndromes: long and short.* Lancet, 2008. **372**(9640): p. 750-63.

164. January, C.T. and H.A. Fozzard, *Delayed afterdepolarizations in heart muscle: mechanisms and relevance.* Pharmacol Rev, 1988. **40**(3): p. 219-27.

165. Luo, C.H. and Y. Rudy, *A dynamic model of the cardiac ventricular action potential. II. Afterdepolarizations, triggered activity, and potentiation.* Circ Res, 1994. **74**(6): p. 1097-113.

166. Shusterman, V., A. Goldberg, and B. London, *Upsurge in T-wave alternans and nonalternating repolarization instability precedes spontaneous initiation of ventricular tachyarrhythmias in humans.* Circulation, 2006. **113**(25): p. 2880-7.

167. Salerno-Uriarte, J.A., et al., *Prognostic value of T-wave alternans in patients with heart failure due to nonischemic cardiomyopathy: results of the ALPHA Study.* J Am Coll Cardiol, 2007. **50**(19): p. 1896-904.

168. Berger, R.D., et al., *Beat-to-beat QT interval variability: novel evidence for repolarization lability in ischemic and nonischemic dilated cardiomyopathy.* Circulation, 1997. **96**(5): p. 1557-65.

169. Nemec, J., et al., *QT interval variability and adaptation to heart rate changes in patients with long QT syndrome.* Pacing Clin Electrophysiol, 2009. **32**(1): p. 72-81.

170. Atiga, W.L., et al., *Beat-to-beat repolarization lability identifies patients at risk for sudden cardiac death.* J Cardiovasc Electrophysiol, 1998. **9**(9): p. 899-908.

171. Kaufman, E.S., et al., *Electrocardiographic prediction of abnormal genotype in congenital long QT syndrome: experience in 101 related family members.* J Cardiovasc Electrophysiol, 2001. **12**(4): p. 455-61.

172. Nemec, J., et al., *Catecholamine-provoked microvoltage T wave alternans in genotyped long QT syndrome.* Pacing Clin Electrophysiol, 2003. **26**(8): p. 1660-7.

173. Couderc, J.P., et al., *Beat-to-Beat repolarization variability in LQTS patients with the SCN5A sodium channel gene mutation.* Pacing Clin Electrophysiol, 1999. **22**(11): p. 1581-92.

174. Nemec, J., et al., *Catecholamine-induced T-wave lability in congenital long QT syndrome: a novel phenomenon associated with syncope and cardiac arrest.* Mayo Clin Proc, 2003. **78**(1): p. 40-50.

175. Hondeghem, L.M., L. Carlsson, and G. Duker, *Instability and triangulation of the action potential predict serious proarrhythmia, but action potential duration prolongation is antiarrhythmic.* Circulation, 2001. **103**(15): p. 2004-13.

176. Viswanathan, P.C. and Y. Rudy, *Pause induced early afterdepolarizations in the long QT syndrome: a simulation study.* Cardiovasc Res, 1999. **42**(2): p. 530-42.

177. Xie, L.H., et al., *Oxidative-stress-induced afterdepolarizations and calmodulin kinase II signaling.* Circ Res, 2009. **104**(1): p. 79-86.

178. Zabel, M., et al., *Electrophysiologic features of torsades de pointes: insights from a new isolated rabbit heart model.* J Cardiovasc Electrophysiol, 1997. **8**(10): p. 1148-58.

179. Choi, B.R. and G. Salama, *Simultaneous maps of optical action potentials and calcium transients in guinea-pig hearts: mechanisms underlying concordant alternans.* J Physiol, 2000. **529 Pt 1**: p. 171-88.

180. Milberg, P., et al., *Inhibition of the Na+/Ca2+ exchanger suppresses torsades de pointes in an intact heart model of long QT syndrome-2 and long QT syndrome-3.* Heart Rhythm, 2008. **5**(10): p. 1444-52.

181. Rosen, M.R., *Cellular electrophysiology of digitalis toxicity.* J Am Coll Cardiol, 1985. **5**(5 Suppl A): p. 22A-34A.

182. Liu, N., et al., *Arrhythmogenesis in catecholaminergic polymorphic ventricular tachycardia: insights from a RyR2 R4496C knock-in mouse model.* Circ Res, 2006. **99**(3): p. 292-8.

183. Terentyev, D., et al., *Abnormal interactions of calsequestrin with the ryanodine receptor calcium release channel complex linked to exercise-induced sudden cardiac death.* Circ Res, 2006. **98**(9): p. 1151-8.

184. Sato, D., et al., *Synchronization of chaotic early afterdepolarizations in the genesis of cardiac arrhythmias.* Proc Natl Acad Sci U S A, 2009. **106**(9): p. 2983-8.

185. Terentyev, D., et al., *Calsequestrin determines the functional size and stability of cardiac intracellular calcium stores: Mechanism for hereditary arrhythmia.* Proc Natl Acad Sci U S A, 2003. **100**(20): p. 11759-64.

186. Lakireddy, V., et al., *The kinetics of spontaneous calcium oscillations and arrhythmogenesis in the in vivo heart during ischemia/reperfusion.* Heart Rhythm, 2006. **3**(1): p. 58-66.

187. Rosen, M.R. and P. Danilo, Jr., *Effects of tetrodotoxin, lidocaine, verapamil, and AHR-2666 on Ouabain-induced delayed afterdepolarizations in canine Purkinje fibers.* Circ Res, 1980. **46**(1): p. 117-24.

188. Orchard, C.H., D.A. Eisner, and D.G. Allen, *Oscillations of intracellular Ca2+ in mammalian cardiac muscle.* Nature, 1983. **304**(5928): p. 735-8.

189. Wier, W.G., et al., *Cellular calcium fluctuations in mammalian heart: direct evidence from noise analysis of aequorin signals in Purkinje fibers.* Proc Natl Acad Sci U S A, 1983. **80**(23): p. 7367-71.

190. Eisner, D.A. and M. Valdeolmillos, *A study of intracellular calcium oscillations in sheep cardiac Purkinje fibres measured at the single cell level.* J Physiol, 1986. **372**: p. 539-56.

191. Rousseau, E. and G. Meissner, *Single cardiac sarcoplasmic reticulum Ca2+-release channel: activation by caffeine.* Am J Physiol, 1989. **256**(2 Pt 2): p. H328-33.

192. Kimura, S., et al., *Delayed afterdepolarizations and triggered activity induced in feline Purkinje fibers by alpha-adrenergic stimulation in the presence of elevated calcium levels.* Circulation, 1984. **70**(6): p. 1074-82.

193. Sicouri, S. and C. Antzelevitch, *A subpopulation of cells with unique electrophysiological properties in the deep subepicardium of the canine ventricle. The M cell.* Circ Res, 1991. **68**(6): p. 1729-41.

194. Restivo, M., et al., *Spatial dispersion of repolarization is a key factor in the arrhythmogenicity of long QT syndrome.* J Cardiovasc Electrophysiol, 2004. **15**(3): p. 323-31.

195. Sicouri, S., J. Fish, and C. Antzelevitch, *Distribution of M cells in the canine ventricle.* J Cardiovasc Electrophysiol, 1994. **5**(10): p. 824-37.

196. Maruyama, M., et al., *Genesis of phase 3 early afterdepolarizations and triggered activity in acquired long-QT syndrome.* Circ Arrhythm Electrophysiol. **4**(1): p. 103-11.

197. Baader, A.P., et al., *Real time, confocal imaging of Ca(2+) waves in arterially perfused rat hearts.* Cardiovasc Res, 2002. **53**(1): p. 105-15.

198. Marx, S.O., et al., *PKA phosphorylation dissociates FKBP12.6 from the calcium release channel (ryanodine receptor): defective regulation in failing hearts.* Cell, 2000. **101**(4): p. 365-76.

199. Zhang, Y.M., M. Miura, and H.E. ter Keurs, *Triggered propagated contractions in rat cardiac trabeculae. Inhibition by octanol and heptanol.* Circ Res, 1996. **79**(6): p. 1077-85.

200. Igarashi-Saito, K., et al., *Endocardial versus epicardial differences of sarcoplasmic reticulum Ca2+-ATPase gene expression in the canine failing myocardium.* Basic Res Cardiol, 1999. **94**(4): p. 267-73.

201. Janse, M.J., et al., *Flow of "injury" current and patterns of excitation during early ventricular arrhythmias in acute regional myocardial ischemia in isolated porcine and canine hearts. Evidence for two different arrhythmogenic mechanisms.* Circ Res, 1980. **47**(2): p. 151-65.

202. Liu, J. and K.R. Laurita, *The mechanism of pause-induced torsade de pointes in long QT syndrome.* J Cardiovasc Electrophysiol, 2005. **16**(9): p. 981-7.

203. Yan, G.X., et al., *Phase 2 early afterdepolarization as a trigger of polymorphic ventricular tachycardia in acquired long-QT syndrome : direct evidence from intracellular recordings in the intact left ventricular wall.* Circulation, 2001. **103**(23): p. 2851-6.